COMPUTER MODELING OF A SOLAR THERMAL SYSTEM FOR SPACE HEATING

A thesis submitted in partial fulfillment
of the requirements for the degree of
Master of Science in Renewable and Clean Energy Engineering

By

DHANANJAY D. DESHPANDE
B.E., Nagpur University, 2013

2016
WrightStateUniversity

WRIGHT STATE UNIVERSITY
GRADUATE SCHOOL

December 16, 2016

I HEREBY RECOMMEND THAT THE THESIS PREPARED UNDER MY SUPERVISION BY Dhananjay D. Deshpande ENTITLED Computer Modeling of a Solar Thermal System for Space Heating BE ACCEPTED IN PARTIAL FULFILLMENT OF THE REQUIREMENTS FOR THE DEGREE OF Master of Science in Renewable and Clean Energy Engineering.

_____
James Menart, Ph.D.
Thesis Director

_____
Joseph Slater, Ph.D.
Chair
Department of Mechanical and Materials Engineering

Committee on Final Examination

_____
James Menart, Ph.D.

_____
Allen Jackson, Ph.D.

_____
Amir Farajian, Ph.D.

_____
Robert E.W. Fyffe, Ph.D.
Vice President for Research and
Dean of the Graduate School

Abstract

Deshpande, Dhananjay D. M.S.R.C.E.E. Department of Mechanical and Materials Engineering, Wright State University, 2016 Computer Modeling of a Solar Thermal System for Space Heating.

Computer Modeling of a Solar Thermal System for Space Heating

Most applications of flat plate, low-temperature solar thermal panels are for water heating, such as producing domestic hot water or raising the temperature of swimming pools. This is reasonable given that the large masses of water present in these systems inherently provide built-in thermal energy storage so that a separate energy storage tank does not have to be purchased. For a space heating system, extra thermal energy storage generally has to be purchased and is a detriment to the economics of these systems. Despite the economic drawbacks of solar thermal space heating, this thesis focuses on the size of thermal systems required to heat an average size home in Minneapolis, MN and Dayton, OH. For these two locations and for a standard test case, this thesis studies the effect of solar panel size and orientation, heat exchanger size, and operation parameters including flow rates through the solar panels and heat exchanger.

Liquid, flat plate collectors are one of the simplest methods for collecting solar energy. These panels are generally inexpensive and can have collection efficiencies above 50%. This makes solar thermal panels more efficient than solar photovoltaic panels, which generally have efficiencies less than 20%. Since the solar thermal panels chosen for study in this work heat a liquid with the sun's energy and the fluid being heated in the building is air, a heat exchanger has to be included in the model. Lastly, because solar thermal systems are inherently unsteady, thermal energy storage must be included in the model. These components of a solar thermal space heating system are modeled by writing and adding routines to the Wright State developed simulation program called Solar_PVHFC. Solar_PVHFC is a simulation program which models solar photovoltaic panels coupled with fuel cells and hydrogen storage tanks. Because of this work, Solar_PVHFC is now capable of modeling a solar thermal system. The advantage of coupling this solar thermal work to Solar_PVHFC is that Solar_PVHFC does a very detailed calculation of the solar energy

impinging upon a surface at any location, at any time, for any orientation. This is required to properly model solar thermal systems. The program modules that perform the simulation of the solar thermal system components are written in MATLAB, just like the Wright State developed program Solar_PVHFC.

Contents

List of Figures

Nomenclature

A_c	Area of collector
A_p	Area of plate
A	Surface area of heat exchanger
A_{fg}	Flow area on gas side of heat exchanger
A_{bg}	Area of base on gas side
$A_{fins,g}$	Area of fins on gas side
A_{bl}	Area of base on liquid side
$A_{fins,l}$	Area of fins on liquid side
a ,b	Coefficients in empirical relationships used to calculate circumsolar diffuse radiation
B	Function of the day of the year
C_r	Heat capacity ratio
C_p	Specific heat
$c_{p,h}$	Specific heat of hot fluid
$c_{p,c}$	Specific heat of cold fluid
C_p	Specific heat
C_b	Bond conductance
$C_{p,l}$	Specific heat of liquid
$C_{p,g}$	Specific heat of gas
C,e	Factors for calculating the top overall heat transfer coefficient
D, D_i	Diameter of tube
$D_{fins,g}$	Distance between fins on gas side
$D_{hg,fins}$	Hydraulic diameter between fins on gas side
$D_{fins,l}$	Distance between fins on liquid side
$D_{hl,fins}$	Hydraulic diameter between fins on liquid side

E	Equation of time in seconds
F	Fin efficiency
f	Fanning friction factor
$F^{'}$	Collector efficiency factor
F_R	Heat removal factor
$F^{'}$	Collector flow factor
F_g	Fins per meter on gas side
F_{th}	Fin thickness
F_l	Fins per meter on gas side
h_c	Convective heat transfer coefficient
h_r	Radiative heat transfer coefficient
h_{fi}	Heat transfer coefficient
h_w	Wind heat transfer coefficient
h_{rad}	Combination of convective and radiative heat transfer coefficients
h_{p-c2}	Convection heat transfer coefficient between absorber plate and lower glass cover
h_{r-c2}	Radiation heat transfer coefficient between absorber plate and lower glass cover
h_{c2-c1}	Convection heat transfer coefficient between two cover plates
$h_{r,c2-c1}$	Radiation heat transfer coefficient between two cover plates
h_{c1-a}	Convection heat transfer coefficient from top cover to ambient air
$h_{r,c1-a}$	Radiation heat transfer coefficient from top cover and sky
h_g	Heat transfer coefficient at gas side
h_l	Heat transfer coefficient at liquid side
I	Hourly measured radiation on horizontal surface
I_0	Hourly insolation on horizontal surface
I_T	Total hourly radiation on tilted surface
I_b	Beam radiation on horizontal surface
I_d	Diffuse radiation on horizontal surface
KL	Cover plate types

k	Thermal conductivity
k_T	Hourly clearness index
k_i	Thermal conductivity of insulation
k_e	Thermal conductivity of insulation for edge
k_p	Plate thermal conductivity
k_g	Thermal conductivity of gas
k_{mat}	Thermal conductivity of material
k_l	Thermal conductivity of liquid
L_{st}	Standard longitude
L_{loc}	Longitude
L	Characteristic length
L_c	Characteristic length
L_t	Insulation thickness
L_e	Edge insulation thickness
L_{dg}	Gas flow channel depth
L_{hl}	Length of heat exchanger on liquid side
L_{hg}	Length of heat exchanger gas side
L_{dl}	Liquid flow channel depth
L_{hl}	Length of heat exchanger on liquid side
LMTD	Logarithm mean temperature difference
m_h	Mass flow rate of hot fluid in heat exchanger
m_c	Mass flow rate of cold fluid in heat exchanger
$\dot{m}$	Mass flow rate
$\dot{m}_{l,layer}$	Mass flow rate on liquid side per layer
$\dot{m}_{g,layer}$	Mass flow rate on gas side per layer
$\dot{m}_l$	Mass flow rate on liquid side
$\dot{m}_g$	Mass flow rate on gas side
N	Number of cover plates
NTU	Number of transfer Units
n	Day number

$\overline{N_{u_L}}$	Nusselt number for two plates with cavity inclined at angle of β (volumetric thermal expansion) between 0^o to 75^o
N_u	Nusselt number
$N_{u,l}$	Nusselt Number at liquid side
$N_{u,g}$	Nusselt Number at gas side
N_{layers}	Number of layers
N_{fg}	Number of fins on gas side
N_{fl}	Number of fins on liquid side
P	Perimeter of plate
P_r	Prandlt number
$P_{r,l}$	Prandlt's number at liquid side
$P_{r,g}$	Prandlt's number at gas side
P_t	Plate thickness
Q_u	Amount of energy rate collected by solar panel for time period Δt
Q_{fin}	Heat transfer through fin
$Q_{max,fin}$	Maximum heat transfer through fin
$\dot{Q_u}$	Amount of energy rate collected by solar panel
q	Heat transfer rate in heat exchanger
q_{max}	Maximum heat transfer rate in heat exchanger
R_e	Reynolds number
R_b	Average Ratio of tilted surface radiation to horizontal radiation
R_1 , R_2	Convective Resistance
R_3, R_4	Convective Resistance
$R_{a_{L,c}}$, R_a	Rayleigh Number
$R_{fin,g}$	Fin resistance on gas side
$R_{base,g}$	Resistance of base on gas side
$R_{fin,l}$	Fin resistance on liquid side
$R_{base,l}$	Resistance of base on liquid side
R_{wall}	Wall resistance

R_{total}	Total resistance
$R_{e,g}$	Reynold's number at gas side
$R_{e,l}$	Reynold's number at liquid side
S	Solar energy absorbed
T_{pm}	Mean plate temperature
T_a	Ambient Temperature
T_s	Sky temperature for radiative transfer
T_a	Ambient temperature
T_{dp}	Dew point temperature
t	Hour from midnight in hours
$\bar{T}$	Average temperature of fluid
T_1	Initial temperature of fluid
T_2	Final temperature of fluid
T_b	Tube temperature
T_{fo}	Fluid outlet temperature
T_{fi}	Fluid inlet temperature
T_{fm}	Fluid mean temperature
T_{pm}	Plate mean temperature
$T_{h,i}$ $T_{h,o}$	Inlet and outlet temperature of hot fluid in heat exchanger
T_{ci} $T_{c,o}$	Inlet and outlet temperature of cold fluid in heat exchanger
$T_{sp,in}$	Solar panel inlet temperature
$T_{sp,out}$	Solar panel outlet temperature
$T_{in,G}$	Heat exchanger inlet gas temperature
U	Overall heat transfer coefficient in heat exchanger
U_L	Overall heat loss coefficient
U_t	Top overall heat loss coefficient
U_b	Back overall heat transfer coefficient
U_e	Edge overall heat transfer coefficient
V	Wind speed
V_{fg}	Volumetric gas flow rate

V_g	Velocity of gas in heat exchanger
V_l	Velocity of liquid in heat exchanger
∀	House volume
W	Plate width

Greek Symbols

δ	Declination angle
$\emptyset$	Latitude
β	Altitude angle of surface
γ	Azimuthal angle of surface
ω	Hour angle
ω_1	Hour angle at beginning of standard hour
ω_2	Hour angle at end of standard hour
$(\tau\alpha)$	Transmittance-absorbance product, subscripts b, d, g, symbolize beam, diffuse, ground and components respectively
τ	Transmittance
α	Absorptance
θ	Angle of incidence subscripts, d and g symbolize beam, diffuse, ground and components respectively
ϵ_g	Glass emittance
ϵ_p	Plate emittance
ϵ_{c2}	Emissivity of lower cover
ϵ_{c1}	Emissivity of top cover
ρ_g	Ground reflectivity
ρ_D	Diffuse reflectivity
ρ_{liq}	Density of liquid
μ_l	Dynamic viscosity of liquid
ρ_{liq}	Density of liquid
ρ_{gas}	Density of gas
μ_g	Dynamic viscosity of gas

$\eta_{collector}$	Collector Efficiency
$\eta_{fin,g}$	Fin efficiency on gas side
$\eta_{fin,l}$	Fin efficiency on liquid side
ε	Effectiveness of heat exchanger
δ_p	Plate thickness
Δt	Time period

ACKNOWLEDGEMENTS

This thesis signifies my amazing experience of completing two years at Wright State University. Since my first day here at WSU, on August 25th, 2014, it has felt like home. I had always dreamt of doing a thesis right from the day I started grad school. The opportunities here were beneficial to my career goals; an example would be starting this thesis and taking courses related to solar energy. Throughout these years, I have learned many concepts and tools for doing my research for this thesis.

First and foremost, I would like to thank my advisor, Dr. James Menart, for having faith in me and giving me the opportunity to do this thesis. His knowledge and experience is enormous in this field, which helped me throughout my graduate program. He has been supportive throughout the entire project. Dr. Menart is a revered thesis advisor, as he guided me all these years, helped me to come up with my thesis topic, and also gave me moral support and freedom to move on while working on my thesis.

I would also like to express my gratitude to the committee members for their time.

A special acknowledgement to my Windsor Apartment friends for being patient and being supportive for all these years and especially to my officemate, Ashwin Borakhadikar. He is a trusted friend from the time when we started sharing the office (Russ Engineering 224) in 2015. Two other friends I mention are Akshay Bhimanwar and Shraddha Nimbalkar. These two constantly asked “are you done yet” and affectionately mentioned me as their friend “the professional student.” Thank you for the support and most of all your humor. You both kept things light and me smiling.

I would like to finish with my home Nagpur (MH-31), India which is the starting place of love, hope and dreams: my family (Mr. Deepak P. Deshpande, Dr. Padmaja D. Deshpande, Mr. Devendra P. Deshpande, Mrs. Neera D. Deshpande, Miss Dhanashree D. Deshpande). I have an amazing family who stood behind me for all these years and gave me support emotionally towards this tough road to finish this thesis and successfully complete my Masters.

Chapter 1. INTRODUCTION

1.1 Objectives

This project deals with computationally investigating a solar thermal system that is composed of flat plate collectors, a heat exchanger, and fluid storage. This solar thermal system is used for house heating. Various aspects of this solar thermal system, including efficiency, inlet and outlet temperatures of the system, and the amount of heat supplied to the house are studied. The survey of this solar thermal system is carried out for two different locations, Minneapolis, MN and Dayton, OH.

A computer model was created that simulates the operation of a flat plate collector coupled with a heat exchanger. Since this system is inherently unsteady, thermal storage has to be included in the model. This was done by using a very simplistic assumption on the size of the storage tank and assuming that no mixing occurs. This solar thermal model is developed in the currently available computer code called Solar_PVHFC [1]. Solar_PVHFC is a Wright State computer program which models solar energy systems that have photovoltaic panels to convert the sun's energy to electricity. Solar_PVHFC provides a detailed analysis of various types of collectors and enables adjustment of the parameters of the solar panel, the hydrogen storage, and the fuel cell system. The scope of this work does not include hydrogen storage, fuel cells, or photovoltaic panels. However, Solar_PVHFC's modeling of solar resources is applicable to this thesis work and thus is fully utilized. This study included adding separate routines to

Solar_PVHFC for the flat plate thermal collectors, the heat exchanger, and the operation of the solar thermal system.

1.2 Status of Renewable Energy

The environmental issues and the restrictions on the usage of fossil fuels around the world have made the use of renewable energy sources necessary. Some of the more popular renewable energy sources are solar, wind, hydro, biofuels, and geothermal. This study focuses on solar renewable energy.

The use of solar energy is not new; it has been used for many years in various applications. It all started by concentrating the sun's heat with a glass lens to light fires. Most recently, the technology has evolved and has been used in various applications for home heating, water heating, industrial heating, cooking, refrigeration, drying of agriculture crops, electricity generation, water desalination, aircraft propulsion, and automobile propulsion, to name a few. An attractive aspect of solar energy is that it scales to small applications. It is cheaper to use solar on a large scale, but it is still very easy to implement on a small scale. There are many advantages of solar energy utilization; therefore, there has been a substantial development in this energy sector [2].

According to the Lawrence Livemore National Laboratory, the United States uses the most fossil fuels of any country in the world. As can be seen in the energy flow chart in Figure 1, the electrical energy generation sector is a huge percentage of the energy consumption in the United States. The production of electricity is one area to which solar energy is well suited to relieve some of the burden on fossil fuels. Note that there have been significant increases in the use of solar energy for electric power generation since the time that Figure 1 was published in 2014 [2].

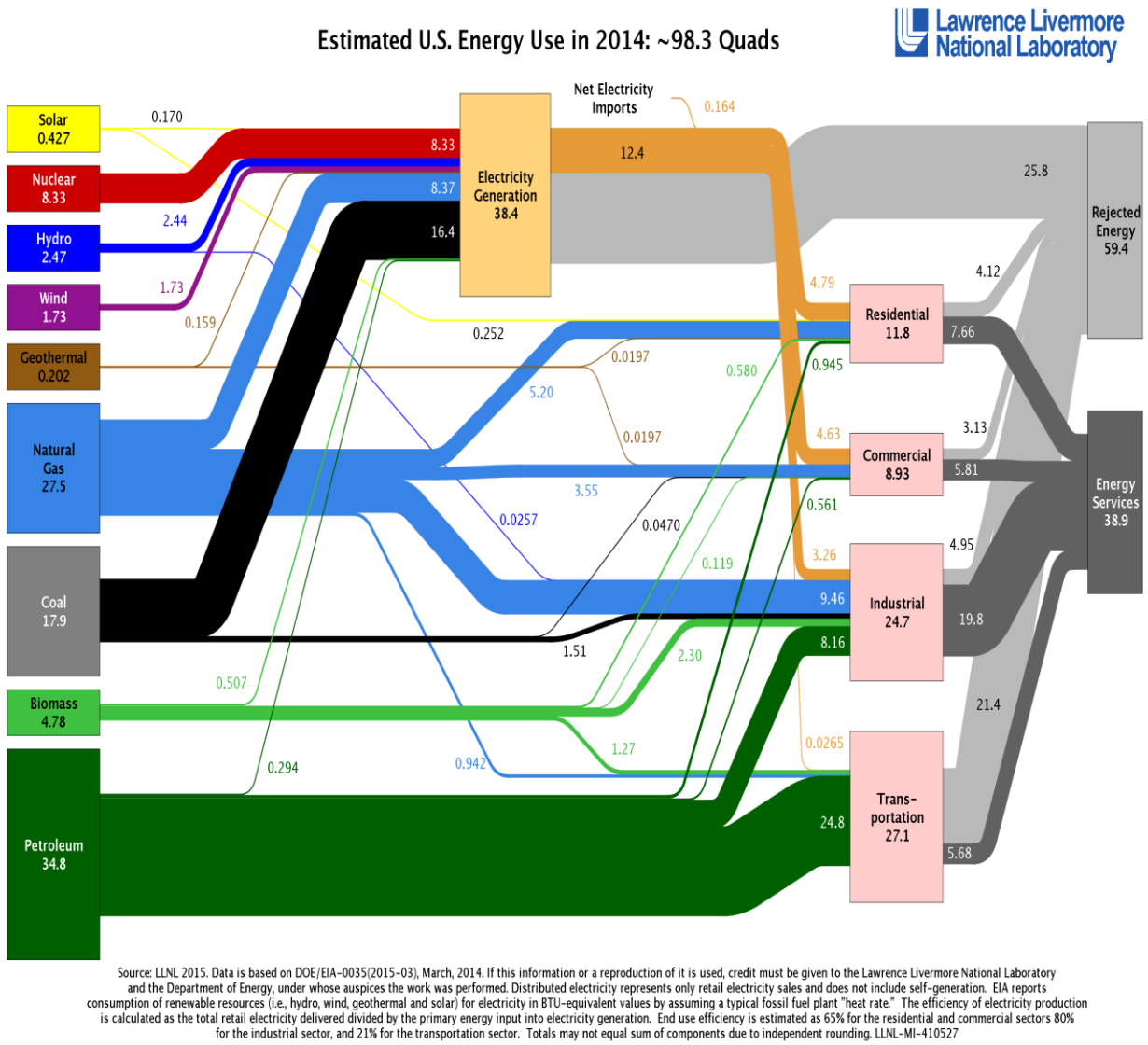

Figure 1: Estimated USA energy use in 2014 [2].

Figure 2 shows different renewable energy sources that were consumed in the year 2014. Biomass is the largest used renewable, which is about 50% of the total renewable energy used. Hydroelectric is the next most used renewable form of energy at 26%. In 2014, solar energy was 2% of the total renewable energy being utilized. This means that it is 0.2% of the total energy utilized by the United States, or 0.2 quadrillion Btu. This growth trend is expected to continue in the coming years [3].

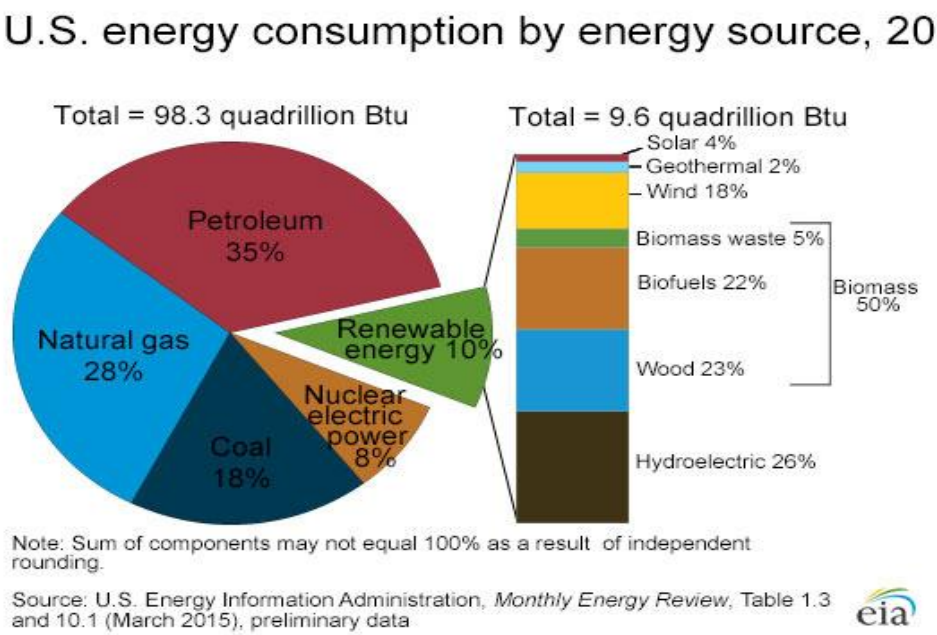

Figure 2: Renewable energy consumption [3].

Due to such developments, the Bureau of Land Management created a solar energy utility program that includes six southwestern states that were open for proposals for solar power installations. These states are supposed to have good weather conditions and land available for utilizing solar energy more efficiently [4].

In Florida, the homeowners having solar water heaters save about 50 to 85% on electricity bills, according to Florida Solar Energy Center. Another major application of solar energy in the USA is solar water heating, which is used in most of the states. In the year 2006, the U.S. Department of Energy estimated that approximately 1.5 million of the population is using solar water heaters. These are usually coupled with flat plate solar panels, so that about 1000 MW of solar thermal power are being produced and used by households. According to the U.S. Department of Energy, there are chances of installations around 400 MW. Solar water heaters save a lot of energy and at the same time reduce the need for conventional heating [5].

1.3 History of Solar Thermal Technology

Solar thermal technology has been used for many years. One of the early uses was in the 18th century when a scientist used a cross-section of a hot box to test how much of the sun's heat is trapped from a glass covered area, as shown in Figure 3 [6].

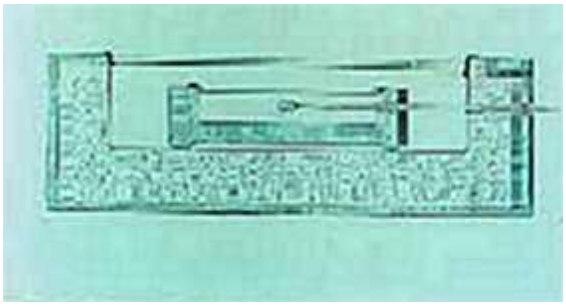

Figure 3 : Cross section of solar powered hot box [6].

In the 19th century, this technology was further developed, as shown in Figure 4; the first solar water heaters were simple, uncovered metal tanks containing water that were painted black and tilted towards the sun when they were in use.

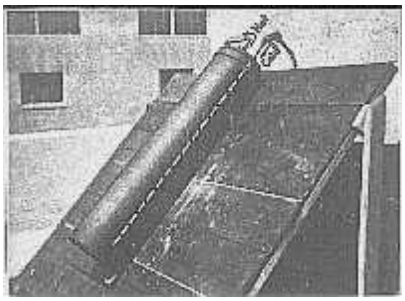

Figure 4 : Solar water heater in 19th century [6].

In the year 1981, the world's first patented commercial solar water heater was advertised (see Figure 5). This solar water heater combined the old methods used in the 18th and 19th centuries and increased the capacity of retaining solar heat [6].

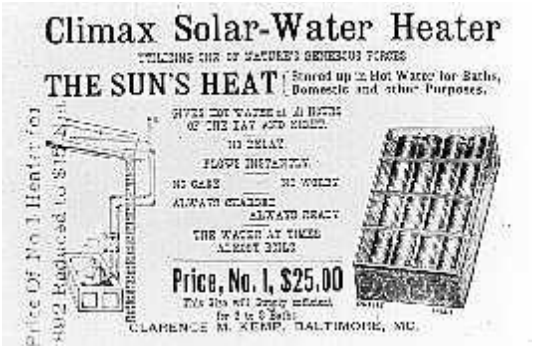

Figure 5: Advertisement for Climax Solar Water Heater [6].

In the early 1900s, a significant evolution occurred in the solar thermal industry. A family in Pomona Valley, California transformed the Climax solar water heater from a glass-covered box system to a solar panel that is placed on the roof of a house to satisfy their hot water requirements (see Figure 6) [6].

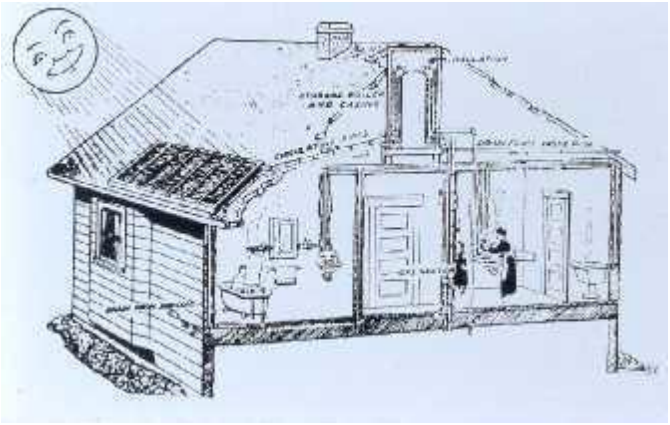

Figure 6 : Climax solar installation on house roof [6].

1.4 Solar Thermal Today

1.4.1 Solar Water Heating

A report published by the Renewable Energy Policy Network for the 21st Century provides a number of interesting statistics regarding the status of solar hot water heating in major countries around the world in recent years. Water collectors, both glazed and unglazed, generated about 313.7 TWh of heat in the year 2013. The contribution to this amount of energy was made

mostly by six countries, with China being the major contributor [7]. The market was on a slower growth path as the year 2014 started due to increases in the total number of collectors that have already been installed. Solar thermal systems provided approximately 341 TWh of heat annually. The year 2014 was the most vital in the application of providing domestic hot water for residential homes [7].

Figure 7 shows percentages by country for solar water heating capacity. As can be seen from this graph, China dominates solar thermal usage. China accounts for 70% of the solar thermal energy generation and use, whereas the rest of the world accounts for the remaining 30%. The United States ranks second for solar water heating at 4.5%, and Germany is third at 3.3%.

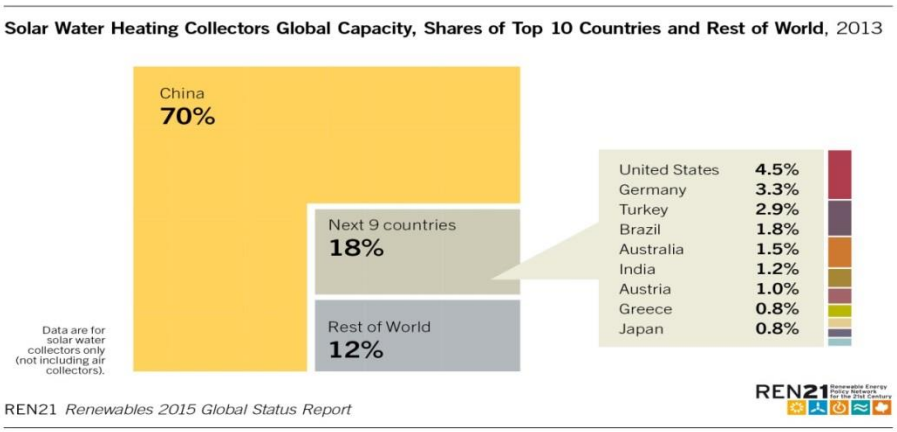

Figure 7 : Global share of solar water heating collectors [7].

Figure 8 shows more clearly, in terms of energy produced by each country, the use of different types of solar thermal collectors. Most of the countries used glazed, water collectors, whereas in the United States there seems to be a preference for unglazed, water collectors for pool heating. In India and China, evacuated tube collectors are primarily used. Evacuated tube collectors are more efficient then unevacuated solar collectors, but they are also more expensive.

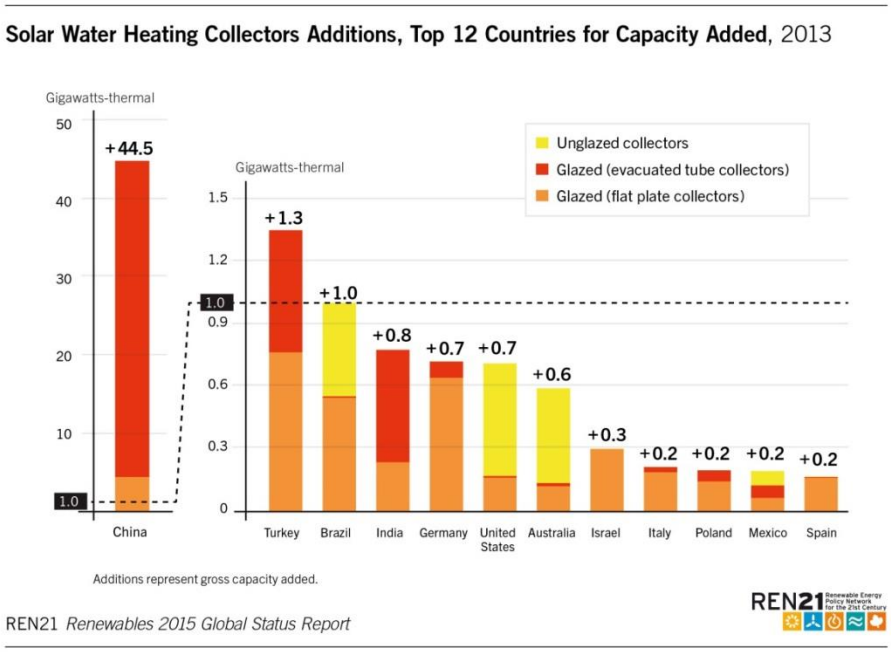

Figure 8 : Solar thermal energy capacity for different countries [7].

1.4.2 Solar electricity generation

Currently, systems using many photovoltaic (PV) panels are being used to produce electricity globally, but it is cheaper to harvest solar energy as heat using a solar thermal panel compared to harvesting it as electricity with PV modules. In addition, low-temperature solar heat can be more efficiently achieved than PV energy harvesting using flat plate collectors and evacuated tube collectors.

In Figure 9, all the segments of solar projects are shown from 2010-2014. The graph for all segments (i.e., Total Solar) is significantly growing. This graph shows that solar PV energy harvesting is about an order of magnitude greater than solar thermal. Residential solar PV and utility scale solar PV are each about five times greater. In addition to solar PV harvesting and producing more energy, solar PV is growing faster than solar thermal. Solar thermal has lower growth within the US, because it is not suitable to install solar thermal systems in every region. It is especially uncommon to find solar thermal installations in the Midwest region due to weather

conditions [8]. This is not to say that solar thermal is not utilized or that it should not be considered as an option.

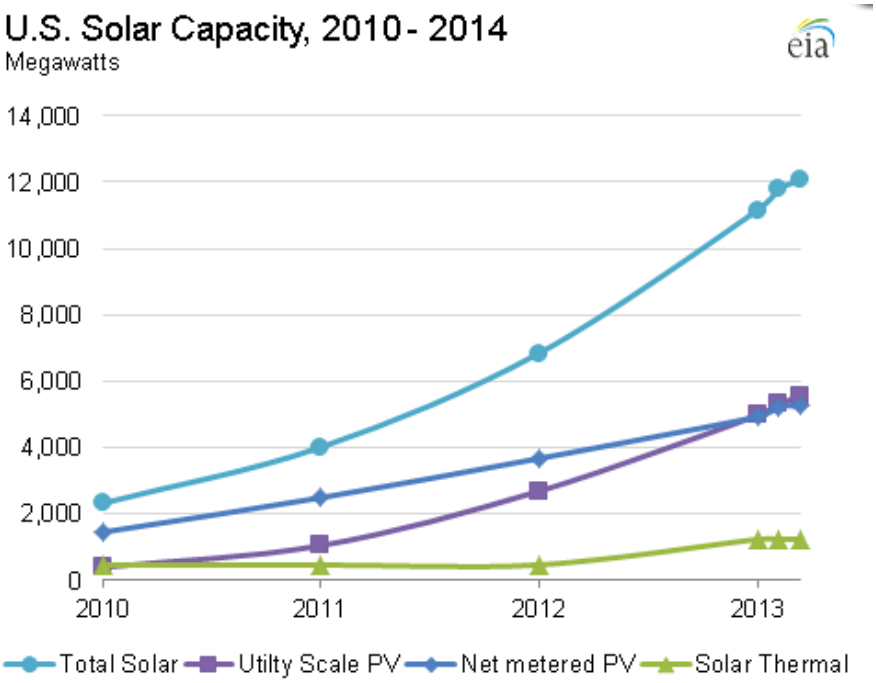

Figure 9 : Graph showing USA solar capacity[9].

In the western regions of the US, there are greater amounts of solar thermal electricity production. One of the major solar thermal plants is located in San Bernardino County, California, and has a capacity of generating up to 250 MW of electric power. The plant is expected to generate 617,000 MW of clean power and eliminate 329,000 tons of carbon dioxide emissions on an annual basis [9]. Another solar thermal electric generating project is further south in the state of Arizona, which has the capacity of generating up to 250 MW of electric power. It is the largest energy storage project and the first in the US that can store more than 1000 MWh of energy [10] .

The northeast region of the US has a high number of solar thermal projects, particularly rooftop collectors used for domestic water heating and space heating. This part of the US has high electricity rates, so the people use solar generated electricity, which is economically the best choice for them [11].

Solar PV panels are used in both commercial and residential areas in the US. A commercial project called the California Valley Solar Ranch is installed in San Luis Obispo County, California and generates about 250 MW. It includes an array of more than 750,000 solar PV panels [12]. Located in Greenville, South Carolina, the Roper Mountain Science Center houses a commercial installation that has a photovoltaic system of 25 kW[13].

Several residential projects also use PV panels. For example, an installation of a PV system that generates 5.32 kW is used for a house located in Cumming, Georgia. This installation uses 19 panels of 280 that are attached to 16 batteries and stores approximately 14.64 kWh of energy[14].

1.4.3 Solar space heating

Solar thermal technology can be used for space heating by using different collectors. Flat plate collectors are usually used for domestic purposes such as space heating and water heating. Solar water heating is more common than space heating. Most of these solar space heating systems use a thermal energy storage tank for delivering the heat to the house. This type of space heating is known as water storage solar heating and allows the system to meet a greater portion of the winter heating loads. This method is used in the southern part of Wisconsin and can supply 50% of a home's heating demand. This is done with one square foot of collector for every four square feet of a home.

Direct solar heating is another option and is the simplest and least expensive for the purpose of space heating. This kind of system does not include a storage unit. These systems can provide nearly 25% of heating in the southern part of Wisconsin by using a square foot of collector for every four square feet of a home's footprint area. These data are provided by the company Full Spectrum Solar that provides these services in Wisconsin[15].

1.5 Outline of Thesis

Although solar thermal space heating is not utilized as much as other solar energy technologies, it is the goal of this thesis to study solar space heating in order to ascertain the percentage of a home's heating load that can be met with flat plate solar panels that use a liquid to transport the thermal energy to the space being heated. A heat exchanger is used to transfer the heat from the working liquid to the air in the home. Because liquid is used as the transport

mechanism from the solar panel to the air in the home, this becomes an unsteady problem and some thermal energy storage must be included. This thesis will identify the percentage of energy requirements that can be met with this type of solar space heating system in a typical home in Minneapolis, Minnesota and Dayton, Ohio. In addition, the effects of a number of the design parameters of the system will be presented.

This thesis is composed of six chapters. Chapter 1 has provided an introduction to solar energy and in particular solar thermal energy. Information on the history of solar thermal energy, its current status, and the different solar thermal applications has been discussed. Chapter 2 of this thesis is the literature survey that provides a review of experimental and modeling studies of flat plate solar collectors carried out by different individuals. Chapter 3 identifies the required paths that solar radiation can take to impinge on a solar panel and the angles that are necessary for modeling of the solar energy impinging on the solar panel. Chapter 4 presents an analysis of the solar thermal system used in this thesis, which includes a detailed description of both the flat plate collector and the heat exchanger, and details of the energy storage assumption used in this study. Furthermore, this chapter discusses the coupling of the flat panel collector with the heat exchanger and energy storage, and provides a control strategy for the system. Chapter 5 presents the results of the study, including those for a one-hour period for standard solar thermal flat plate testing conditions; the yearly results for typical 2000-square foot homes located in Minneapolis, MN and in Dayton, OH; and the design and operating parameters of the solar thermal system. Finally, Chapter 6 presents the conclusions reached as a result of this work.

Chapter 2. LITERATURE SURVEY

The modern flat plate solar thermal collector was designed in the late 1950s by Hottel and Whillier [16]. This is one of the easiest solar collectors to manufacture and is commonly used in today's market. It consists of a dark flat plate absorber, transparent glass cover, heat transport fluid, and insulation on the back. The circulating fluid in the absorber tubes may be of two kinds: air-based or liquid-based. Air-based collectors are usually used for heating buildings and drying crops. Liquid-based collectors can be of two types: glazed and unglazed. Liquid-based collectors are usually used for providing domestic water heating and for space heating purposes [17].

There has been a good deal of research in the area of solar thermal systems. In this chapter, some of this research is discussed. The first subsection of this chapter surveys experimental work on solar thermal systems, and the second subsection surveys modeling work. This division between experimental and modeling work is not perfect, because a number of investigators did both and presented it in the same paper. For this reason, there will be mention of experimental work in the modeling subsection and modeling work in the experimental subsection.

2.1 Experimental Work

Tasdemiroglu [18] carried out experimental evaluation of space heating in Ankara, Turkey. This experimental analysis consisted of a system with two flat plate collectors connected in series, liquid-to-liquid heat exchangers, a storage tank, a liquid-to-air heat exchanger, two pumps for circulation, and a number of valves. Various temperatures were recorded using thermocouples and a digital multimeter. These included fluctuations in the temperatures at intersections of the major system components, room temperatures, and ambient temperatures. Also measured was the total solar radiation incident on the collectors. Data were collected for seven months, from October 1988 to April 1989, and the thermal performance was evaluated, giving 36% and 45% daily efficiencies for direct and indirect modes, respectively.

Chekerovska and Filkoski [19] developed an experimental setup in the city of Shtip to take measurements on flat plate solar panels that have a tracking system. These individuals wanted to investigate the effect of a sun tracking system performance. They had a set of two flat plate solar collectors in which one was fixed and the other was tilted towards the south at 30 degrees with a dual-axis rotation system. The results of that experiment showed a significant increase in the daily energy captured by the moving collector as compared to a stationery collector. The collector with the two-axis tracking system had significantly improved performance, with an increase in collected energy of over 20% in the months of March and April for the afternoon hours. It was also noted that the computational fluid dynamics (CFD) model they developed produced better comparisons to experimental data in the system with the fixed collector.

Esbensen and Korsgaard [20] designed a house at the Technical University of Denmark for heating in the winter season by using solar energy as its main source. The house had insulated walls, and the total energy required for space heating was 2300 kWh per year. The heating system used a flat plate collector that supplied hot water for the whole year. The flat plate collector was 42 m^2 and was attached to an insulated water storage tank of 30 m^3. The absorbed radiation in the solar collector and energy that was accumulated in the storage tank were calculated using a computer model. The wind velocity, ambient temperature, and solar radiation for that particular year were taken as input data from a source to calculate this parameter on an hourly basis. To avoid freezing of the panels in cold weather and cloudy conditions, the water was drained from the collector. The house had a calculated total heat balance such that 7300

kWh of energy was collected in the year; 30% of the energy was used for space heating, 30% was used for water heating, and the remaining was lost heat from the accumulator tank.

Manickavasagan et al. [21] conducted a study on the performance of a solar water heater that used an alternative working fluid. The experimental study had a flat plate solar panel, which was fabricated and had a fixed orientation. This was coupled to a heat exchanger kept inside a water storage drum. The collector, which they operated at a low temperature, had an operating range from ambient temperature to 100^{o} C. They chose acetone as the alternative working fluid, which circulated in a closed loop. This system's heat exchanger was used to transfer heat between the water and acetone. The solar intensity had few changes as the time progressed from morning to evening: 550 W/m^2 in the morning at 8:30 am, 850 W/m^2 from noon to 1:30 pm, and 640 W/m^2 at 6:00 pm in the evening. The absorber plate temperature was constant in the beginning hours, but later increased to 90^{o} C for two hours and then decreased to 72^{o} C in the afternoon. The acetone was found to be at the highest temperature between 1:00 pm and 2:00 pm. The water temperature also had a significant change, from 30^{o} C to 62^{o} C. The overall efficiency of the system was 45% when water was the working fluid in the collector. In the future, alternative fluids that have low boiling points with high latent heats of evaporation such as acetone, methanol, or ethanol could be used as the working fluid for solar collectors.

The absorber plate of a solar thermal panel plays an important role in a solar thermal system. Therefore, its design and the materials used in its construction play a vital role. A cross-corrugated absorber plate was tested experimentally by Lin et al. [22]. This type of absorber plate was also studied mathematically. This solar thermal panel has two plates; the top plate is shaped like a wave and the bottom plate is of the same shape. The bottom plate was placed perpendicular to the airflow direction to increase the heat transfer rate. The thermal performance was measured for these plates, and Lin et al. concluded that selective coatings and glass covers would not be useful.

Ayoub [23] worked on a solar system that included the combination of a solar panel with a tracking system. This system is located in a region with predominately cloudy sky conditions. This tracking option provided better energy capture and efficiency than the non-tracking solar panel. In another experimental procedure, the panels were fixed in three different positions. In this study, Zhong et al. [24] calculated the optimum performance and theoretically investigated the system using a mathematical model developed by Ayoub [23].

In the year 2011, Dupeyrat [25] experimented with hybrid solar thermal panels. These hybrid collectors converted part of the incident sun energy into electricity and recovered the remaining energy as heat. This hybrid system produced higher efficiencies than simple thermal panels or PV panels. There were two solar panels manufactured: PVT-A, which employed a single crystallized silicon solar cell on top of an optimized flat plate heat exchanger, and PVT-B, for which the absorber assembly had square copper channels covered with Cd-Te. This combination was then enclosed in a frame and called a solar collector. This was an experimental setup that was coupled with a domestic solar water heating system. Its aim was to determine the behavior of hybrid collectors compared to a conventional system.

2.2 Modeling Work

Hassan and Beliveau [26] worked on an integrated solar system that included a flat plate collector mounted on the roof of a house and had a storage unit composed of a phase change material (PCM). The collector and PCM storage unit were connected in a loop. This work focused on using solar energy collection and storage to provide space heating to residential units, and a house in Blacksburg, Virginia was used as the site. The weather conditions at this location were suitable for this system, which supplied 88% of the heating and hot water needs over the course of a year; however, the storage system was not suitable from an economical perspective. ABAQUS software version 6.3 was used for modeling the flat plate solar panels. The simulation results were calculated for a year on an hourly basis. The focus of the analysis was the outlet temperature of fluid from the collector and the storage tank. These calculated temperatures are provided in Figure 10, which shows temperature distributions for summer and winter conditions. The other results plotted on this graph provide information on the available solar energy that is available for a single day in January and in July. Figure 11 clearly shows the requirements for space heating and hot water for the home. It shows different parameters such as energy collected and energy consumed by the panel and energy and hot water consumption in the home. The collector could provide heated water all the time or it could supply 33% of the space heating needed in January, 58% in December, 86% in November, 88% in February, and 100% in the rest of the months. The total energy the system could supply was 88% of the home's space and water heating needs over the course of a year.

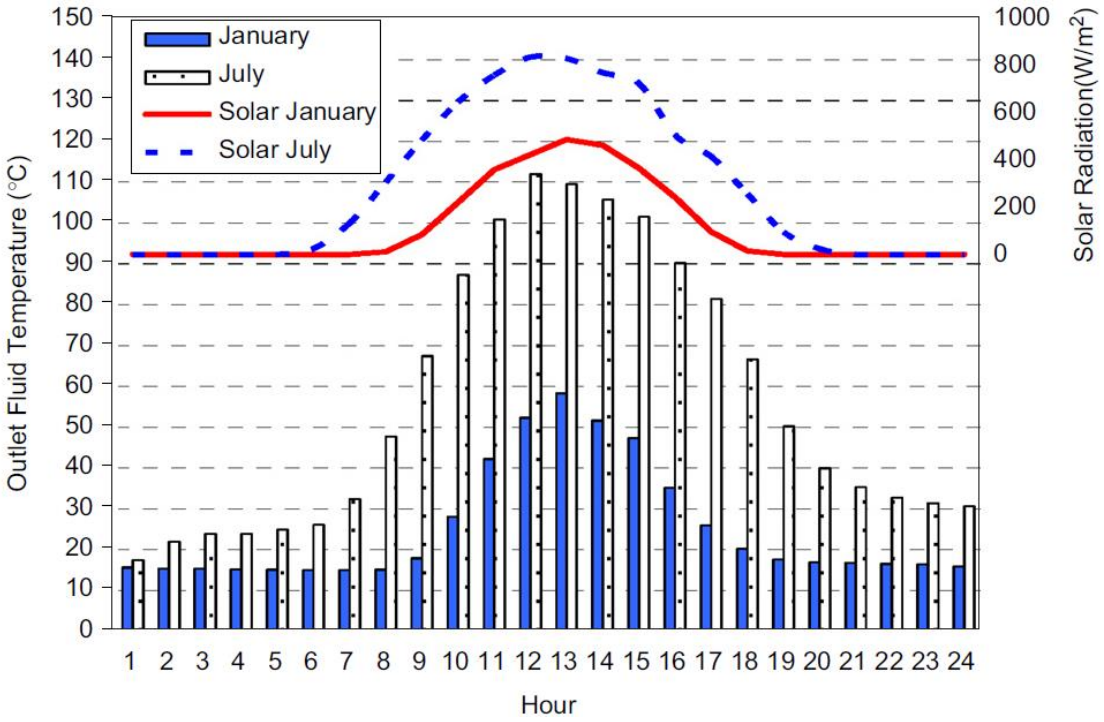

Figure 10 : Solar collector performance in summer and winter conditions [26].

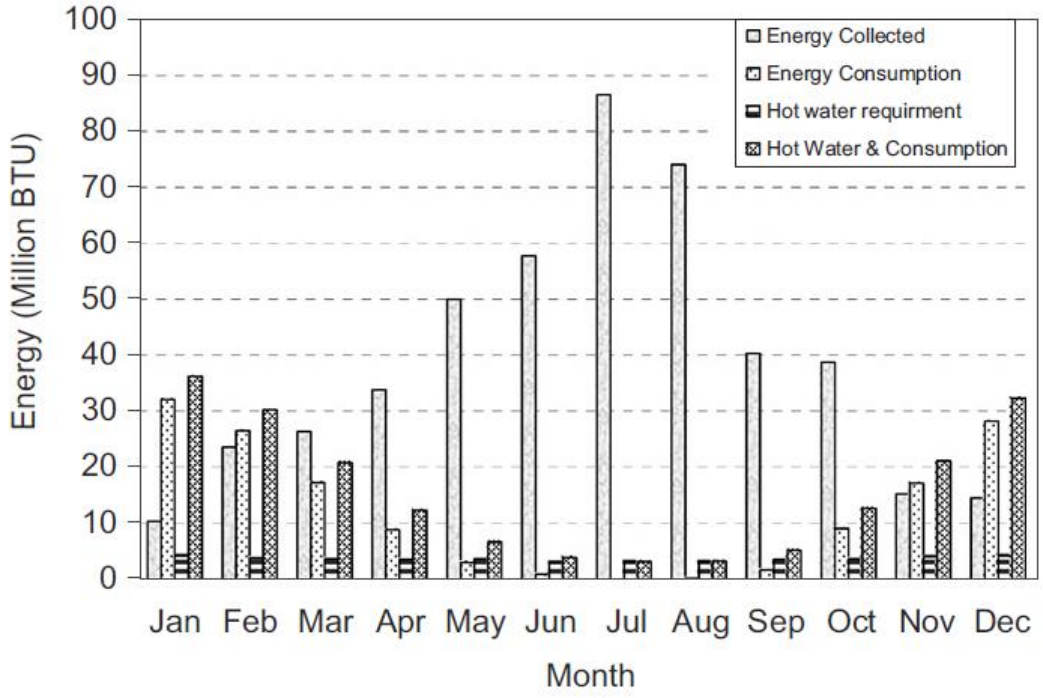

Figure 11 : Solar energy available versus space and water heating requirements [26].

Mehdaoui et al. [27] performed computations and experiments on a prototype model built in Tunis, Tunisia. These computations and experiments were conducted to understand the Tunisian air heating needs. The setup of the prototype apparatus consisted of a flat plate collector, hot water tank, and an active layer for floor heating that is integrated inside a single room. The various modes of heat transfer were considered using a simulation program written in TRNSYS. The experimental tests were carried out in local weather conditions for two months, March and April 2013. Experimental results were compared to the computational results, and the accuracy of the simulation program was determined. Using this same program, Mehdaoui et al. conducted a study to optimize design parameters for the prototype house, which included the collector area, collector mass flow rate, storage tank volume, and thickness of the active layer. The analysis showed that the solar collector with an area of 6m^2, a mass flow rate of $100kg\ \text{m}^{-1}$, and a storage tank of 450 liters achieved maximum performance. In the later part of the project, the long-term performance of the mathematical model was evaluated using data from a typical meteorological year for Tunis, Tunisia.

Oonk et al. [28] carried out research on the modeling of a solar heating and cooling system at Colorado State University. They developed a computational model for this system,

which simulated one year of operation using data from a typical meteorological year. This model was capable of simulating many design features, including a flat plate collector, main storage tank, hot water storage tank, auxiliary heater, absorption air conditioner with cooling tower, and heat exchangers between the collector and storage tank. The results showed the effect on system performance of the collector area, the collector tilt, and the number of cover plates used on the collectors.

Cadafalch [29] created a detailed one-dimensional, numerical model of a solar flat plate collector that has heat and flow characteristics. This particular model is an extension of the model developed by Duffie and Beckman [30], which was verified by an experiment performed on two different collectors at steady state conditions.

Jiandong et al. [31] used a numerical simulation for evaluating solar collector performance. Their analysis was based on the finite volume method. The absorber plate thickness, collector tube spacing, length, diameter, and insulating layer thickness were studied. The study was carried out on a built collector, a numerical simulation of the built system was done, and then the computational results were compared with the experimental results. The results showed that increasing the absorber plate thickness or reducing the collector tube spacing improves the collector efficiency. In one of the conditions studied, the solar intensity was 700 W/m^2, the wind speed was 4 m/s, and the absorber plate thickness varied from 0.1 mm to 2.1 mm. This resulted in a collector efficiency that increased from 46.6% to 64.0%. In another case, the collector tube spacing decreased from 170 mm to 50 mm and the efficiency increased from 52.8% to 66.0%. They also tried reducing collector tube length and increasing the tube diameter; this yielded a significant increase in efficiency to the levels of 55% to 64%. It was also noticed that the insulation thickness on the panel did not have a significant effect on improving efficiency. These results helped in improving the design parameters of flat plate collectors.

Zueva and Magiera [32] developed a mathematical model for a solar collector coupled with a heat exchanger. In this model, they developed an analytical solution for the heat conduction through the collector surface, which is under Cauchy boundary conditions with respect to internal heat sources, which represented the incident solar energy.

Hamed et al. [33] studied flat plate collectors for the city of Gabes, Tunisia and determined their performance. The collector supplied hot water to the required source. They conducted simulations to determine the dynamic behaviour of the collector and studied the outlet

water temperature and overall heat loss coefficient and other parameters. Some of Hamed et al.'s results are presented here. Figure 12 shows outlet water temperatures from the solar panels as a function of the number of flow tubes. The working fluid flows through the tubes, and the number of tubes used in the collector affects flow rate and heat transfer rate. The simulation results show the outlet temperature reaches a peak and then decreases. The mass flow rate of 0.008 kg/s is constant, which indicates that the number of tubes directly affects the velocity of the fluid. The overall heat loss coefficient is plotted as function of time, as seen in Figure 13, which depicts the overall heat loss coefficient as a maximum at noon and decreasing from that point. The highest value in the summer and winter seasons is 3.38 W/m^2K at a mass flow rate of 0.005 kg/s.

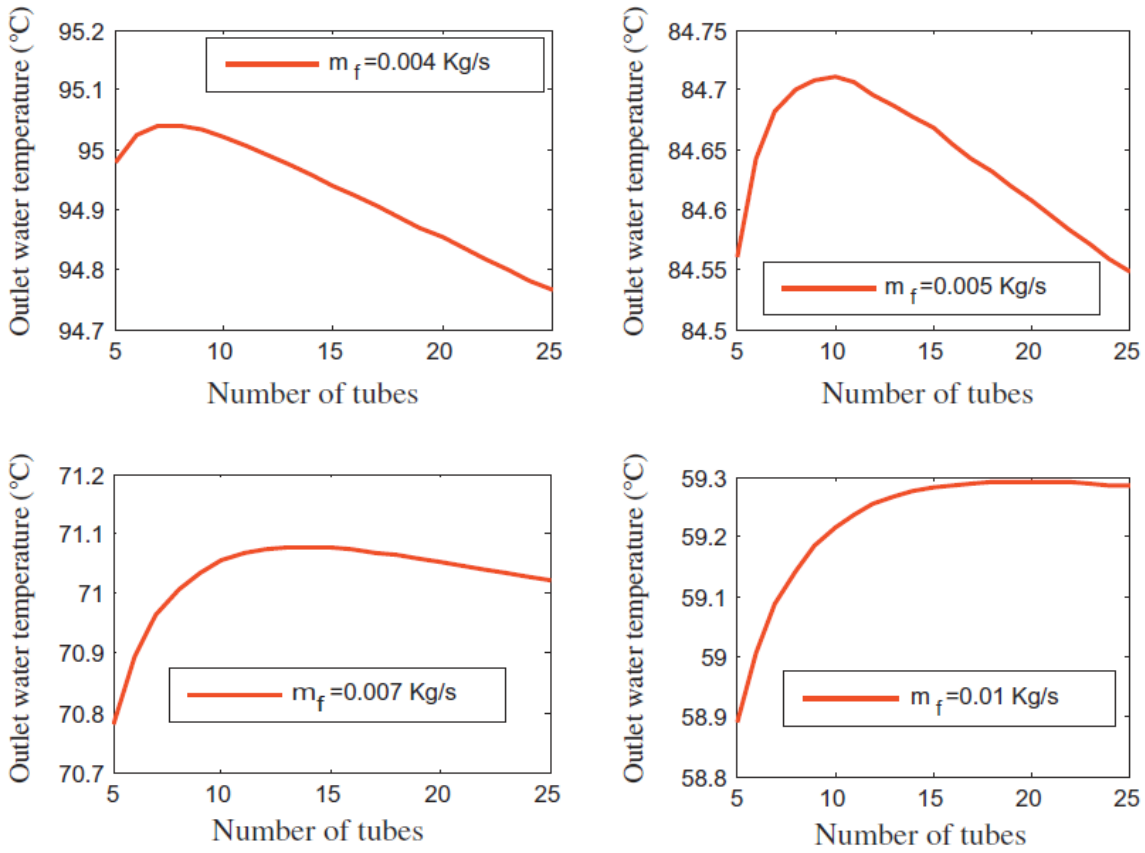

Figure 12 : Outlet water temperature verses number of tubes for various mass flow rates [33].

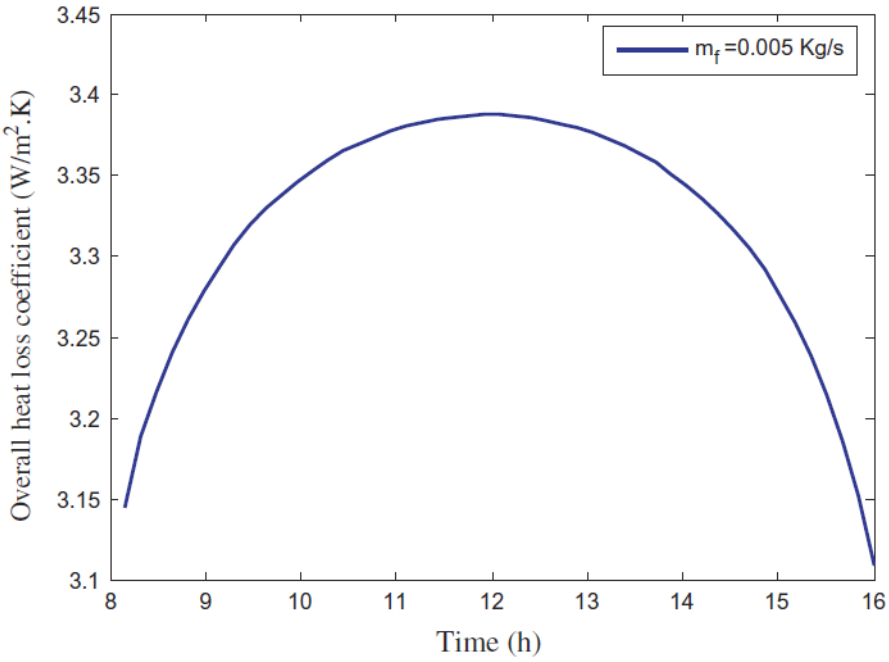

Figure 13: Collector overall heat loss coefficient verses time [33].

Xiao et al. [34] used heat pipes coupled with solar collectors to enhance heat transfer rates. A new theoretical method was developed for analyzing the thermal performance of a heat pipe flat plate solar collector coupled with a cross flow heat exchanger. The results obtained from the analysis were compared with previous results from the literature.

Gunerhan and Hepbasli [35] worked on modeling the performance of solar water heating systems for a building. They performed exergy analysis and evaluated the performance of a solar water heating system. The system consisted of a flat plate collector, a heat exchanger, and a pump for circulation. Their study included the evaluation of varying water inlet temperatures to the solar collector on the efficiencies of the system components and their effect on other thermodynamic parameters. This particular analysis was checked by using the experimental data taken in Izmir Province, Turkey. The energy efficiency values were found to be 2.02% to 3.37%, respectively. These results were obtained while carrying out eight test runs from around 1:10 pm to 3:35 pm for the overall system.

Oliva et al. [36] presented a numerical technique that accounted for the thermal behavior of a solar collector. The multidimensional and transient heat transfer properties that describe the solar collector were all taken into account. This numerical simulation studied different aspects of the systems, such as dimensions and arrangement of the components, the combination of inlet

velocity and inlet temperature of fluid, and different outdoor conditions. This analysis is for an air collector that has rectangular ducts. The heat transfer caused by the free convection between the air gap zones was calculated using empirical relationships, and the solar irradiance was taken to be constant hourly.

The dynamic modeling of flat plate collector plays a significant role in evaluating the performance of a flat plate collector. The flat plate collector was introduced to time-varying meteorological data. The dynamic modeling gave a better result as compared to steady state models. The dynamic model presented here used differential equations, which were solved using the Runge-Kutta and Taylor Series expansion method. The fluid temperature, plate temperature, and cover temperature were represented using three different equations. Later, this model was compared with experimental results obtained using a liquid-cooled flat-plate solar collector having a corrugated transparent fibreglass cover. The results obtained from the dynamic model closely matched the experimental flat plate collector results. The temperature varied $\pm 3^{o}$ C for the experimental collector compared to the predicted model. The model was coupled with a 1 kW ammonia-water absorption refrigeration system having 30% ammonia by weight and an inlet fluid temperature of 30^{o} C. This dynamic modelling produced better results compared to measured experimental data for the above system [37].

Saleh [38] modelled flat plate solar panels, which are in the transient state. The study included a one-dimensional mathematical model, which simulates the transient processes occurring in panels. The model developed in MATLAB simulates the complete system, which comprises the collector and storage tank. Experiments were carried out for several days to verify the results produced by the model. The results were satisfactory, which showed a significant change in transient fluid temperature at the outlet of the collector. These transient temperatures were measured and computed from a MATLAB program that had an acceptable convergence factor when calculating the overall efficiency and heat loss factor for the complete system.

Chapter 3. DETERMINATION OF SOLAR ENERGY IMPINGING ON PANELS

3.1 Solar_ PVHFC

Solar_PVHFC stands for Solar_PhotoVoltaic Hydrogen Fuel Cell and is a program written by Michael Gustafson while he was a Master's student at Wright State University [1]. This program is written in the computer language MATLAB. The program models available solar radiation impinging on the solar panels, PV panels, reversible fuel cells, and hydrogen storage. The program is capable of reading supplied demand files and comparing them to the energy produced by the PV, fuel cell, and hydrogen system. A few demand files come with the program and can be utilized by the user.

This subsection of Chapter 3 gives a brief overview of Solar_PVHFC and the additions made to this program for the solar thermal system analysis in this study. More details about Solar_PVHFC are available in Michael Gustafson's Master's thesis entitled "A Computational Approach to Simulating the Performance of a 24-Hour Solar Hydrogen Fuel Cell Electric Power Plant" [1].

Solar_PVHFC is a user-friendly program in that it gives freedom to the user to change as many inputs as desired through easy-to-use GUI interfaces, which are used for much of its input and output. Large data set inputs are done through input files and are used for the Typical Metrological Year, Version 3 (TMY3) experimentally measured solar data required to perform the detailed solar resource calculations performed in Solar_PVHFC.

When Solar_PVHFC is started, the user is given the choice to run a new simulation or to load a previous simulation. The discussion given below will focus on the new simulation option. If the new simulation option is selected, the next GUI that pops up is the choice of location for the simulation. The current program has Dayton, OH and Yuma, AZ as built-in locations, but users can load a TMY3 file of the location of their choosing. TMY3 data is available for many cities in the US and for locations outside the US. The next step in the program simulation is to choose the energy demand profile from a drop-down menu or create a new demand file. This is simply done by writing over one the of Excel spreadsheet demand files already available with the program. Next, there are four options for determining the solar resource. In this work, the isotropic diffuse model was used and is described in the next subsection of this chapter. The next step is optional and irrelevant to this study—selecting one of three GUIs (PV panel design, the reversible fuel cell design and the hydrogen storage tank design). Next, a GUI that allows the user to enter the time frame of the simulation is available. All calculations are done on an hourly basis, but the entered time frame needs to be specified in days. The user can control the starting and ending time, which provides the user with control of the time of year for which a simulation is performed. After this GUI, calculations are done and the final GUI at the end of the simulation allows the user to save the results.

There were two large coding additions made to Solar_PVHFC to perform the solar thermal analysis discussed in this thesis: adding a program module that analyzes a flat plate, liquid, solar thermal panel and adding a module that analyzes a plate-fin compact heat exchanger. The thermal solar panel and the heat exchanger, along with a fluid storage tank with a large enough capacity to handle one hour's worth of liquid flowing through the solar panel, comprise the solar system studied in this thesis. A system control was also developed for this system. The system control, which is simple to use despite being time-consuming to develop, is discussed in Section 4.3 of this thesis.

3.2 Solar Flux on Tilted Surface

The quantity of solar insolation impinging on a solar panel at a given location and time is a strong function of the orientation of the surface. This is true for a solar PV panel or a solar thermal panel. The calculation of the impinging radiation for either of these types of solar panels is exactly the same. This is the reason that this portion of the computer program Solar_PVHFC can be used for this thesis work without changes. However, given that the solar energy impingement on a solar thermal panel is so critical to its operation, the analysis used to determine the solar radiation impinging on a flat surface is explained in this thesis.

The solar radiation impinging on a surface has three primary components: beam, diffuse, and ground-reflected radiation. The sky dome is where diffuse radiation originates, and it is a function of atmospheric conditions. For the most precise modeling of the diffuse radiation, it is divided into three components: isotropic diffuse, circumsolar diffuse, and horizon brightening diffuse. In this work, all types of diffuse solar radiation are lumped into one isotropic diffuse term. This is commonly done and is fairly accurate, since the circumsolar and horizon brightening components are usually small.

The model used in this study for determining the solar radiant energy impinging on a flat surface is the three component isotropic sky model, as put forth by Liu and Jordan [39]. As part of the isotropic sky model, the total solar energy impinging on a tilted surface is the sum of the beam, diffuse, and ground-reflected components of radiation. The equation for the total radiation on tilted surface is

$$I_T = I_b R_b + I_d \left(\frac{1+cos\beta}{2}\right) + \mathrm{I}\, \rho_g \left(\frac{1-cos\beta}{2}\right). \tag{3.1}$$

For the meaning of the symbols used in this equation, the reader is directed to the Nomenclature section. No description of any of the symbols used in the equations presented in this thesis is given in the text portion of the document unless more than what is provided in the Nomenclature is deemed to be necessary for adequate understanding of the quantity. It is assumed that the reader will refer to the Nomenclature to find the meaning of any symbols used.

3.2.1 Beam, Diffuse, and Ground-Reflected Radiation

Firstly, we consider the hourly beam radiation on a horizontal surface, which is radiation received directly from the sun without getting scattered by the atmosphere. The equation for this is

$$I_b = I - I_d. \tag{3.2}$$

In this equation, I is the total solar energy impinging on a horizontal, unit area surface in one hour. This quantity is measured experimentally and made available to researchers through published TMY3 data sets. The other important radiation component in Equation (3.2) is the diffuse radiation, which is received by a unit area, horizontal surface after getting scattered by the atmosphere. An hourly clearness index is required to calculate I_d. The hourly clearness index leads to a relationship between the diffuse radiation I_d and the horizontal radiation I. The hourly clearness index is defined as

$$k_T = \frac{I}{I_0} \tag{3.3}$$

where I_0 is the hourly insolation on a horizontal surface above the atmosphere and is given as

$$I_0 = \left(\frac{12\,3600}{\pi}\right)\left(1 + 0.033\cos\frac{360n}{365}\right)\left\{\cos\emptyset\cos\delta(\sin\omega_2 - \sin\omega_1) + \frac{\pi(\omega_2-\omega_1)}{180}\sin\emptyset\sin\delta\right\}. \tag{3.4}$$

Equations for many of the quantities in I_0 are angles that describe the solar geometry and are given later in this chapter. Using this clearness index in three empirically determined correlations that give the ratio of diffuse radiation to the total radiation on a horizontal surface allows one to determine the diffuse radiation from the experimentally determined total radiation on a horizontal surface. These empirically determined correlations are

$$\frac{I_d}{I} = \begin{cases} 1.0 - 0.09k_T \quad for\ k_T \le 0.22 \\ 0.9511 - 0.1604 * k_T + 4.388 * {k_T}^2 - 16.638 * {k_T}^3 + 12.336 * {k_T}^4 \quad for\ 0.22 < k_T \le 0.8 \\ 0.165\ for\ k_T > 0.8 \end{cases}. \tag{3.5}$$

Another parameter in Equation (3.1) that needs to be determined is the geometric factorR_b, which is the average ratio of the tilted surface beam radiation to horizontal surface beam radiation. This is simply a geometric quantity that is the ratio of the cosines of two important angles in solar energy impingement: the angle of incidence of beam radiation on the tilted surface and the angle of incidence of beam radiation on a horizontal surface. The equation for R_b at a given instant of time is

$$R_b = \frac{cos\theta}{cos\theta_z}. \tag{3.6}$$

This version of R_b causes problems when calculating the beam hourly radiation during sunrise and sunset. Using Equation (3.6) can cause very large values of R_b at sunrise and sunset, which will cause poor results for the hour being analyzed. To avoid this issue, it is suggested to use the average value over an hour,

$$R_b = \frac{a}{b} \tag{3.7}$$

where

$$\begin{aligned} a = {} & (\sin\delta \sin\emptyset \cos\beta - \sin\delta \cos\emptyset \sin\beta \cos\gamma)\frac{\pi}{180}(\omega_2 - \omega_1) \\ & + (\cos\delta \cos\emptyset \cos\beta + \cos\delta \sin\emptyset \sin\beta \cos\gamma)(\sin\omega_2 \\ & - \sin\omega_1) - (\cos\delta \sin\beta \sin\gamma)(\cos\omega_2 - \cos\omega_1) \end{aligned} \tag{3.8}$$

and

$$b = (\cos\emptyset \cos\delta)(\sin\omega_2 - \sin\omega_1) + (\sin\emptyset \sin\delta)\frac{\pi}{180}(\omega_2 - \omega_1). \tag{3.9}$$

As with the Equation (3.4), many of the quantities are solar angles, which are described in the next subsection of this chapter.

The remaining quantities in Equation (3.1) are the ground reflectivity ρ_g and the angular tilt of the solar panel from a horizontal plane. Both of these quantities are inputs to the analysis.

3.2.2 Required Angles

In Equations (3.4), (3.8), and (3.9), many angular quantities were used. Some of these angles are easy to calculate, whereas others are rather complex. In this section, equations for all these angles are presented.

Firstly, consider the hour angle ω. Hour angles vary throughout the day and are a way to track the sun's east to west motion across the sky. Technically, the hour angle is defined as the longitudinal angular displacement of the sun east or west of the local meridian where the solar panel is located. This means that the hour angle changes at the same rate at which the earth rotates, 15 degrees per hour and can be determined with the equation

$$\omega = 15(\text{solar time in hours} - 12) \quad . \tag{3.10}$$

This equation gives the hour angle in degrees relative to the location of the solar panel. At solar noon, the sun is directly above the meridian where the panel is located. In the solar morning, the sun is to the east of the solar panel, and these sun positions are defined with negative hour angles. In the solar afternoon, the sun is to the west of the solar panel, and these hour angles are negative. The problem with using this equation is that solar time needs to be determined and solar time is not the same as the time read off a clock.

Solar time is time based on the position of sun. When the sun is directly above the meridian at which solar time is desired, this is called solar noon. This is the "12" shown in Equation (3.10). Solar time has to be used in all sun angle relationships as opposed to local clock time. It is essential to convert the standard time to solar time by using the two correlations:

$$\text{Solar time} = \text{Standard time} + \frac{4 * (L_{st} - L_{loc}) + E}{60} \tag{3.11}$$

and

$$\mathrm{E} = 229.2(0.000075 + 0.001868\cos B - 0.032077\sin B - 0.014615\cos 2B - 0.04089\sin 2B) \tag{3.12}$$

where

$$\mathrm{B} = (n-1)\frac{360}{365} \tag{3.13}$$

and

$$\omega_2 = \omega_1 + 15\,. \tag{3.14}$$

Standard time used in Equation (3.11) is clock time without daylight savings time applied.

The declination angle is another angle that describes the position of the sun in the sky, and it pertains to how high the sun rises in the sky on any given day. Technically, the declination angle gives the tilt of the earth's axis of rotation relative to the plane of its orbit around the sun. Although the declination angle actually is a measure of the tilt of the earth, it must be recognized

that the tilt of the earth is what determines the maximum altitude angle of the sun in the sky for a given day. The declination angle is calculated as a function of the day using

$$\delta = 23.45 \sin\left(360 \frac{284+n}{365}\right). \tag{3.15}$$

A location angle found in (3.4), (3.8), and (3.9) is the latitude where the solar panel is located. This is the angular location of the solar panel with respect to the equator. Locations north of the equator are expressed as positive, and locations south of the equator are expressed as negative angles. The latitude is important because of the earth's curvature, which changes the way the sun appears in the sky at a given time. Longitude is another location angle that is important and is used in Equation (3.11). It is an angular distance of the solar panel west or east of the prime meridian, which is located in Greenwich, London, England.

The remaining two angles in Equations (3.4), (3.8), and (3.9) describe the orientation of the solar panel. The first is the altitude angle of the surface, β, otherwise known as the slope angle of the panel, which is the angle between the surface of the panel and a horizontal plane. The other panel orientation angle is the azimuthal angle. The azimuthal angle is denoted by γ. This is an angular measure of the orientation of the panel from due south. This angle is found by projecting the panel surface normal into a horizontal plane and then measuring the angular distance of this vector from due south.

Now all the required angles in Equations (3.4), (3.8), (3.9), and (3.11) have been discussed and the necessary equations presented. Therefore, all information required to calculate the total solar energy impinging on a tilted panel per unit area of the panel for one hour I_T has been given. This quantity is used in the next chapter to evaluate the solar energy absorbed by a solar thermal collector.

Chapter 4. SOLAR THERMAL SYSTEM ANALYSIS

As stated in the objectives of this thesis, a model of a flat plate collector and heat exchanger has been added to the computer program Solar_ PVHFC. In this chapter, the details and modeling of a flat plate collector, heat exchanger, and the system as a whole are discussed.

4.1 Solar Panel

Solar thermal collectors are differentiated by a number of factors. They can be differentiated by whether they concentrate the sun or not, by the shape of the panel, by the type of fluid running through the panel, or by the means through which heat loss is reduced. In this work, a non-concentrating, flat plate, liquid, solar thermal collector that uses glass covers on the front and insulation on the back to reduce heat losses is modeled. This is one of the simplest and most basic solar thermal collectors. More complex solar thermal collectors are available, but are beyond the scope of this project. The goal here is to use a typical, inexpensive flat plate collector to study the feasibility of solar space heating. Some of the more complex thermal collectors were mentioned in the literature survey presented in Chapter 3.

A typical flat plate, liquid, solar thermal collector is shown in Figure 14. This is the thermal collector modeled in this work. Figure 15 shows this same solar panel from a cross-sectional perspective. The cross sectional view of this panel shows two cover plates; however, one or three cover plates can be used.

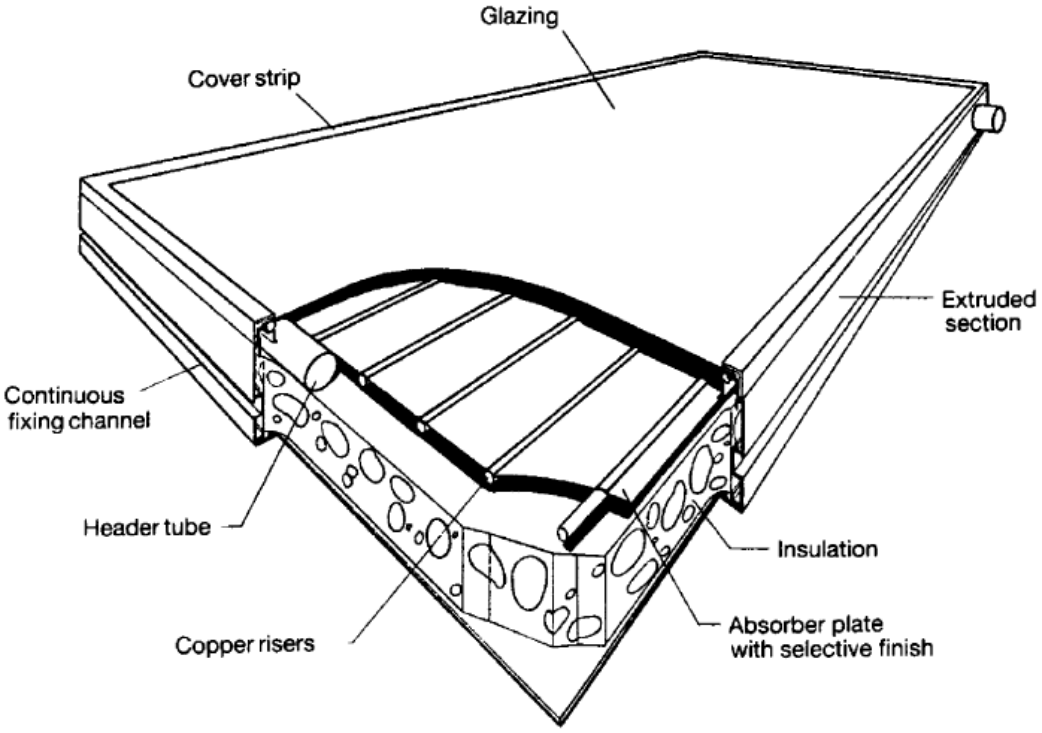

Figure 14 : Parts of a typical flat plate, solar thermal collector [40].

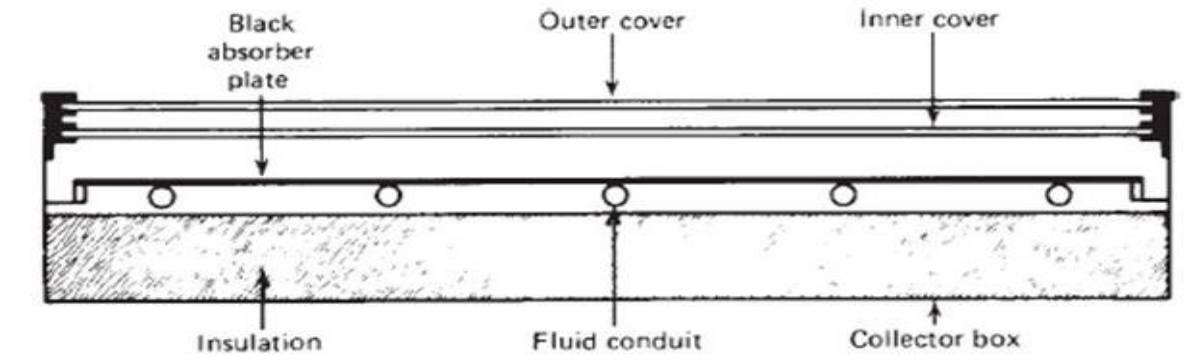

Figure 15: Cross-section of a flat plate collector [41].

The working principle of a flat plate collector is simple: Solar radiation travels through the glass cover plates and impinges on the absorber plate of the panel. The absorber plate is usually made of a high thermal conductive metal that has been blackened in such a manner that it has a high absorptivity for wavelengths typical of solar radiation. This same absorber plate has tubes embedded in it such that water or some other liquid (e.g., ethylene glycol) can pass through the plate. The goal of this plate is to transfer the absorbed solar radiant energy to the liquid passing through the tubes. To do this, the absorber plate must be a good conductor and the spacing between the tubes carrying the liquid must not be too large. If it is difficult for the absorbed solar energy to travel through the absorber plate to the liquid flowing through the tubes, larger amounts of energy will be lost to the environment. Because the absorber plate heats up to a higher temperature than its surroundings, there will be some absorbed solar energy convected back to the environment. To reduce convective losses, glass cover plates are usually used over the top of the absorber plate and insulation is used on the back and sides of the absorber plate. Glass is used to stop convection on the top side because it allows the solar radiation to pass through to the absorber plate. All of the components that make up the solar panel are bound together by a frame that gives the panel structural strength.

4.1.1 Overall Thermal Energy Delivered by Solar Panel

The important factor to be considered in flat plate panel performance is the amount of solar energy the collector transfers to the liquid flowing through the tubes. The symbol used for this quantity on a rate basis is $\dot{Q}_u$. An equation giving this quantity is

$$\dot{Q}_u = A_c \left[\frac{S}{\Delta t} - U_L\left(T_{pm} - T_a\right)\right]. \tag{4.1}$$

This equation states that the useful thermal power output of a collector having a frontal area of A_c is the difference between the rate of absorbed solar radiation and the rate of thermal losses from the panel. The collector loses thermal energy to the surroundings by means of conduction, convection, and radiation, which is all accounted for in the overall heat loss coefficient, $U_{L,}$ and the difference of mean plate and ambient temperatures. The above equation is modified later to be a function of the fluid inlet temperature, which is usually a known quantity.

4.1.1.1 Solar Energy Absorbed by Panel

As the solar radiation impinges on the collector surface, most of it is transmitted through the glass cover plates and absorbed by the absorber plate. The amount of radiation that is absorbed depends on the transmissivity of the glazing and the absorptivity of absorber plate. As mentioned previously, the incident radiation on a tilted solar panel is composed of three components that are incident on the collector at different angles.

The absorptance of radiant energy by the solar panel is a product of the radiant energy incident on the panel and the transmittance absorptance product of the glass covers and the absorber plate as

$$S = I_T(\tau\alpha). \tag{4.2}$$

The transmittance absorptance product is placed in parentheses for a special reason. The parentheses mean that the glass cover plate transmittance times the absorber plate absorptance product must be calculated as a unit so that multiple reflections are included. This multiple reflection process is shown in Figure 16. Part of the radiation incident on the absorber plate gets absorbed and part gets reflected back to the glass cover plates; $(1-\alpha)\tau$ is reflected back to the cover plates. Part of $(1-\alpha)\tau$ incident on the underside of the glass cover plates gets transmitted to the surroundings while part gets reflected back to the absorber plate; $(1-\alpha)\tau\rho_D$ is reflected back to the absorber plate where ρ_d is the diffuse reflectivity of the glass cover plates. As shown in Figure 16, there are multiple reflections of diffuse radiation that continue until the incident energy is absorbed. Also, it should be noted that value of ρ_D is a function of the number of cover plates. Therefore$(\tau\alpha)$, or the fraction of radiation incident on absorber plate that is absorbed, after taking into account all the reflections is

$$(\tau\alpha) = \frac{\tau\alpha}{1-(1-\alpha)\rho_D}. \tag{4.3}$$

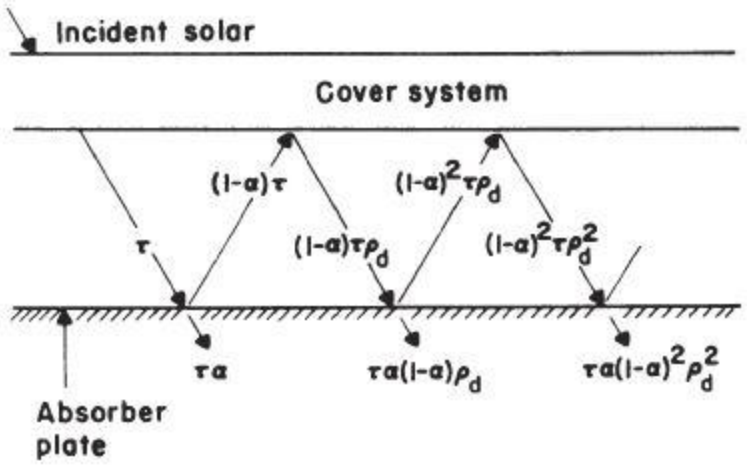

Figure 16: Absorption of solar radiation through cover plates[41] .

Because the beam radiation, diffuse radiation, and ground-reflected radiation all are incident on the solar panel at different angles, Equation (4.3) must be solved separately for each of these components. This means a beam $(\tau\alpha)_b$, a diffuse $(\tau\alpha)_d$ and a ground $(\tau\alpha)_g$ need to be calculated.

The absorptance of the absorber plate as a function of the incident angle of the radiation is determined using an empirical curve fit of

$$\alpha = \epsilon_{p,s}(1 - 0.0015879\theta + 0.00027314\theta^2 - 0.000023026\theta^3 + 0.00000090244\,\theta^4 - 0.000000018\,\theta^5 + 0.0000000001773 4\theta^6 - 0.0000000000069937\,\theta^7) \quad (4.4)$$

where θ is the incident angle of the particular radiation component. The incident angle for beam radiation is

$$cos\theta = \sin\delta sin\emptyset\cos\beta - sin\delta cos\delta sin\beta cos\gamma + cos\delta cos\emptyset\, cos\beta cos\omega + cos\delta sin\phi sin\beta cos\gamma cos\omega + cos\delta sin\beta sin\gamma sin\omega \quad (4.5)$$

where explanations and equations for all the angles on the right-hand side of this equation are given in Chapter 3. The incidence angle for the diffuse radiation is given by

$$\theta_d = 59.7 - 0.1388\beta + 0.001497\beta^2 \quad (4.6)$$

and that for the ground reflected radiation is

$$\theta_g = 90 - 0.5788\beta + 0.002693\beta^2. \quad (4.7)$$

Now, the individual transmittances are obtained using a tabulated representation of the transmittances shown in Figure 17. These transmittance values have been checked and verified

by experiments done by Hottel and Woertz [42]. This figure shows transmittances as a function of the angle of incidence of the radiation, the type of glass, and the number of cover plates used on the collector. The type of glass is identified with the extinction coefficient–glass thickness product, KL. The incident angles used to enter Figure 17 are calculated from the same equations used to determine the incident angles for the absorber plate absorptance given in Equations (4.5) – (4.7). To obtain values of transmittances between the digitized values, straight line interpolation routines are used.

At this point all the required absorptance and transmittances required can be determined and substituted into Equation (4.3) to obtain the transmittance-absorptance product($\tau\alpha$). This quantity can then be substituted into Equation (4.2) to get the absorbed solar radiation. The absorbed solar radiation value can then be substituted into Equation (4.1) as a start to determining I_T. However, before I_T can be determined, the heat loss from the panel must be determined. The procedure for doing this is shown in the next subsection.

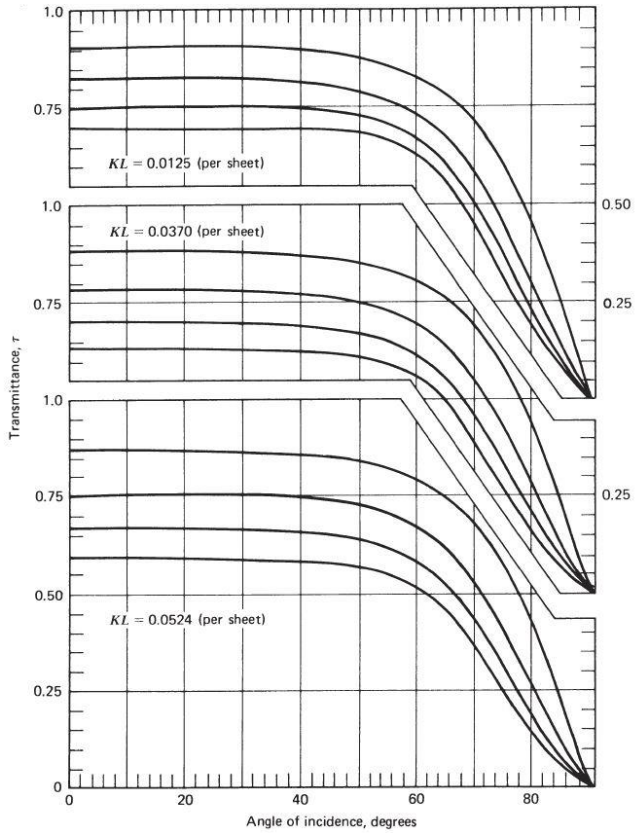

Figure 17: Transmittance values for different types of glass, for one, two, three, and four cover plates as a function of the incident angle of the incoming radiation[41].

4.1.1.2 Heat Loss from Panel

The absorber plate of a solar collector gathers solar energy; most of this energy will be utilized as useful energy. However, there will be losses by different modes of heat transfer, which are unavoidable. The heat loss from a flat plate collector can be given as

$$Q_{loss} = \frac{T_{pm} - T_a}{R_c} = U_L A_c (T_{pm} - T_a). \tag{4.8}$$

In Equation (4.8), the overall heat loss coefficient, U_L, is one of the important terms to be calculated, and it is significant in determining the amount of thermal energy finally delivered to the home by the solar panel. To do this, we first have to look at the thermal network for a flat plate collector. This will be done for a collector having two cover plates. In the future, more or fewer plates can be used by making slight adjustments to the analysis given below. Figure 18 shows a typical thermal network for a solar panel with two cover plates.

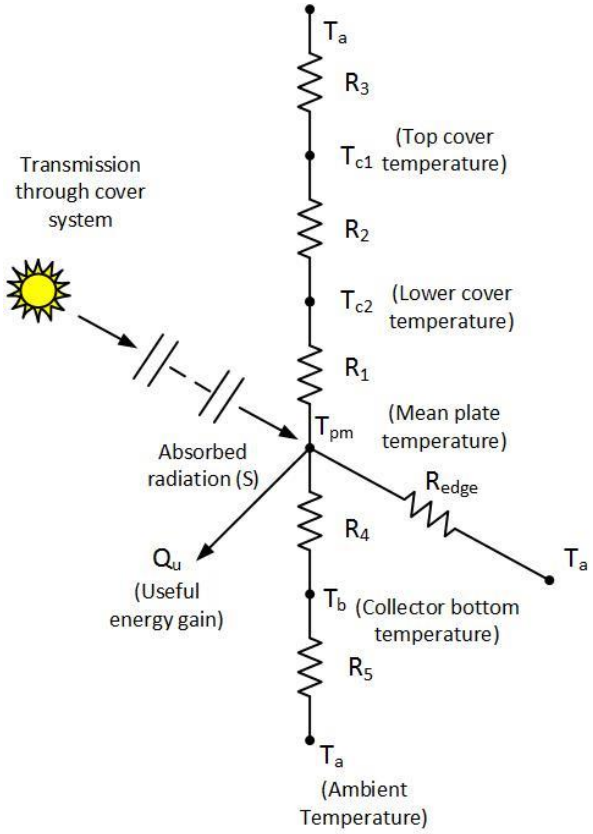

Figure 18: Thermal resistive network for two cover flat plate collector.

To combine all the resistances shown in Figure 18, they must be attacked in three parts: the top, the bottom, and the sides. First, the resistances for the top of the collector are determined. These resistances account for losses out the transparent covers of the collector. Because this is a steady state analysis, the heat transfer from the absorber plate to the lower cover, from the lower cover to the top cover, and from the top cover to the atmosphere are the same. This means these resistances are in series. In this analysis, the conductive resistance of the actual glass is assumed to be small.

The heat transfer in the upward direction, starting from the absorber plate at a temperature T_{pm} to the lower cover at T_{c2} occurs due to convection and radiation. This is heat transfer between two parallel surfaces that are separated by a small distance, and the heat loss is given by

$$Q_{absorber\ plate-lower\ cover} = A_c h_{p-c2}\left(T_{pm} - T_{c2}\right) + \frac{A_c\sigma\left({T_{pm}}^4 + {T_{c2}}^4\right)}{\frac{1}{\varepsilon_p}+\frac{1}{\epsilon_{g2}}-1}. \tag{4.9}$$

The radiation heat transfer coefficient between the absorber plate and the lower glass cover is given by

$$h_{r,p-c2} = \frac{\sigma\left(T_{pm}+T_{c2}\right)\left({T_{pm}}^2+{T_{c2}}^2\right)}{\frac{1}{\varepsilon_p}+\frac{1}{\epsilon_{g2}}-1}. \tag{4.10}$$

Therefore Equation (4.9) can be written as

$$Q_{absorber\ plate-lower\ cover} = A_c\left(h_{p-c2} + h_{r,p-c2}\right)\left(T_{pm} - T_{c2}\right) = \frac{\left(T_{pm} - T_{c2}\right)}{R_1} \tag{4.11}$$

where

$$R_1 = \frac{1}{A_c*\left(h_{p-c2}+h_{r,p-c2}\right)}. \tag{4.12}$$

In the same way the heat transfer from T_{c2} to the top cover plate T_{c1} is given by

$$Q_{lower\ cover-top\ cover} = A_c\left(h_{c2-c1} + h_{r,c2-c1}\right)(T_{c2} - T_{c1}) = \frac{(T_{c2} - T_{c1})}{R_2} \tag{4.13}$$

where

$$h_{r,c2-c1} = \frac{\sigma(T_{c2}+T_{c1})\left({T_{c2}}^2+{T_{c1}}^2\right)}{\frac{1}{\epsilon_{c2}}+\frac{1}{\epsilon_{c1}}-1} \tag{4.14}$$

and

$$R_2 = \frac{1}{A_c\left(h_{c2-c1} + h_{r,c2-c1}\right)} \tag{4.15}$$

The next consideration for heat loss is from the top cover plate to the ambient air having a temperature of T_a through convective heat transfer and to the sky at a temperature of T_{sky} through radiative heat transfer. Equation (4.16) shows the combined convection-radiation heat transfer, which depends on the ambient temperature and the sky temperature,

$$Q_{top\ cover-ambient} = A_c\left(h_{c1-a} + h_{r,c1-a}\right)(T_{c1} - T_a) = \frac{(T_{c1} - T_a)}{R_3} \tag{4.16}$$

where

$$h_{r,c1-a} = \epsilon_{c1}\sigma\left(T_{c1} + T_{sky}\right)\left({T_{c1}}^2 + {T_{sky}}^2\right)\frac{\left(T_{c1} - T_{sky}\right)}{T_{c1} - T_a}. \tag{4.17}$$

Therefore,

$$R_3 = \frac{1}{A_c\left(h_{c1-a} + h_{r,c1-a}\right)}. \tag{4.18}$$

The sky temperature buried in the radiative heat transfer coefficient is given as

$$T_s = T_a * \left(0.711 + 0.0056T_{dp} + 0.000073{T_{dp}}^2 + 0.013\cos(15t)\right)^{1/4}. \tag{4.19}$$

The sky temperature is different than the ambient temperature because convection interacts with the air right around the panel, whereas radiation interacts with the air up to very high altitudes. The sky temperature is an altitude-weighted temperature with which the radiation interacts.

As in Figure 18, we can see that the thermal resistances are in series and thus the total resistance for the top of the collector is given by

$$R_{top} = R_1 + R_2 + R_3 = \frac{1}{A_c U_t\left(T_{pm} - T_a\right)}. \tag{4.20}$$

Thus,

$$Q_{top\ loss} = \frac{T_{pm} - T_a}{R_{top}} = U_{top}A_c\left(T_{pm} - T_a\right). \tag{4.21}$$

Now, we will consider the loss of energy from the bottom of the collector. The heat transfer occurs through conduction in the bottom insulation and convection and radiation transfer to the surroundings. The bottom of the collector is at a low temperature and the resistance to heat flow due to radiation and convection to the surroundings can be neglected as it is minor relative to the conductive resistance. Thus, the heat loss form the bottom of the collector is

$$Q_{bottom,loss} = \frac{T_{pm} - T_a}{R_{bottom}} = U_b A_c \left(T_{pm} - T_a\right) \tag{4.22}$$

where

$$R_{bottom} = \frac{\Delta x}{k_{ins} A_c}. \tag{4.23}$$

The other heat loss that should be considered is the edge losses, which are given by

$$Q_{edge\ loss} = \frac{T_{pm} - T_a}{R_{edge}} = U_e A_c \left(T_{pm} - T_a\right) \tag{4.24}$$

where

$$R_{edge} = \frac{\mathrm{L}_e}{k_{ins} A_{edge}}. \tag{4.25}$$

It should be noted that the overall heat transfer coefficient for the edge is written based on the frontal area of the collector and thus the reason for A_c in Equation (4.23). This can be done as

$$U_e = \frac{U_e A_e}{A_c}\,. \tag{4.26}$$

Since the top, bottom, and side resistances are in parallel they combine as

$$R_L = \frac{1}{R_{top}} + \frac{1}{R_{bottom}} + \frac{1}{R_{edge}}. \tag{4.27}$$

The overall heat transfer coefficients combine as

$$U_L = U_t + U_b + U_e\,. \tag{4.28}$$

At this point in the analysis, a number of convective heat transfer coefficients are required. These convective heat transfer coefficients are in Equations (4.12), (4.15), and (4.18). Firstly, the heat transfer coefficients in a cavity are determined (see Equations 4.12 and 4.15). Figure 19 is a simple diagram that shows a cavity for an absorber plate which is tilted at an angle β. The Nusselt number correlation for two plates that form a cavity and are inclined at angle of β between 0^o to 75^o [43] is given by

$$\overline{N_{u_L}} = 1 + 1.44\left[1 - \frac{1708(\sin 1.8\beta)^{1.6}}{R_{a_L}\cos\beta}\right]\left[1 - \frac{1708}{R_{a_L}\cos\beta}\right]^{+} + \left[\left(\frac{R_{a_L}\cos\beta}{5830}\right)^{1/3} - 1\right]^{+} \tag{4.29}$$

for

H/L≥ 12

$$H/L < w/L$$

and

$$0 \leq \beta \leq \beta * critical\ tilt\ angle = 75^o.$$

If the tilt of the panel is greater than 75^o, Equation (4.29) should be evaluated at 75^o. There is little chance of finding solar collectors sloped between 75^o and 90^o. The + sign in Equation (4.29) means that if this term is less than zero, it should be set equal to zero. The above equation has a nondimensional number called the Rayleigh number, which needs to be calculated. This is done by

$$R_{a_{L,c}} = \frac{g\beta_T(T_1 - T_2)L^3}{\nu\alpha} \tag{4.30}$$

where β_T is the volumetric thermal expansion coefficient. For air, the volumetric thermal expansion coefficient is

$$\beta = \frac{1}{T}. \tag{4.31}$$

The fluid properties needed in these equations are all taken at an average temperature of

$$\bar{T} = \frac{T_1 + T_2}{2}. \tag{4.32}$$

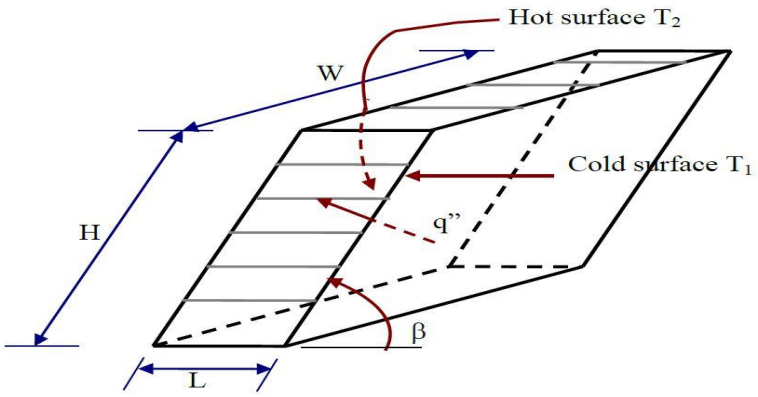

Figure 19: Cavity between absorber plate and lower glass plate [43].

The heat transfer coefficient in Equation (4.18) depends on the ambient conditions, the orientation of the panel, and where the panel is mounted. This is external flow that is between the outside air in the environment and the top of the glass plate collector. One possible correlation for the heat transfer coefficient between the top cover plate and the ambient air is for the case

where the collector plate is located on the ground at an angle to the wind. The Nusselt number correlation for this situation is

$$\overline{N_{u_L}} = 0.86{R_e}^{1/2}\ {P_r}^{1/3} \tag{4.33}$$

where

$$L = 4A_p/P \tag{4.34}$$

and the Reynolds number should be between the values of

$$2 \times 10^4 < R_e < 9 \times 10^4. \tag{4.35}$$

Another case that may occur is when the collector is mounted on the roof of a house. This situation is often encountered as many solar collectors are mounted on roofs for domestic purposes. The equation for this case is

$$\overline{N_{u_L}} = 0.42{R_e}^{0.6}. \tag{4.36}$$

The assumption made in this case is that the house is considered to be a sphere with the same volume as the house. The length scale used in this equation is

$$L_c = \sqrt[3]{\forall}\,. \tag{4.37}$$

If the collector is mounted flush to the roof of the house, then

$$h_w = max\left[5, \frac{8.6V^{0.6}}{{L_c}^{0.4}}\right] \tag{4.38}$$

may be a better correlation to use. In this equation L_c is again determined by Equation (4.37).

Other quantities that have to be known to determine the heat loss from a solar thermal collector are the temperatures between the plates. These temperatures are needed to determine fluid properties and to determine the radiative heat transfer coefficients. For all interfaces, these temperatures can be determined with

$$T_j = T_i - \frac{q_{loss\ top}}{h_{c,i-j}+h_{r,i-j}}. \tag{4.39}$$

This makes the calculation an iterative procedure that depends on temperatures to the fourth power. This can cause convergence problems in a computer simulation. To lessen the problems encountered in the iteration process, the equation

$$U_t = \left(\frac{N}{\frac{C}{T_{pm}}\left[\frac{T_{pm} - T_a}{N + f}\right]} + \frac{1}{h_w} \right)^{-1} + \frac{\sigma\left(T_{pm} + T_a\right)\left({T_{pm}}^2 + {T_a}^2\right)}{\frac{1}{\epsilon_p + 0.00591 N h_w} + \frac{2N + f - 1 + 0.133\epsilon_p}{\epsilon_g} - N} \tag{4.40}$$

where

$$f = \left(1 + 0.089 h_w - 0.1166 h_w \epsilon_p\right)(1 + 0.07866N) \tag{4.41}$$

$$C = 520(1 - 0.000051\beta^2)\ for\ 0^o \leq \beta \leq 70^o\ and\ for\ 70^o < \beta \leq 90^o\ use\ \beta = 70^o \tag{4.42}$$

$$e = 0.43\left(1 - \frac{100}{T_{pm}}\right) \tag{4.43}$$

can be used for the top overall heat transfer coefficient. This is what is done in this work. The calculation is still iterative in nature, but it is a more stable iterative process. This equation can be used to calculate the top losses for any tilt angle β or any number of cover plates.

4.1.2 Heat Recovery Factor

There are still two issues that need to be addressed in Equation (4.1). The first issue is varying temperatures along the length and width of the solar panel. These two directions are also referred to as the flow direction and the spanwise direction. The second issue is that T_{pm} is not a known quantity. As mentioned before, T_{pm} needs to be replaced with the fluid inlet temperature. This will be done in this sub-subsection. While doing this, a few quantities that are important for flat plate collector performance are defined.

As soon as the absorbing plate absorbs solar energy, it causes temperature gradients to develop across the width of the panel. There has to be temperature gradients between the tubes to drive the absorbed energy between the tubes to the fluid. Normally, the fluid tubes are uniformly spaced across the width of the absorber plate. There has to be a temperature increase in the fluid along the plate if it is to absorb any solar energy without undergoing a phase transformation. No solar thermal collector allows the working fluid in a collector to change out of the liquid phase. This means that there will be temperature gradients in the flow direction and in the spanwise

direction. In the flow direction, the temperature increases continually, whereas in the spanwise direction, it is periodic change. Both of these temperatures are accounted for in the model used in this work. This is done via the heat recovery factor, which is discussed in this sub-subsection.

Figure 20a shows a section of the absorber plate for a flat plate collector between two fluid flow tubes. Note that the x-direction is in a direction normal to the flow direction and the y-direction is in the same direction as the flow. Figures 20b, 20c and 20d show temperature profiles in different directions in the absorber plate. Considering any region in the collector, the general temperature can be found by knowing the temperature of the fluid at that location. Figure 20d shows how the fluid temperature varies in the flow direction. In Figure 20c, the temperature variation between flow tubes in the x-direction is shown. The temperatures above the tubes are taken as being uniform because heat is transferred directly downwards at these locations. Figure 20b shows a three-dimensional temperature profile.

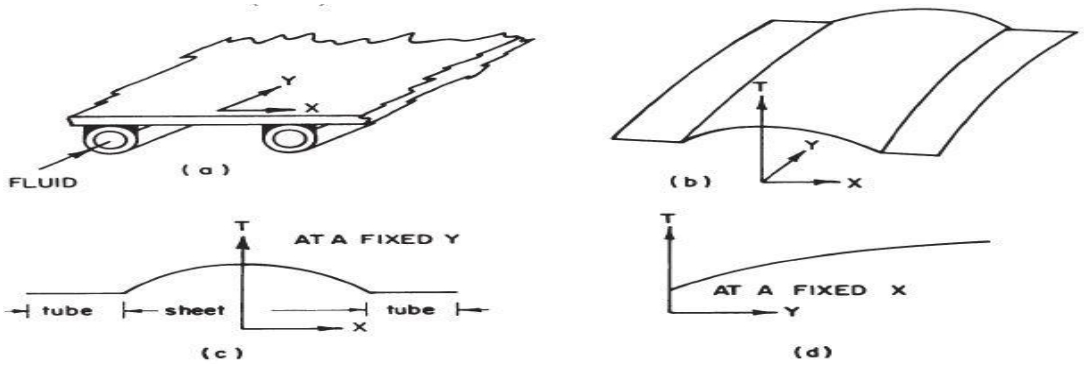

Figure 20: Absorber plate temperature distribution[43].

In the spanwise direction, the temperature distribution can be calculated by modeling one section of the absorber plate between the tubes as fins. The total heat to the fluid per unit length of collector for all the tubes, $\dot{q}$, is the heat gain from the fin on each side of one tube and the heat gain right above the tubes multiplied by the number of tubes. To calculate the heat collected by the fin, the fin efficiency is required. The fin efficiency is given as

$$F = \eta_{fin} = \frac{\dot{q}_{fin}}{\dot{q}_{max,fin}} = \frac{\tanh[mL]}{mL} \tag{4.44}$$

where

$$m = \sqrt{\frac{U_L}{k_p \delta}}. \tag{4.45}$$

Thus, the heat transfer rate from the fins per unit length of the collector is

$$\dot{q}_{fin} = F\dot{q}_{max,fin} = (depth)(number\ of\ tubes)F(W-D)\left[\frac{S}{\Delta t} - U_L(T_b - T_a)\right]. \quad (4.46)$$

The heat transfer rate from the area above the tube per unit length is

$$\dot{q}_{tube} = (depth)(number\ of\ tubes)D\left[\frac{S}{\Delta t} - U_L(T_b - T_a)\right]. \quad (4.47)$$

The total heat transfer per unit length of the collector is the sum of these two quantities:

$$\dot{q} = \dot{q}_{fin} + \dot{q}_{tube}. \quad (4.48)$$

The heat gain per unit length of collector must be transferred from right above the absorber plate into the fluid. This means that two more thermal resistances must be overcome, which are the contact resistance between the fluid tubes and the absorber plate and the convective resistance of the liquid flowing in the tube. These two resistances are generally buried in a collector performance factor called the collector efficiency factor. The meaning of the collector efficiency factor is defined as

$$F' = \frac{U_o}{U_L} \quad (4.49)$$

where U_o is the overall heat transfer coefficient that includes all thermal resistances the heat from the sun must travel through to get to the liquid flowing through the tubes, and U_L is the overall heat transfer coefficient for heat losses from the solar panel. This important solar panel performance quantity is calculated from

$$F' = \frac{\frac{1}{U_L}}{W\left\{\frac{1}{U_L[F(W-D)+D]} + \frac{1}{h_{fi}\pi D_i} + \frac{1}{C_b}\right\}} \quad (4.50)$$

where

h_{fi} = heat transfer coefficient = $\frac{N_u\, k}{D}$ = $\frac{nusselt\ number * thermal\ conduvtivity}{diameter\ of\ tube}$

and h_{fi} can be obtained from the Nusselt number correlation

$$N_u = \left\{\frac{\left(\frac{f}{8}\right)R_e - 1000P_r}{1 + 12.7\left(\frac{f}{8}\right)^{0.5}\left(P_{r,g}^{0.66}\right) - 1}\right\} \quad (4.51)$$

where

$$f = (0.79\log(R_e) - 1.64)^{-2} \tag{4.52}$$

if turbulent flow is assumed. Other Nusselt number correlations can be used if laminar flow exists. The quantity C_b is a contact conductance and is usually taken as a large value and is not important to the analysis. It is interesting to note that F' is fairly constant for a given collector.

To account for temperature changes along the length of the collector, the heat removal factor is used. The collector heat removal factor F_R is a ratio of useful energy gained by the collector to the energy gained by the collector if it were entirely at the inlet fluid temperature. The equation for the heat removal factor is

$$F_R = \frac{\dot{m}C_p}{A_c U_L}\left\{1 - exp\left(-\frac{A_c U_L F'}{\dot{m}C_p}\right)\right\}. \tag{4.53}$$

The collector heat removal factor allows one to swap the fluid inlet temperature into Equation (4.1) in place of the plate mean temperature. When this is done, the useful energy gained by the collector is given by

$$\dot{Q}_u = F_R A_c \left[\frac{S}{\Delta t} - U_L(T_{fi} - T_a)\right]. \tag{4.54}$$

This is the form of the useful energy gain of a thermal collector that is solved in the computer routines developed for this work. The difficulty in solving this equation is in the determination of S, U_L, and F_R. The technique for determining all three of these parameters has been presented in this chapter.

With the collector heat removal factor formulation of the useful energy gain equation, a plate mean temperature can be calculated. Although Equation (4.1) no longer requires this parameter, it may be interesting to see its value. The plate mean temperature can be calculated from

$$T_{pm} = T_{fi} + \frac{\frac{\dot{Q}_u}{A_c}}{F_R U_L}(1 - F_R). \tag{4.55}$$

An average temperature that is important for obtaining fluid properties is the fluid mean temperature, which is determined from

$$T_{fm} = T_{fi} + \frac{\frac{\dot{Q}_u}{A_c}}{F_R U_L}(1 - F'). \tag{4.56}$$

Another collector performance factor that is sometime useful is the collector flow factor F'', which is the ratio of collector heat removal factor to the collector efficiency factor,

$$F'' = \frac{F_R}{F'}. \tag{4.57}$$

The collector flow factor can be written in terms of more fundamental parameters as

$$F'' = \frac{\dot{m}C_p}{A_c U_L F'}\left\{1 - exp\left(-\frac{A_c U_L F'}{\dot{m}C_p}\right)\right\}. \tag{4.58}$$

The last performance factor presented is the collector efficiency, which is the ultimate determiner of good collector performance. This collector efficient is the ratio of the useful energy gathered by the collector to the energy incident on the collector,

$$\eta_{collector} = \frac{\dot{Q}_u \Delta t}{I_T A_c}. \tag{4.59}$$

4.2 Heat Exchanger Analysis

Heat exchangers are devices that make possible the transfer of thermal energy between two or more fluids that are at different temperatures. The two fluids, which are at different temperatures generally, are separated by a solid wall. Usually, in heat exchangers, there is neither external heat transfer nor work. Figure 21 shows a drawing of a heat exchanger, where it can be seen that the hot fluid and the cold fluid are injected into the heat exchanger from different inlets. Each liquid passes through the heat exchanger, where the warm fluid loses its thermal energy, which is gained by the cold fluid. Usually, a heat exchanger involves convection between each fluid and the separation wall and then conduction through the separation wall.

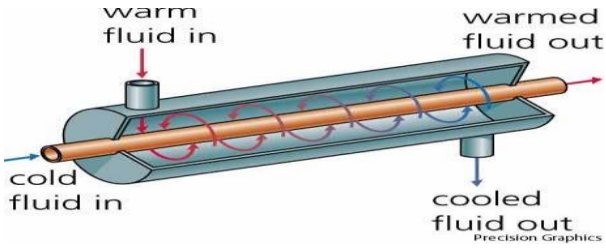

Figure 21: Working of heat exchanger [44].

4.2.1 Type of heat exchanger used

Typical applications of a heat exchanger include heating and air-conditioning or space heating in houses and commercial buildings. They are also used in the chemical processing

industry and for power generation in large plants. There are many types of heat exchangers used in industry for different applications, which require different types of hardware and different configurations. Therefore, it is very important to use the right heat exchanger in the right application. Reaching a required heat transfer with a known number of constraints has led to manufacturing various kinds of heat exchangers.

One way of classifying heat exchangers is according to the flow arrangement. Parallel flow heat exchangers have both the hot and cold fluid inlets at the same end of the heat exchanger so that the fluids flow in the same direction. Counter flow heat exchangers have the fluids entering at opposite ends of the heat exchanger so they flow in opposite directions (see Figure 23). Cross-flow heat exchangers have the fluids entering at right angles to one another so that the fluids move perpendicular to each other. There are two types of cross-flow heat exchangers: mixed (at least one of the fluids can move spanwise to its main flow direction) and unmixed (spanwise motion is not permitted). Figure 23 shows types of cross-flow heat exchangers. This study uses a cross-flow, single-pass type of heat exchanger in which both fluids are unmixed.

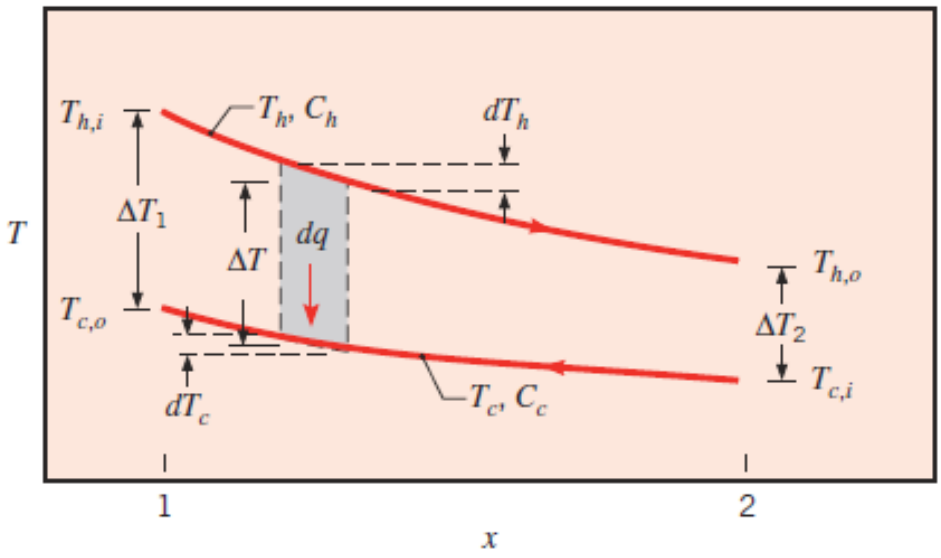

Figure 22: Temperature distribution in heat exchanger [45].

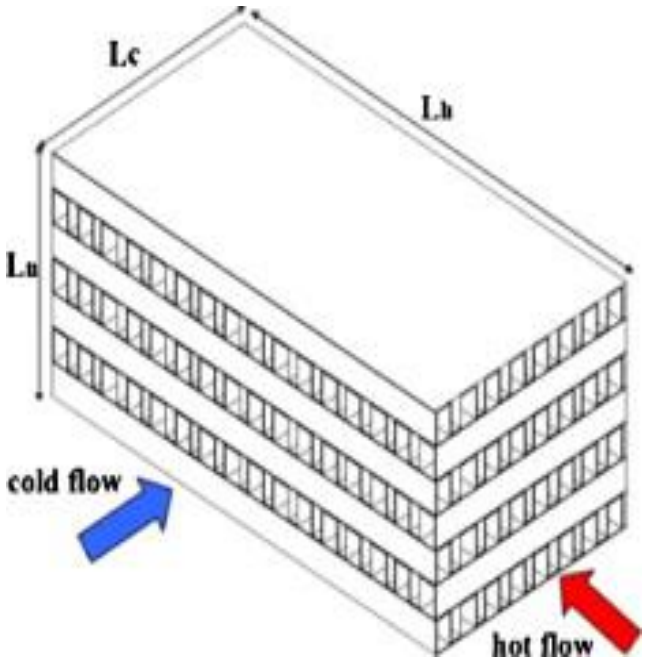

Figure 23: Cross flow heat exchangers [46].

4.2.2 Method for Heat Exchanger Analysis

The heat exchanger analysis is an important part of this solar thermal system analysis and is directly coupled with the solar panel to control the inlet conditions. The heat exchanger also dictates how much heat is transferred from the working fluid running through the solar panel to the space being heated. For this reason, the analysis used to simulate the performance of the heat exchanger in the solar thermal system being studied in this thesis work is detailed.

Heat exchanger analyses can be conducted using one of two methods: logarithmic mean temperature difference (LMTD) and the effectiveness-number of transfer units (effectiveness-NTU) method. LMTD is the preferred technique when the inlet and outlet temperatures of the fluids are known or when these temperatures can be easily found with an energy balance. The effectiveness-NTU method is preferred when both the outlet temperatures are unknown. Since both the outlet temperatures are unknown in the solar thermal system being analyzed in this work, the effectiveness-NTU method is used.

4.2.2.1 Effectiveness-NTU method

The heat transfer between the fluids in a heat exchanger can be determined in one of two ways,

$$\dot{Q} = m_h c_{p,h}(T_{h,i} - T_{h,o}) \tag{4.60}$$

and

$$\dot{Q} = m_c c_{p,c}(T_{c,i} - T_{c,o}). \tag{4.61}$$

The first equation shows the heat transfer from the hot fluid side, and the second equation shows the heat transfer from the cold fluid side. These both have to be equal because the heat from the hot fluid must pass into the cold fluid. The subscripts h and c on these equations represent the hot and cold fluids.

In the effectiveness-NTU method, both the heat exchanger effectiveness and the number of transfer units must be determined. The effectiveness of a heat exchanger is an important parameter to determine the performance of a heat exchanger. Firstly, the maximum possible heat transfer rate is determined. This term is denoted by $\dot{Q}_{max}$. To determine $\dot{Q}_{max}$, one of the fluids flowing through the heat exchanger will have to undergo the maximum possible temperature difference termed as $T_{h,i} - T_{c,i}$, where $T_{h,i}$ and $T_{c,i}$ are the inlet temperatures of the hot and cold fluids, respectively. The temperatures $T_{h,0}$ and $T_{c,o}$ are the outlet temperatures of the hot and cold fluids, as shown in Figure 22. The fluid that will undergo the maximum temperature difference is the fluid with the minimum heat capacity. The heat capacity of the fluids is defined as

$$C_h = \dot{m}_h c_h \tag{4.62}$$

and

$$C_c = \dot{m}_c c_c. \tag{4.63}$$

To illustrate more clearly the maximum possible temperature difference in a heat exchanger, a couple of situations will be considered. Firstly the case where $C_c < C_h$ is considered. In this case, the maximum possible heat transfer rate is

$$\dot{Q}_{max} = C_c(T_{h,i} - T_{c,i}). \tag{4.64}$$

If the case where $C_c > C_h$ is considered, then

$$\dot{Q}_{max} = C_h(T_{h,i} - T_{c,i}). \tag{4.65}$$

If Equations (4.64) and (4.65) are written as a single equation, then

$$\dot{Q}_{max} = C_{min}(T_{h,i} - T_{c,i}) \tag{4.66}$$

where C_{min} is C_h or C_c, whichever is smaller.

Now, the effectiveness for a heat exchanger can be defined. The heat exchanger effectiveness is the ratio of the actual heat transfer rate to the maximum possible heat transfer rate

$$\varepsilon = \frac{\dot{Q}}{\dot{Q}_{max}}. \tag{4.67}$$

The effectiveness is a dimensionless quantity that has a value between 0 and 1. Using Equations (4.60), (4.61), and (4.66) the effectiveness can be written as

$$\varepsilon = \frac{C_h(T_{h,i}-T_{c,i})}{C_{min}(T_{h,i}-T_{c,i})} \tag{4.68}$$

or

$$\varepsilon = \frac{C_c(T_{c,o}-T_{c,i})}{C_{min}(T_{h,i}-T_{c,i})}. \tag{4.69}$$

If parameters like ε, $T_{h,i}$, and $T_{c,i}$ are known, then the actual heat transfer rate can be determined with

$$q = \varepsilon\, C_{min}\left(T_{h,i} - T_{c,i}\right). \tag{4.70}$$

The next important parameter in the effectiveness-NTU method is the dimensionless number NTU,

$$NTU = \frac{U\,A}{C_{min}}. \tag{4.71}$$

This number can be used to determine the heat exchanger effectiveness, which is considered to be a function of NTU and $\frac{C_{min}}{C_{max}}$,

$$\varepsilon = f\left(NTU, \frac{C_{min}}{C_{max}}\right) \tag{4.72}$$

where $\frac{C_{min}}{C_{max}}$ is equivalent to $\frac{C_c}{C_h}$ or $\frac{C_h}{C_c}$ relative to magnitudes of cold and hot fluid heat capacity rates. The ratio $\frac{C_{min}}{C_{max}}$ is called the heat capacity ratio given as C_r. For a cross-flow, single-pass heat exchanger where both fluids are unmixed, the effectiveness is expressed as a function of the NTUs as

$$\varepsilon = 1 - exp\left[\left(\frac{1}{C_r}\right)(NTU)^{0.22}\{exp[-C_r(NTU)^{0.78}] - 1\}\right]. \tag{4.73}$$

4.2.3 Thermal Resistive Network for Heat Exchanger

A heat exchanger usually involves two working fluids that are divided by a wall. The resistive network involves the conduction and convection resistances in the fluids and the wall. The heat exchanger, which is being used for this analysis, is a cross-flow heat exchanger. Figure 24 shows the thermal resistive network that depicts the heat transfer from the hot fluid to the wall by convection, through the wall by conduction, and ends with convection from the wall to the cold fluid. In the heat exchanger used in this solar space heating system, the cold fluid is air, which is called the gas side of the heat exchanger, and the hot fluid is a mixture of ethylene glycol and water, which is called the liquid side of the heat exchanger.

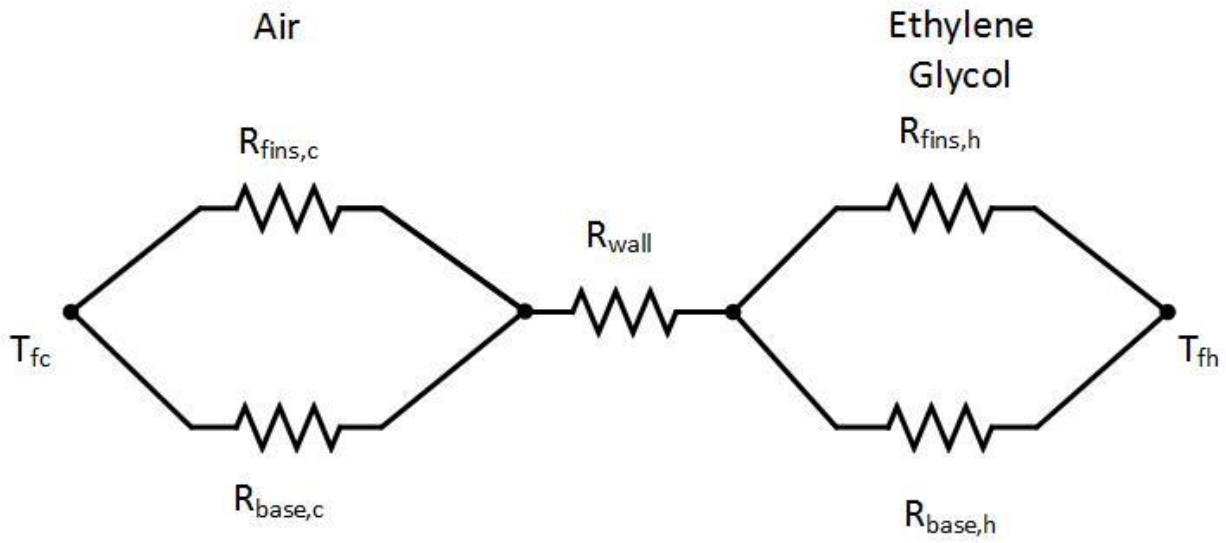

Figure 24: Thermal resistive network for heat exchanger.

As shown in Figure 24, there are two paths for heat transfer from the hot fluid to the wall and two paths for heat transfer from the wall to the cold fluid. One of these paths is through the fins, and the other directly through the wall. The two resistances on the gas side are given as

$$R_{fin,g} = \frac{1}{h_g \eta_{fin,g} A_{fins,g}} \tag{4.74}$$

and

$$R_{base,g} = \frac{1}{h_g A_{bg}}. \tag{4.75}$$

Similarly the liquid side fin and base resistances are given as

$$R_{fin,l} = \frac{1}{h_l \eta_{fin,l} A_{fins,l}} \tag{4.76}$$

and

$$R_{base,l} = \frac{1}{h_l A_{bl}}. \tag{4.77}$$

The resistance to the heat transfer through the wall is given by

$$R_{wall} = \frac{P_t}{k_{mat} L_{hl} L_{hg} N_{layers}}. \tag{4.78}$$

The fin efficiencies required in Equations (4.74) and (4.76) are obtained from

$$\eta_{fin,g} = \frac{\frac{\tanh m_{g,g} L_{dg}}{2}}{\frac{m_{g,g} L_{dg}}{2}} \tag{4.79}$$

where

$$m_{g,g} = \sqrt{\frac{2h_g}{k_{mat} F_{th}}} \tag{4.80}$$

for the gas side and

$$\eta_{fin,l} = \frac{\frac{\tanh m_{l,l} L_{dl}}{2}}{\frac{m_{l,l} L_{dl}}{2}} \tag{4.81}$$

where

$$m_{l,l} = \sqrt{\frac{2h_l}{k_{mat} F_{th}}} \tag{4.82}$$

for the liquid side. Combining all five of these resistances properly is done as

$$R_{total} = \frac{1}{\frac{1}{\frac{1}{R_{base,g}} + \frac{1}{R_{fin,g}}} + R_{wall} + \frac{1}{\frac{1}{R_{fin,l}} + \frac{1}{R_{base,l}}}}. \tag{4.83}$$

An overall heat transfer coefficient can be defined using this total resistance as

$$U = \frac{1}{R_{total}(A_{bg} + A_{fins,g})}. \tag{4.84}$$

4.2.4 Geometry

The cross flow heat exchanger used in this analysis has a number of geometrical quantities that need to be calculated and a number of geometrical quantities that need to be

entered. The inputs are the flow length of the gas, the flow length of the liquid, the number of gas-liquid flow layer pairs, the fins per inch on each side of the heat exchanger, the height of each of the flow channels, and the thickness of the separator plates. The flow length of the gas determines the overall thickness of the heat exchanger, and the flow length of the liquid determines the width of the heat exchanger. The flow length of the gas should generally be taken to be much smaller than the flow length of the liquid. The flow length of the liquid determines the frontal area for the gas flow, which should be large. The number of layers used also determines the frontal area for the gas flow. One layer of this heat exchanger is composed of one gas flow channel and one liquid flow channel. The heat exchanger analysis in this thesis assumes that every layer behaves exactly the same.

Some of the geometrical parameters that need to be calculated are given below. The gas side quantities are given first and then the liquid side quantities are given. This list is not complete; some geometrical parameters are deemed to be self-evident and not discussed. There are three areas that need to be known to perform these heat transfer calculations. One of these areas is the frontal flow area for the gas to move through the heat exchanger, which is

$$A_{fg} = \left(\frac{L_{dg}}{2\left(L_{hl} - N_{fg}F_{th} - 2P_t\right)}\right) N_{layers} \tag{4.85}$$

where

$$N_{fg} = F_g L_{hl}. \tag{4.86}$$

The second of these areas is the area on the wall separating the gas from liquid that is not covered by gas side fins, which is given by

$$A_{bg} = \left\{\left(L_{hl} - N_{fg}F_{th}\right)L_{hg}\right\}N_{layers}. \tag{4.87}$$

The third of these areas is the surface area of the fins available for heat transfer, which is

$$A_{fins,g} = \left\{2\left(N_{fg} + 1\right)\left(\frac{L_{dg}}{2}\right)L_{hg}\right\}N_{layers}. \tag{4.88}$$

The hydraulic diameter used on the gas side is

$$D_{hg,fins} = \left(\frac{2L_{dg}D_{\,fins,g}}{L_{dg} + D_{\,fins,g}}\right). \tag{4.89}$$

Similarly, the same quantities on the liquid side of the heat exchanger are determined using the following equations:

$$A_{fl} = \left(\frac{L_{dl}}{2\left(L_{hg} - N_{fl}F_{th} - 2P_t\right)}\right) N_{layers}, \tag{4.90}$$

$$N_{fl} = F_l L_{hg}, \tag{4.91}$$

$$A_{bl} = \left\{\left(L_{hg} - N_{fl}F_{th}\right)L_{hl}\right\} N_{layers}, \tag{4.92}$$

$$A_{fins,l} = \left\{2\left(N_{fl} + 1\right)\left(\frac{L_{dl}}{2}\right)L_{hl}\right\} N_{layers}, \tag{4.93}$$

and

$$D_{hl,fins} = \left(\frac{2L_{dl}D_{\,fins,l}}{L_{dl} + D_{\,fins,l}}\right). \tag{4.94}$$

4.2.5 Heat Transfer Coefficients

Heat transfer coefficients are important quantities for heat exchanger analysis. Two heat transfer coefficients are required, one for the convective heat transfer between the gas and the wall and one for the convective heat transfer between the wall and the liquid. These heat transfer coefficients are used in the thermal resistance equations shown in Equations (4.74 – 4.77). Only one heat transfer coefficient is calculated for the gas side and one for the liquid side. This means the heat transfer coefficient between the fin and the fluid is taken to be the same as the heat transfer coefficient between the fluid and the separating wall. Thus, the same heat transfer coefficient is used in both Equations (4.74) and (4.75) for the gas side of the heat exchanger; and the same heat transfer coefficient is used in Equations (4.76) and (4.77) for the liquid side of the heat exchanger. The flow on either the gas or liquid side of the heat exchanger can be laminar or turbulent. For this reason, both laminar and turbulent heat transfer coefficients correlations are included in the developed MATLAB code, and the proper one is determined by the value of the Reynolds number.

To determine Reynolds numbers, it is necessary to determine fluid velocities by entering the mass flow rate on the liquid side and the volumetric flow on the gas side. Fluid velocities are obtained from these input quantities using

$$V_g = \frac{\dot{\forall}_g / N_{layers}}{\rho_g} \tag{4.95}$$

and

$$V_l = \frac{\dot{m}_l / N_{layers}}{\rho_l A_{fl}}. \tag{4.96}$$

It should be noticed that in both of these equations, the total flow rates are divided by the number of flow layers in the heat exchanger. This is done because the fluid velocity in one heat exchanger layer is desired. Every layer of the heat exchanger is the same, so once results are obtained for one layer, they are obtained for every layer. The Reynolds numbers on both the gas and liquid side of the heat exchanger are

$$R_{e,g} = \frac{\rho_g D_{hg,fins} V_g}{\mu_g} \tag{4.97}$$

and

$$R_{e,l} = \frac{\rho_l D_{hl,fins} V_l}{\mu_l}. \tag{4.98}$$

Heat transfer coefficients are generally obtained from Nusselt number correlations. The heat transfer coefficient can be obtained from a known Nusselt number using

$$h_l = \frac{N_{u,l} k_l}{D_{hl,fins}} \tag{4.99}$$

for the gas side and

$$h_g = \frac{N_{u,g} k_g}{D_{hg,fins}} \tag{4.100}$$

for the liquid side. On the gas side of the heat exchanger, the Nusselt number correlation for laminar flow, $R_{e,g}$ < 3000, is

$$N_{u,g} = 1.86 * \left(\frac{R_{e,g} * P_{r,g} * D_{hg,fins}}{L_{hg}} \right)^{0.33} \tag{4.101}$$

and for turbulent, $R_{e,g} \geqslant 3000$, the Nusselt number used is

$$N_{u,g} = \left\{ \frac{\left(\frac{f_g}{8}\right) * R_{e,g} - 1000 * P_{r,g}}{1 + 12.7 * \left(\frac{f_g}{8}\right)^{0.5} * \left(P_{r,g}^{0.66}\right) - 1} \right\} \tag{4.102}$$

where f_g is the friction factor,

$$f_g = \left(0.79 * \log R_{e,g} - 1.64\right)^{-2}. \tag{4.103}$$

Similarly the Nusselt number correlations for the liquid side are

$$N_{u,l} = 1.86 * \left(\frac{R_{e,l} * P_{r,l} * D_{hl,fins}}{L_{hl}}\right)^{0.33} \tag{4.104}$$

if $R_{e,l}$ < 3000; and

$$N_{u,l} = \left\{\frac{\left(\frac{f_l}{8}\right) * R_{e,l} - 1000 * P_{r,l}}{1 + 12.7 * \left(\frac{f_l}{8}\right)^{0.5} * \left(P_{r,l}^{0.66}\right) - 1}\right\} \tag{4.105}$$

if $R_{e,l} \geqslant$ 3000, where

$$f_l = \left(0.79 * \log(R_{e,l}) - 1.64\right)^{-2}. \tag{4.106}$$

4.3 Coupling of Solar panel and Heat Exchanger Analysis

The complete solar thermal space heating system analyzed for this thesis work is shown in Figure 25. The two key components are the solar thermal panel and the heat exchanger. It is these two components on which this modeling work has focused. The analysis of each of these components has been discussed in the prior sections of this chapter. The third component of this system is the storage system, which is the focus on this section.

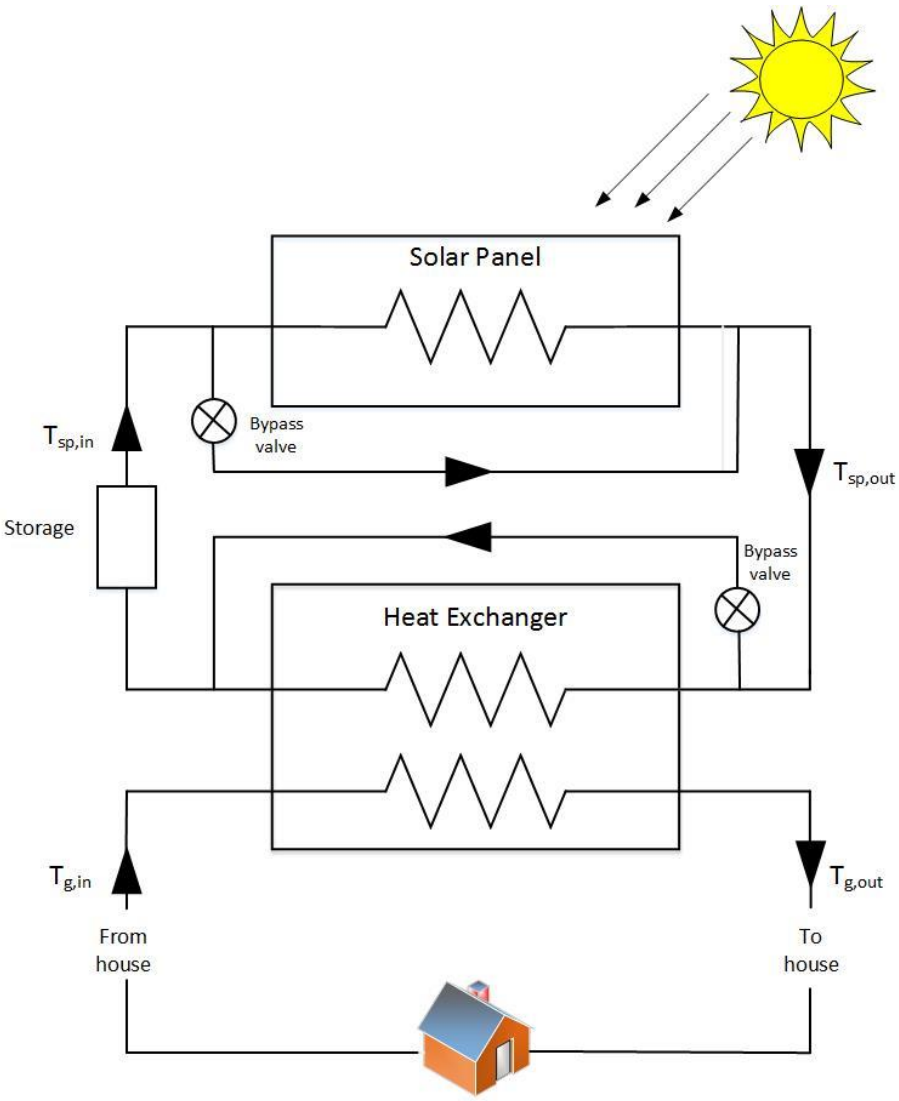

Figure 25 : Diagram of solar thermal system.

There are two fluids involved in this system: a liquid (i.e., ethylene glycol) and a gas (i.e., house air). The major flow of the liquid through this system is from the top of the storage container, through the solar panel, through the heat exchanger, and back to the bottom of the storage container. On the gas side of the system, air is sucked from the house, run through the heat exchanger where it is heated by the liquid on the other side of the heat exchanger, and then the air is dumped back into the house to keep it warm. Figure 25 depicts two bypass flow conduits on this system. The bypass associated with the solar panel is used when the solar panel cannot deliver heat to the working fluid, such as times when the sun is not shining. The bypass associated with the heat exchanger is used if the house does not require heating. On an actual

home, the solar panels will be placed on the roof of the house, the heat exchanger would be placed inside the house, and the storage container would be placed in the basement of the house. Tubing would be used to connect these components in the manner shown in Figure 25. Also required in this system are flow valves and control equipment.

There are four temperatures present in this solar thermal system: two are in the liquid loop and two are in the gas loop. The two temperatures present in the liquid loop are $T_{sp,in}$, which is the temperature of the liquid going into the solar panel, and $T_{sp,out}$, which is the temperature of the liquid going out of the solar panel. The temperature $T_{sp,out}$ will be equal to or larger than $T_{sp,in}$ because it is the job of the solar panel to heat the liquid. If the solar panel is incapable of heating the liquid, the liquid goes around the solar panel and $T_{sp,out}$ is taken to be equal to$T_{sp,in}$. The other two temperatures in the system are $T_{g,in}$ and $T_{g,out}$. The temperature $T_{g,in}$ is nothing more than the chosen indoor air temperature. This is the temperature at which a home owner chooses to set the thermostat. A reasonable indoor air temperature for the heating season, and the heat exchanger inlet air temperature used in the results presented in this thesis, is 23^{o}C. The temperature $T_{g,out}$ is the temperature of the air going back into the house. The air being returned to the house is at a higher temperature than the air taken from the house. This is the way the home is heated and kept at a temperature of 23^{o}C during the heating season. The heat required to keep the temperature of the home at 23^{o}C is equal to the heat loss from the home. This is called the heating load of the home. For this air to have any heating value, it must be at a higher temperature than $T_{g,in}$. This will happen if the solar panel is supplying heat to the liquid side of the loop. $T_{g,out}$ is one of the desired quantities calculated by the computer model developed as part of this work.

In order to avoid having more than four different temperatures in this solar space heating system and to avoid doing a detailed storage system model, it was assumed that the size of the storage container is such that it holds one hour's worth of liquid flow. In equation form, this means the volume of the storage tank in cubic meters is

$$\forall_{storage} = \frac{3600\dot{m}_l}{\rho_l}, \tag{4.107}$$

where the mass flow rate of the liquid is specified in kg/s, the density is specified in kg/m^3, and the number 3600 converts the mass flow rate per second to the amount of mass required for one hour. Thus, if the mass flow rate of liquid in the thermal system is 0.1 kg/s, the storage volume

required in the system is 0.35 m^3. If the liquid mass flow rate in the system is 1.0 kg/s, the storage volume is 3.5 m^3. These calculations were done using an ethylene glycol density of 1025 kg/m^3. The other assumption made in regards to energy storage is that there is no mixing of liquid or heat conduction occurring in the storage tank. This means the fluid coming into the tank builds up from the bottom of the tank and the fluid going out of the tank is taken from the top. This allows for a step change in the fluid temperature within the storage tank and eliminates the need to model thermal energy storage in a detailed manner.

The operation of the solar panels and the heat exchanger in this solar space heating system are coupled to one another. The way one of these components behaves, affects the way the other component behaves. The output temperature from the solar panels affects the way the heat exchanger behaves, and the output temperature from the heat exchanger affects the way the solar panels behave. A higher liquid inlet temperature to the heat exchanger will mean more heat delivered to the space being heated. A higher liquid inlet temperature to the solar panel, means the solar panel will have more heat losses to the environment. Although it may seem that the storage container does not affect the system, it does. The storage container allows thermal energy to be delivered to the space being heated even when there is no energy gain in the solar panel, for example, during the night.

The control of this solar space heating system is necessary to obtain the best performance. There are few controls in this analysis, but they are chosen to obtain the best performance of the system. The first control is that liquid only passes through the solar panel when there is the possibility of gaining energy. This is done by calculating the useful heat gain in the solar panel with the analysis shown in Section 4.1. When this quantity comes out to be negative, the panel is losing heat to the environment, the liquid is set to bypass the solar panel for that hour, and the useful heat gain is set to zero. The second control used is associated with the heat exchanger; liquid is passed through the heat exchanger whenever there is a demand for space heating. If there is no demand, the liquid bypasses the heat exchanger. This is essentially what a control thermostat in a home would do.

As will be seen in the results section of this thesis, this type of control scheme will cause some high temperatures to occur in the liquid in the summer time. This occurs because the solar system is allowed to collect heat whenever it is capable of doing so. In the summer, a good deal of heat can be collected, but little heat is demanded. This means heat is going into the liquid, but

is not being taken out of the liquid driving the liquid temperature up. A type of equilibrium is reached when the liquid temperature reaches levels well above the ambient temperature so that just as much heat is convected and radiated from the solar panel to the surroundings as is gained from the sun.

Chapter 5. SOLAR THERMAL SYSTEM PERFORMANCE

In this chapter, the performance of the solar thermal system shown in Figure 25 is presented. The performance of this system is carried out using a MATLAB program based on the analysis described in Chapter 4 of this thesis. A number of output performance parameters are given in this chapter as a function of a number of operational or design parameters. The design and operational parameters are the size and orientation of the solar panel array, the tilt angel at which the solar panels are installed, the arrangement of the solar panel array, the liquid flow rate through the solar array, the size of the heat exchanger, and the flow rate of room air through the heat exchanger. The performance parameters presented are the liquid inlet temperature to the solar array, the liquid outlet temperature from the solar array, the room air temperature coming out of the heat exchanger, the heat recovery factor of the solar array, the efficiency of the solar array, the overall system efficiency, the useful heat gain of the solar array, the heat transfer between the two fluids in the heat exchanger (this is the same as the heat delivered to the home, and the fraction of the heating load of the home that is satisfied by the solar thermal system. The ultimate goal of installing a solar thermal space heating system on a home or building is to heat the space inside the home or building. Thus, the two most important performance parameters presented here are the amount of heat delivered to the home and the fraction of the home's

heating load met by the solar thermal system. Another important aspect of these systems is the cost. A cost analysis is outside the scope of the present work and will not be presented here. This work is meant to be a technical investigation of a simple solar thermal space heating system. Having said this, it is reasonable for the reader to assume that the larger the system, the higher the initial cost of the system.

There are three solar system performance investigations presented below. The first investigation only looks at the performance of the solar system operating for one hour with some standard input conditions specified by the Solar Rating and Performance Corporation (SRCC). The second performance study looks at system performance for a typical home located in Minneapolis, MN and presents detailed hourly results for a typical metrological year and integrated results over the entire year. The third performance study looks at a typical home located in Dayton, OH and again presents detailed hourly results and integrated yearly results. The reader should look at the Minneapolis, MN and Dayton, OH studies as real world results; although the one-hour results provide simpler observation of the component performances. This one hour study analyzes the solar thermal system using a given liquid inlet temperature and eliminates the energy storage system from the analysis. It also isolates the solar array performance from the heat exchanger performance. In this one-hour analysis, the heat exchanger performance still depends on the outlet temperature from the solar array.

5.1 One-Hour Analysis

The one-hour analysis utilizes operating conditions specified by the SRCC [47]. This organization sets conditions at which solar thermal panels can be rated. A report published by the SRCC provided this work with the initial start for evaluating different parameters. The conditions used for this one-hour analysis come from a report rating a flat plate collector manufactured by Guangdong Fivestar Solar Energy Co. Ltd. [48, 49]. This report provided standard temperature differentials and standard solar irradiances for a number of solar thermal panel applications. Because our solar thermal system is designed for space heating, the temperature differential used is 50°C ($T_{sp,in} - T_a = 50\,^oC$). The SRCC also provided solar irradiation data for the test conditions for latitude of 50^oN. This is the latitude used in this one-hour analysis. The collector was assumed to be facing due south and tilted at an angle equal to

the latitude. The hour of the calculation was solar noon to 1 pm. The beam and diffuse components were given by the ratings report as well, but these quantities were calculated by the analysis used in this work. By picking September 22 as the day on which the analysis was performed, the calculated beam and diffuse components were made to match the rating report's values closely. The normal incidence condition specified by the rating report was also met. It should be noted that the SRCC has different solar irradiation and temperature differential conditions for each hour of an entire day. Thus the SRCC presents a standard test day. However, we have only looked at a standard test hour in this study.

5.1.1 Ethylene Glycol Flow Rate

For all the results presented in this thesis, the liquid used in the solar collector is a mixture of ethylene glycol and water: 50% water and 50% ethylene glycol. This is a typical solar thermal panel working fluid because it resists freezing. This ethylene glycol solution also flows through the hot side of the heat exchanger, as can be seen in Figure 25. The flow rate of ethylene glycol is what is surveyed in this sub-subsection. For this liquid flow rate survey, the area of the solar array is 25 m^2 and the tube spacing is 0.118 m, which is the tube spacing recommended by SRCC.

Figure 26 shows the four fluid temperatures present in this solar thermal system; two of the temperatures are for the ethylene glycol flowing through the solar array and two of the temperatures are for the air that comes from and returns to the home. The two ethylene glycol temperatures are the solar array inlet temperature and the solar array outlet temperature. As can be seen by looking at Figure 25, these are also the heat exchanger outlet temperature and the heat exchanger inlet temperature, respectively, on the ethylene glycol side of the heat exchanger. All four of these temperatures have been plotted against the mass flow rate of the ethylene glycol. This plot shows that the inlet solar array temperature is kept at a constant 64^{o}C and the inlet air temperature to the heat exchanger is kept at a constant 23^{o}C. For reference sake, these temperatures are shown in all temperature plots presented.

The optimum fluid flow rate efficiently removes the heat from the panel that the sun is depositing in it. The flow rate that is lower will not remove sufficient heat from panel and thus will affect the efficiency. On the other hand, if the mass flow rate is high, the panel will have

higher efficiency. The solar array outlet temperature shows a significant change in the function of the ethylene glycol flow rate. As should be expected, the temperature greatly increases as the ethylene glycol flow rate goes to zero. For the size of solar array used in this simulation, 25 m^2, these results show that a mass flow rate above 1.5 kg/s is sufficient to keep the ethylene glycol outlet temperature essentially at the inlet temperature. This flow rate also essentially keeps the heat exchanger from noticeably changing the temperature of the ethylene glycol. Note that the air side flow rate in this analysis is held at a constant 0.05m^3/sec. Figure 26 shows the effect of the ethylene glycol flow rate on the air outlet temperature. Effects are only seen at very low ethylene glycol flow rates. This indicates the proper ethylene glycol flow rate in this system should be based on panel performance and pumping power requirements, not on the heat exchanger performance.

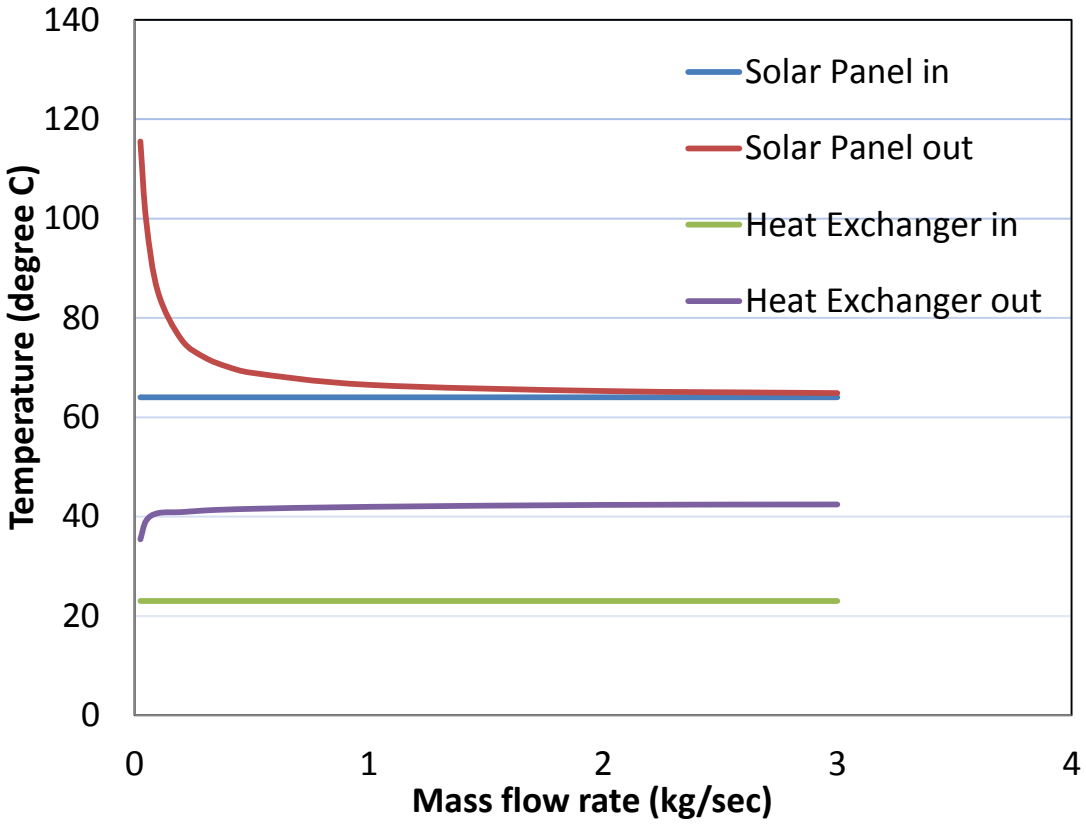

Figure 26: Component inlet and outlet temperatures as function of ethylene glycol mass flow rate.

The next parameters that are presented as a function of ethylene glycol flow rate are the useful energy gained by the solar array and the heat transfer between the ethylene glycol side of the heat exchanger and the air side of the heat exchanger. The heat transfer in the heat exchanger is the thermal energy delivered to the space to be heated. Figure 27 shows both of these heat transfer rates. As shown, the solar panel useful energy gain increases as the mass flow rate increases; this is due to the decrease in temperature throughout the solar array, which lowers the heat lost to the surroundings. As shown in Figure 27, the solar array heat removal factor increases as a function of the ethylene glycol flow rate. It is easy to see from Equation (4.69) that the heat removal factor increases as the mass flow rate increases. An increasing heat removal factor generally indicates increased panel performance. The heat transfer in the heat exchanger tends to follow the same trend as the heat transfer in the solar array. This occurs because more heat delivered to the ethylene glycol in the solar array, means more heat is available to be transferred to the air in the heat exchanger. The one unusual aspect of the heat transfer results shown in Figure 27 is that the heat exchanger heat transfer is larger than the heat transfer in the solar array. Quite obviously, this could not happen if the solar system were run for many hours. This happens for this one-hour analysis because the inlet temperature to the solar array is taken as 64^{o}C. This means the ethylene glycol has a good deal of stored energy relative to the 23^{o}C inlet air. This stored thermal energy is causing the heat transfer in the heat exchanger to be larger than the heat transfer in the solar array.

Figure 28 also shows the heat exchanger effectiveness. This heat exchanger performance parameter quickly decreases for small ethylene glycol mass flow rate increases and then starts to increase with further ethylene glycol mass flow rate increases. The initial rapid decrease is believed to be due to the rapid rise in the heat capacitance of the ethylene glycol, and the slower rise is believed to be due to the rise in the heat transfer coefficient between the ethylene glycol and the heat exchanger wall with increased flow. For the particular solar system being analyzed, Figure 27 and Figure 28 would indicate an ethylene glycol flow rate larger than 0.4 kg/s is used. In this work, the base ethylene glycol flow rate adopted is 0.5 kg/s.

5.1.2 Arrangement of Solar Panels

This particular survey is about varying the arrangement of the individual solar panels in the solar array. The question being asked is: Should the solar panels be connected in series or parallel with respect to the ethylene glycol flow? For this work, the length of the solar array in the flow direction is increased from 0.5 m to 3.5 m; whereas the width of the solar array is appropriately decreased to keep the total solar panel area constant. In this survey, the area of the solar panel array is kept at 25 m^2, the ethylene glycol flow rate is kept at 0.5 kg/s, and the air flow

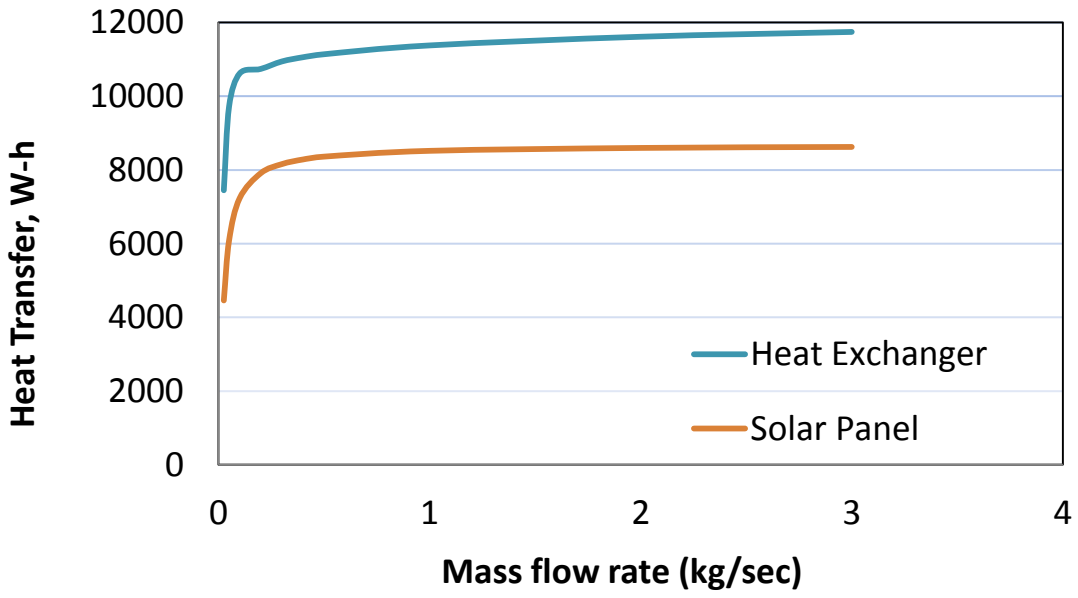

Figure 27: Hourly useful heat gain in solar array and hourly heat transfer in heat exchanger as a function of the ethylene glycol flow rate.

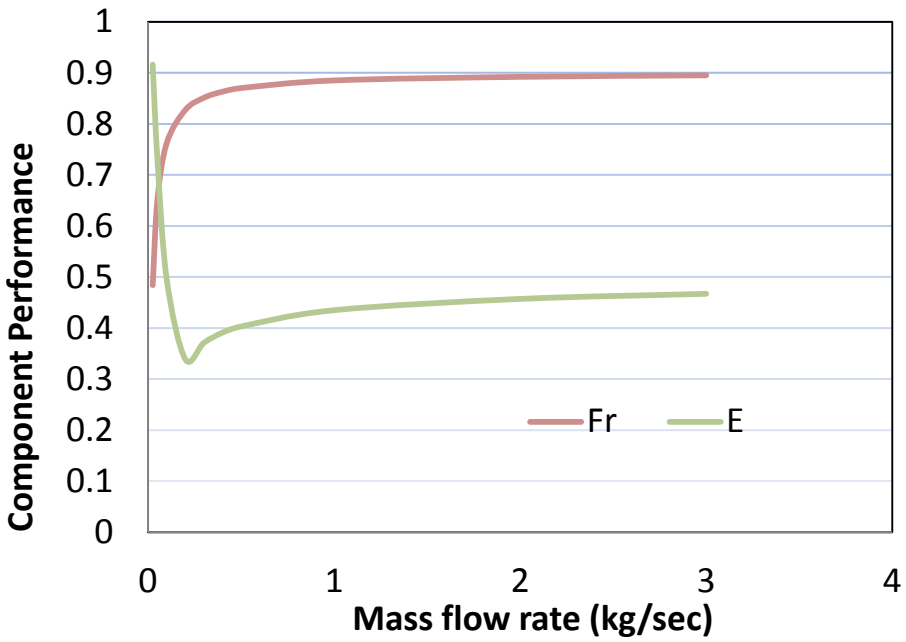

Figure 28: Solar array heat removal factor and heat exchanger effectiveness as a function of the ethylene glycol flow rate.

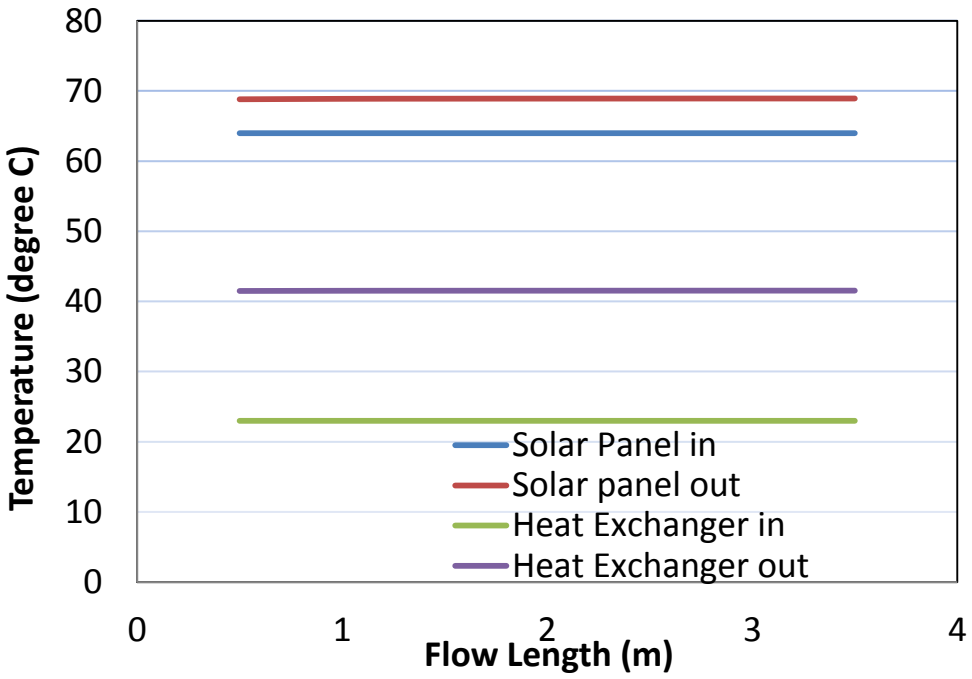

Figure 29: Temperatures of system as function of solar array flow length.

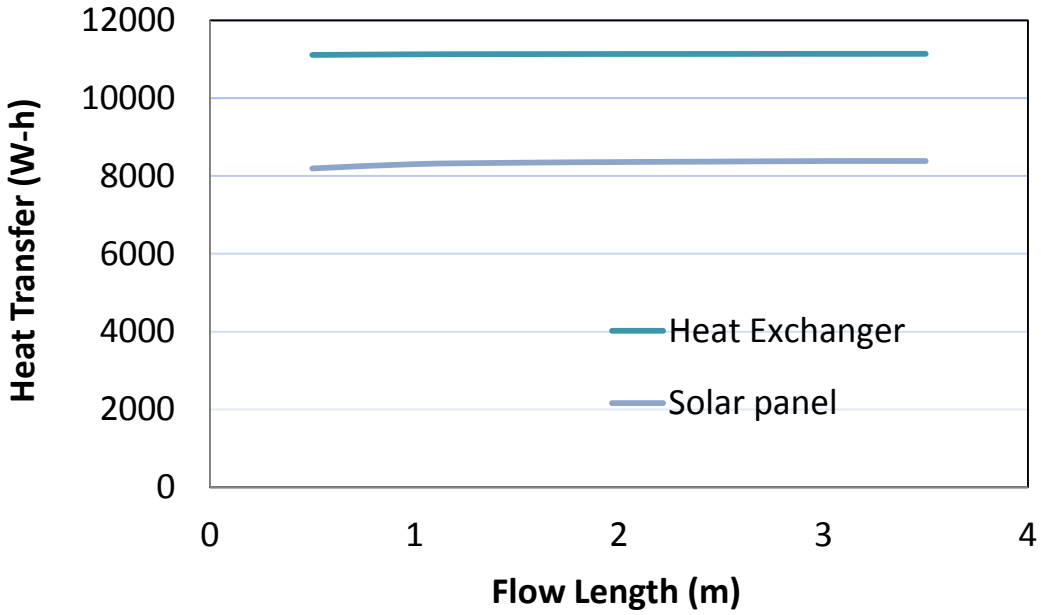

Figure 30: Hourly useful heat gain in solar array and hourly heat transfer in heat exchanger as a function of the solar array flow length.

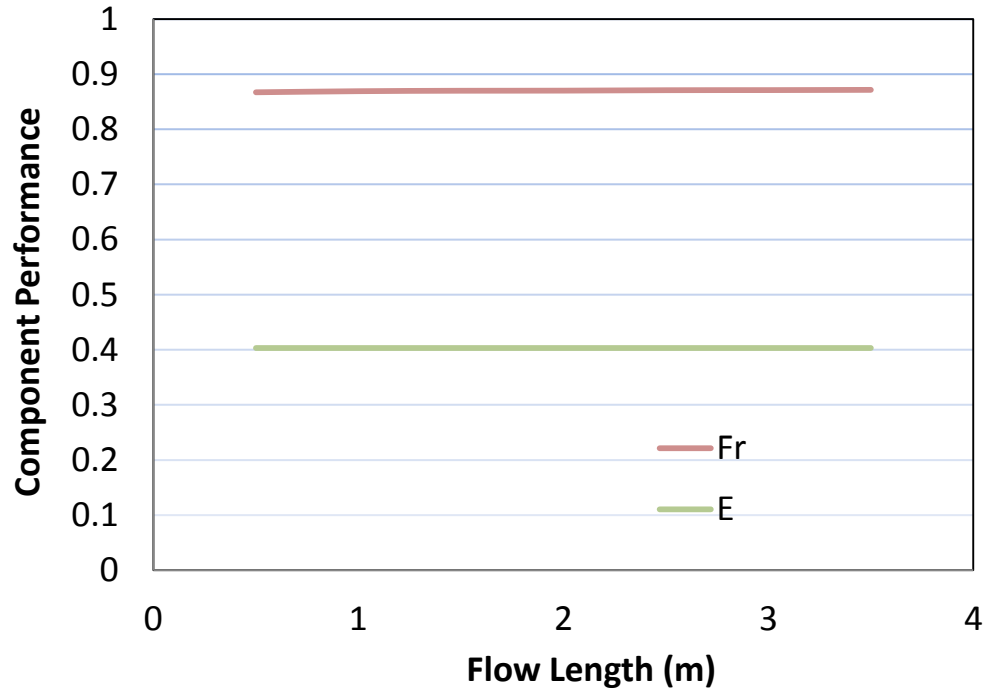

Figure 31: Component performance as function of solar array flow length.

rate through the heat exchanger is kept at 0.5 m^3/s. Figures 29, 30, and 31 show that the shifting of area from being in parallel to being in series has little effect on the system performance. Figure 29 indicates the system temperatures do not change, Figure 30 indicates the heat transfers do not change much, and Figure 31 indicates the solar array heat removal factor and the heat exchanger effectiveness do not change. For the mass flow rates used in this survey, the results indicate that the arrangement of the solar panel surface area is not a factor in the performance of the system. It must be stressed that these same results would probably not be obtained if the flow rate per flow tube remained constant, instead of the total ethylene glycol flow rate. In this work, the base solar array flow length is taken as 2 m. This is done because many commercial panels are about this length.

5.1.3 Size of Heat Exchanger

This survey is carried out to see the effect over the system when the size of the heat exchanger is varied. This is done by changing the length of the heat exchanger on the liquid side as well as gas side. The heat exchanger is a cross-flow heat exchanger that has 93 layers. The base case lengths on the liquid and gas sides are 0.9 meters and 0.05 meters, respectively, and all computations use these lengths unless stated otherwise. The lengths of the heat exchanger are varied one at time, keeping the other side of the length of heat exchanger constant.

Figure 32 represents the effect on system temperatures of changing the heat exchanger length on the air side, and Figure 33 represents the effect on system temperatures of changing the heat exchanger length on the ethylene glycol side. For the results in both these figures, the other side flow length is held constant at the base case values listed above. In these figures, the ethylene glycol temperatures are labeled as “solar panel in” and “solar panel out”. As shown in Figure 25, the solar panel, ethylene glycol in temperature is the same as the heat exchanger, ethylene glycol out temperature. Likewise, the solar panel, ethylene glycol out temperature is the same as the heat exchanger, ethylene glycol in temperature. Figure 32 clearly shows that the heat exchanger ethylene glycol temperatures are not changing as the gas side length is increasing. Figure 33 also clearly shows that the gas outlet temperature from the heat exchanger is

increasing. The highest temperature achieved is approximately 48°C for the longest gas flow length surveyed. Figure 33 also shows the gas side outlet temperature increasing as the ethylene glycol flow length is increased. The reason for this is that the heat capacity of the ethylene glycol flow is large compared to the air flow. This means an increase in heat transfer, because the heat exchanger surface area is increased, which will show up as a temperature increase in the gas. The heat transferred from the ethylene glycol is exactly the same as the heat transferred to the gas. The fluid with the minimum heat capacity is the one that will show the biggest temperature change.

The heat exchanger heat transfer for one hour is shown in Figure 34 as a function of the gas flow length and in Figure 35 as a function of the ethylene glycol flow length. As expected, as the flow lengths increase, the heat transfer increases. Both Figure 34 and Figure 35 show a similar trend of increasing the energy transferred by the heat exchanger as the lengths increase. This is due to the increase in size of the heat transfer area. For the 2-meter length, for either side, the heat exchanger delivers near to 15000 W-h. Therefore, increasing the lengths would deliver higher temperatures, have higher energy exchange, and improve the performance of the solar thermal system. However, the size of the heat exchanger may be restricted due to space and cost constraints.

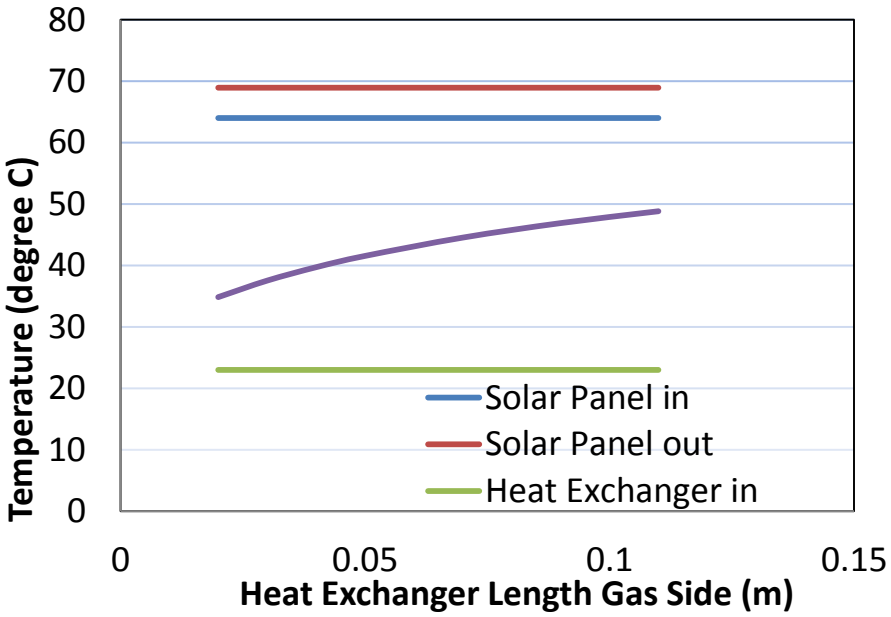

Figure 32: System temperatures as a function of heat exchanger length on the air side.

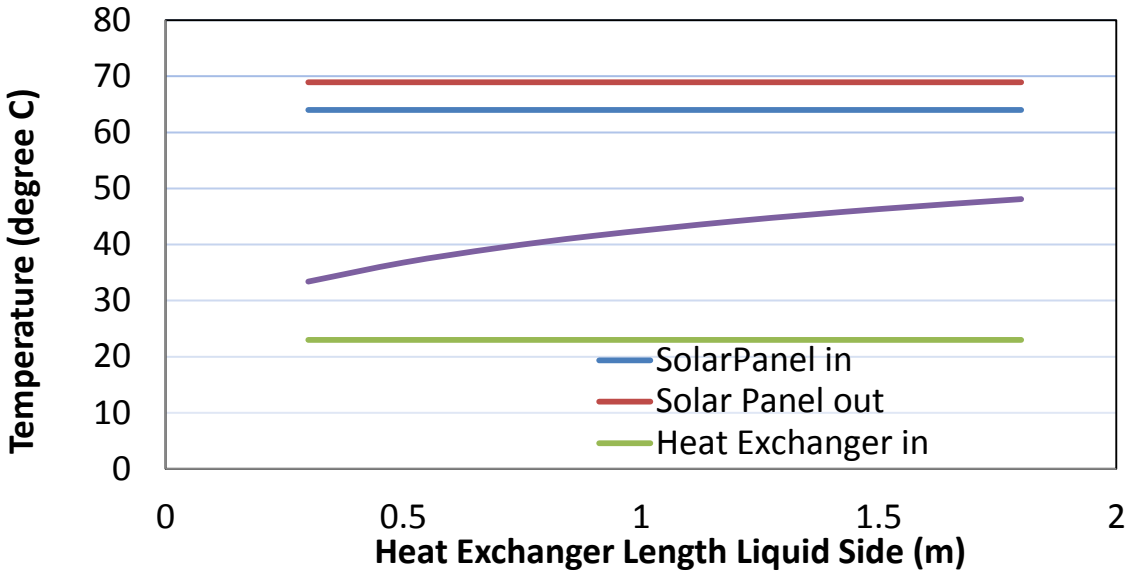

Figure 33: System temperatures as a function of heat exchanger length on the ethylene glycol side.

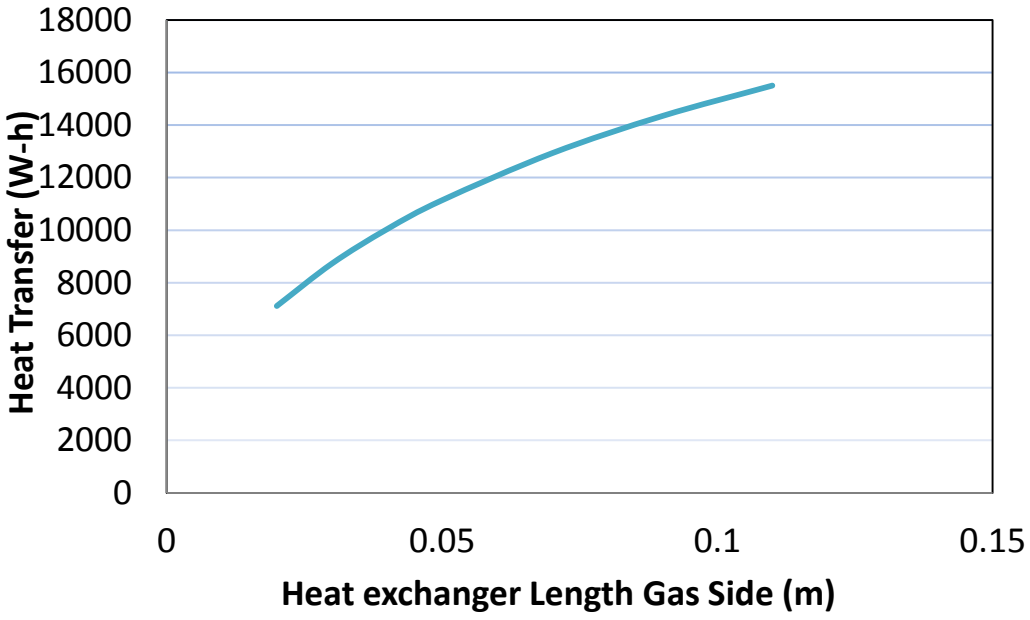

Figure 34: Heat transfer in heat exchanger as function of length on the air side.

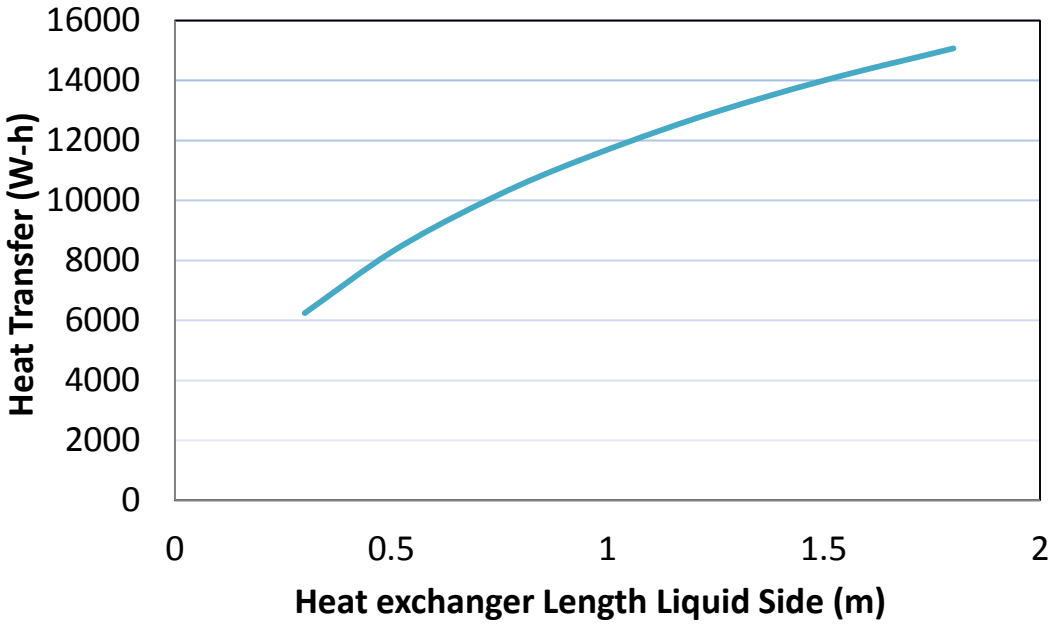

Figure 35: Heat transfer in heat exchanger as function of length on the ethylene glycol side.

The next parameters to study as a function of the air and ethylene glycol flow lengths are the component performances, which are shown in Figure 36 and Figure 37. The component performance for the heat exchanger, which is the heat exchanger effectiveness, follows a growth trend as either heat exchanger length is increased. As expected, the panel performance, which is the heat recovery factor, is not affected by changes in the heat exchanger size. The effectiveness, ε, rises to approximately 0.55 as the lengths are increased, which can be seen in the figures.

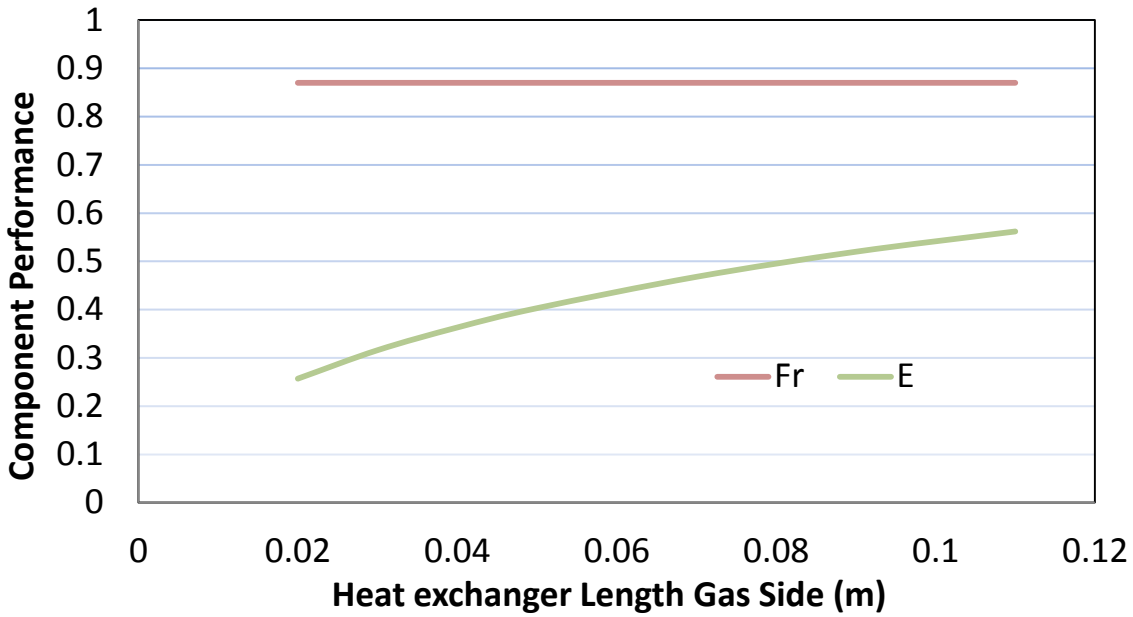

Figure 36: Component performance as function of heat exchanger length on the gas side.

5.1.4 Air Side Flow Rate

This is another fluid used in the cross flow heat exchanger. The fluid used is air, which is usually used when a solar thermal system is used for space heating purposes. The air flow rate affects the heat exchanger performance, thereby affecting the overall system performance. The exact effect can be seen on the air side of the heat exchanger that will be shown in Figures 38-40.

Figure 38 shows inlet and outlet temperatures for the solar array and the heat exchanger. The solar array side temperatures are constant throughout the process because only a one-hour analysis is done; the mass flow rate and inlet temperature to the panel are kept constant. The inlet of the air into the heat exchanger is maintained at 23^{o}C for all the flow rates. As can be seen from Figure 38, there is a drop in heat exchanger outlet temperature as the air flow rate increases.

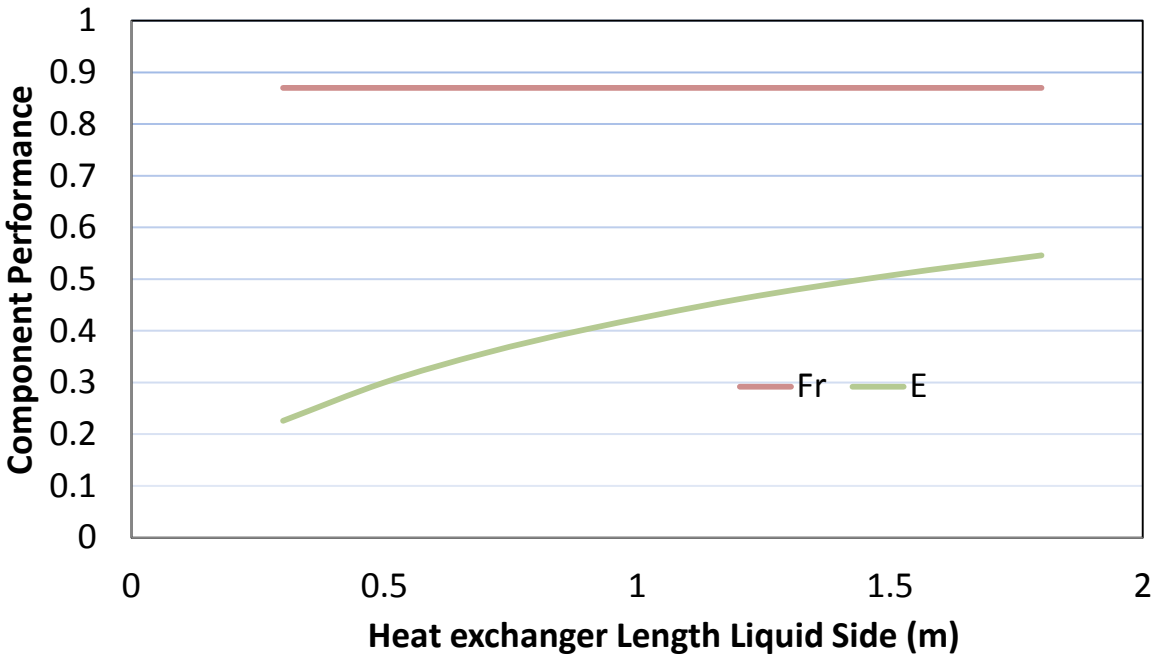

Figure 37: Component performance as function of heat exchanger length on the liquid side.

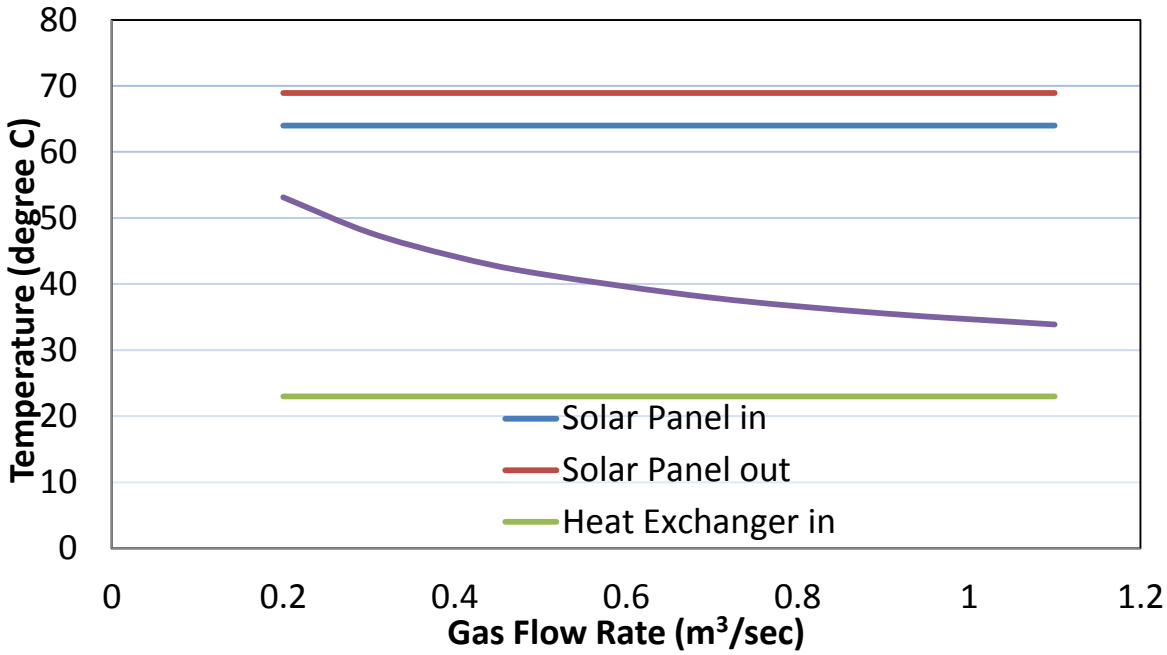

Figure 38: System temperatures as function of air volumetric flow rate.

The next parameter to view is how the heat transfer changes with air side flow rate. This is shown in Figure 39. It can be seen that there is a significant amount of rise in heat transferred

by the heat exchanger as the air flow rate increases. This is due to a larger temperature difference between the ethylene glycol and air as the air flow rate increases. This can be seen in Figure 39.

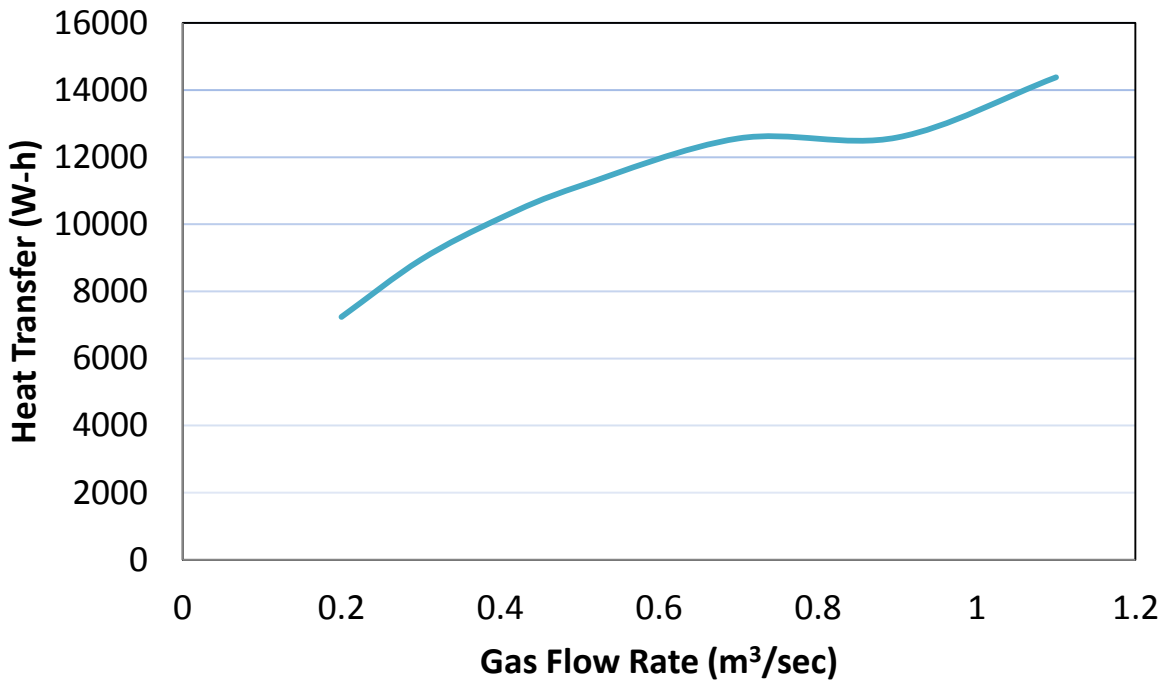

Figure 39: Heat transferred in heat exchanger as a function of air volumetric flow rate.

The plot in Figure 39 depicts the performance of the solar array and the heat exchanger. The solar array has a constant heat removal factor F_r of 0.87. The solar panel has a steady performance because there is no change in the input in the flow rate and inlet temperature. Figure 40 shows that there is a significant drop in the heat exchanger effectiveness, ε, as the airflow rate increases. The rate of rise decreases as the air flow rate increases.

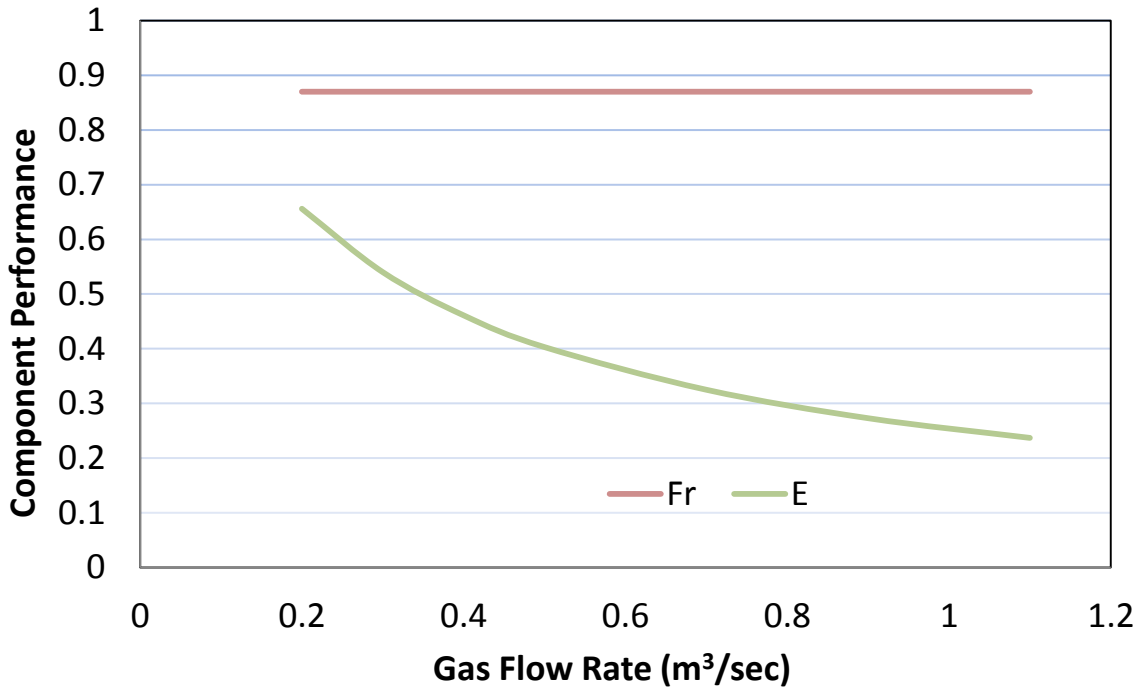

Figure 40: Component performance as function of air volumetric flow rate.

5.2 Results for Minneapolis, Minnesota

The results in this section are for a 2000 ft^2 home located in Minneapolis, MN with an average amount of insulation. This location was chosen because of its relatively long heating season. The results presented below are of two basic types. First, hourly results are presented, which are not the same as the one-hour results presented in Section 5.1, as they were for just one hour and eliminated the storage from the analysis and decoupled the performance of the solar array from the heat exchanger. The hourly results in this sub-section are for 8760 hours, every hour in a year. Storage and coupling between the components in the solar system come into play for every hour after the first one.

5.2.1 Detailed Hourly Results

The size of the solar system used for the detailed hourly results for the Minneapolis, MN analysis is the base results mentioned in the Section 5.1. The solar array is 25 m^2, the flow length

through the solar array is 2 meters, the width of the solar array is 12.5 m, the tilt of the panels is 58.43^0, and the tube spacing in the panels is 0.118 meters. The heat exchanger has 93 layers, an ethylene glycol flow length of 0.9 m, and an air flow length of 0.05 m. The mass flow rate of the ethylene glycol through the system is 0.5 kg/s, and the volumetric air flow rate through the heat exchanger is 0.5 m^3/s. Figure 41 shows four different plots that are given as a function of time in hours. The first plot is Q_{inc}, where Q_{inc} is the amount of solar energy that actually hits the solar array. This plot has a large scale that varies from 0 kW to 40 kW. The second plot, labeled Q_{panel} in Figure 41, shows the amount of energy that the solar array is able to collect and deliver to the ethylene glycol. As can be seen, all the energy that hits the panel does not make it into the ethylene glycol. The difference between these two plots is the amount of energy that is lost back to the environment. On average, half of the energy incident on the solar array makes it into the working fluid, about 10 kW-15 kW, and is carried to the heat exchanger. The third plot in Figure 41 is the amount of energy transferred in the heat exchanger to the air, which is then supplied to the house; Q_{HX} denotes this. For many hours, Q_{HX} is smaller than Q_{panel}, but what is hard to see is that the peaks in the Q_{HX} are wider than in the Q_{panel} plot. The peaks are lower because the heat exchanger is incapable of transferring this much energy between the ethylene glycol and the air, or the demand for heat is not as large as the energy supplied by the solar array. This energy is not lost, it is stored. However, it should be understood that the hotter the ethylene glycol coming out of the heat exchanger, the hotter the ethylene glycol going into the solar array. The hotter the fluid going into the solar array, the less energy collected in the solar array. Thus, there is a reason not to run the system at hot levels. Lastly, in the fourth plot in Figure 41, there are two different colored lines. The green line shows the energy delivered to the room, and the red line shows the heat the home needs. The red line can be called the required heating load of the home. The heat loads for this home in Minneapolis, MN were calculated using the program Energy Plus, which was written by the United States Department of Energy. As mentioned above, the home size was taken to be 2000 ft^2 and to have an average amount of insulation. The forth plot in Figure 41 shows that only a fraction the energy demand is met by the solar system chosen. In the late spring, summer, and early fall, most of the energy demands of the home are met by the solar system. In Figure 41, late spring, summer and early fall runs from about 3000 hours to 6000 hours. Hour number one in the plot is January 1 from midnight to 1 am. It is hard to see that most

of the demand is met between the hours of 3000 and 6000 because the red line lies over the green line. The energy supplied by the heat exchanger is never larger than the energy required by the home. This is made to occur by the control system used.

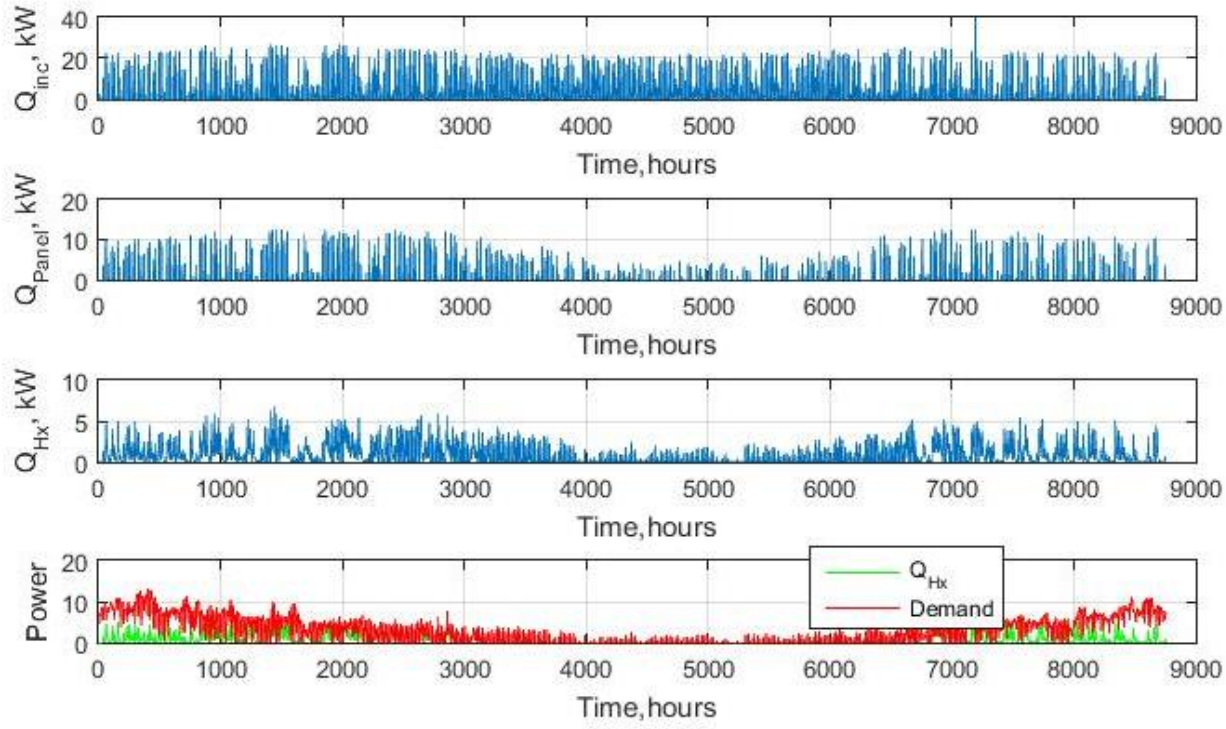

Figure 41: Hourly heat rates for Minneapolis, Minnesota.

Figure 42 shows three different temperatures for all hours of a full year that are important to the operation of the solar system. The first plot is the ambient temperature in Minneapolis. The ambient temperature in Minneapolis varies from -10^{o}C to 0^{o}C in the winter. Therefore, a large amount of heating is required. The second and third plots show the inlet and outlet temperature of the ethylene glycol running through the solar array, which are denoted by $T_{sp,in}$ and $T_{sp,out}$, respectively. A number of rapid ups and downs are seen in the graph, but there is a definite increase in ethylene glycol temperatures in the summer as compared to the winter. This occurs because the solar array puts a good deal of solar energy into the ethylene glycol in the summer, but little is being taken out, because little heating is required in the summer time. In winter, a great deal of heating is required, so the ethylene glycol temperatures are lower. It should be

noted that the ethylene glycol in temperatures look just like the ethylene glycol out temperature. Over half of them are exactly the same because no heat is transferred to the ethylene glycol when there is not sun. The location where there are differences cannot be seen very well because the differences are not that big relative to the temperature scale used in these plots.

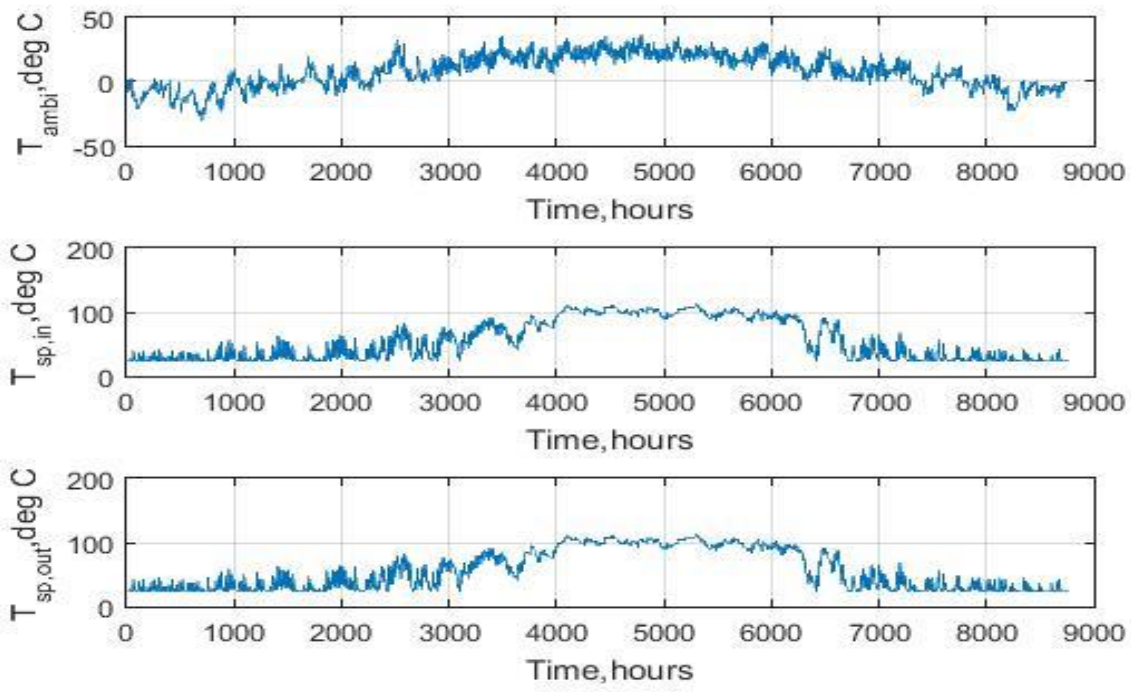

Figure 42: Hourly ambient and ethylene glycol temperatures for Minneapolis, MN.

Figure 43 shows two plots that are temperatures in the system, but these are on the air side of the heat exchanger. These are the temperatures of the air from the home and the air being delivered to the home. $T_{load,in}$ is the set temperature of the air in the house, which is taken as 23^{o}C for this work. As seen in Figure 43, this temperature does not change. $T_{load,out}$ is the temperature of the air that comes out of the heat exchanger and is delivered to the home. This air maintains the home at 23^{o}C and therefore must be higher than 23^{o}C. It can be seen in the second plot that this temperature is about 30^{o}C in the winter on many days, which is sufficient to heat the home.

In the remaining subsections of Section 5.2, yearly-integrated results are presented for the 2000 ft^2 home in Minneapolis, MN. A number of design and operating parameters for the solar system were surveyed to see how they affect the system performance, including the area of the

solar array, the tilt of the solar panels, the arrangement of the solar panels in the solar array, the size of heat exchanger, the mass flow rate of ethylene glycol through the solar array, and the volumetric flow rate of air through the heat exchanger. These survey results give a clearer idea of how the solar thermal system behaves as a function of design parameters and operating parameters.

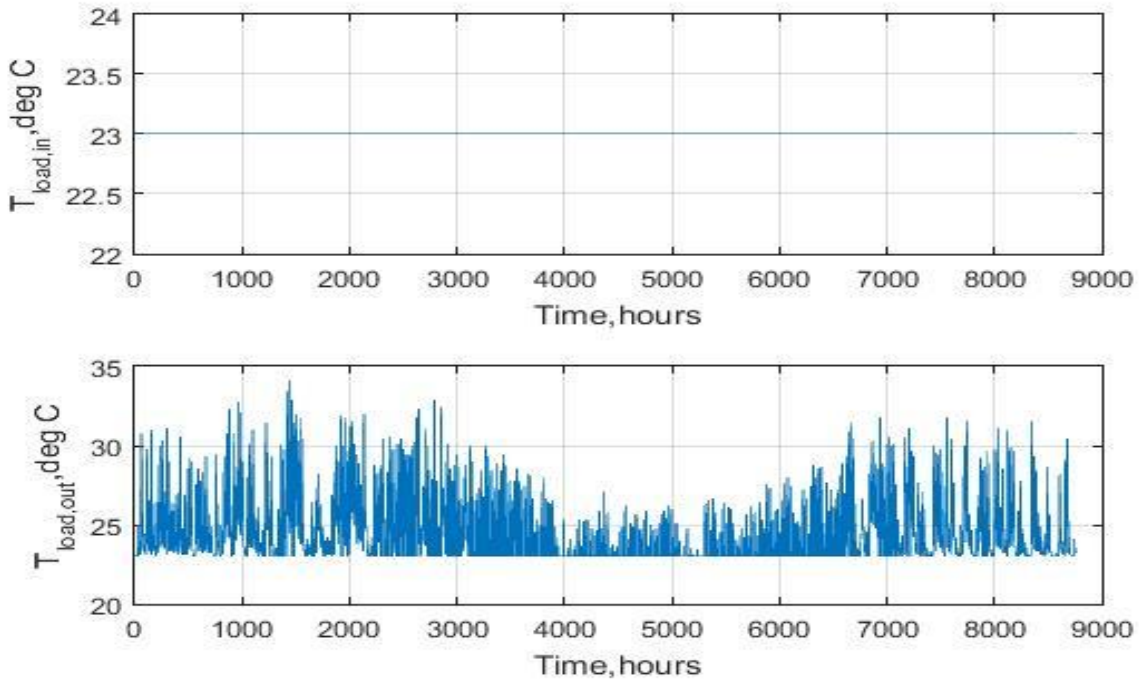

Figure 43: Hourly air temperatures for Minneapolis, MN.

5.2.2 Area of Solar Array

This is an important parameter to be studied because the amount of solar energy intercepted is directly proportional to the area of the solar array. This is a major design parameter. Figure 44 shows the efficiency of the solar array and overall efficiency of the solar thermal system as a function of the area of the solar array. Areas from 10 m^2 to 60 m^2 are surveyed. The array length is taken as 2 m, and the width of the array is varied to change the total collection area. All other parameters of the system are the base values presented for the detailed hourly results in Sub-Section 5.2.1. At the start of the analysis, which is January 1 at midnight,

the ethylene glycol inlet temperature is taken as 23°C. Figure 44 shows the efficiency of the solar array and the overall solar system efficiency. The solar array efficiency curve cannot be seen because it lies right under the overall system efficiency. This occurs due to small energy storage, which happens on an hourly basis (see Figure 41), but not on a yearly basis. When it comes to yearly results, the heat transfer values are integrated over a year so it averages out (see Figure 41). Therefore, the all the energy coming into the panel goes out the heat exchanger. There are no losses in our storage system or heat exchanger in our model. Therefore, we can see both lines overlapping each other. This phenomenon will be seen in all the upcoming results as the storage system is always small. Both the solar array efficiency and the overall solar system efficiency decrease as the panel area is increased. This occurs because a greater fraction of the energy collected by a small solar array is used as heat to keep the home comfortable as compared to a large solar array. When the array becomes larger, the time when the energy collected by the solar array cannot be used increases. This means the ethylene glycol running through the solar panels runs hotter and loses more energy to the environment in the solar panels.

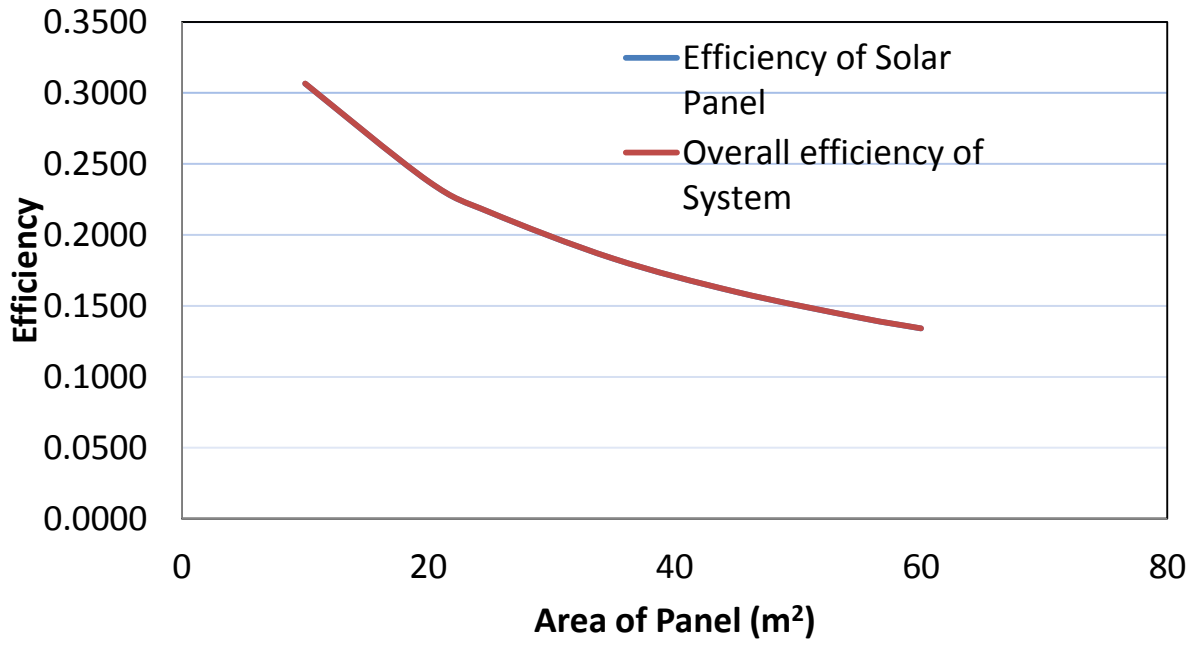

Figure 44: Efficiency of solar array and solar system as a function of the area of solar array for Minneapolis, MN.

The next performance parameters displayed (see Figure 45) are the energy collected by the solar array and the energy transferred in the heat exchanger. Just like the efficiencies, these two curves fall on top of one another and only one of the lines can be seen. The energy collected by the solar panels is the line that is visible and the energy transferred in the heat exchanger is directly underneath this line. Both of these energy flows increase as the area of the solar array increases. The maximum energy gain by the collector for this survey is near to 12000 kW-h for a panel size of 60 m^2 and the heat exchanger has a comparable gain of approximately 12000 kW-h for the same size of solar array. The reader should note that the energies increase with array area (see Figure 45), and the efficiencies decrease with increasing array area (see Figure 44), because efficiencies deal with fractions of energies not the total energies.

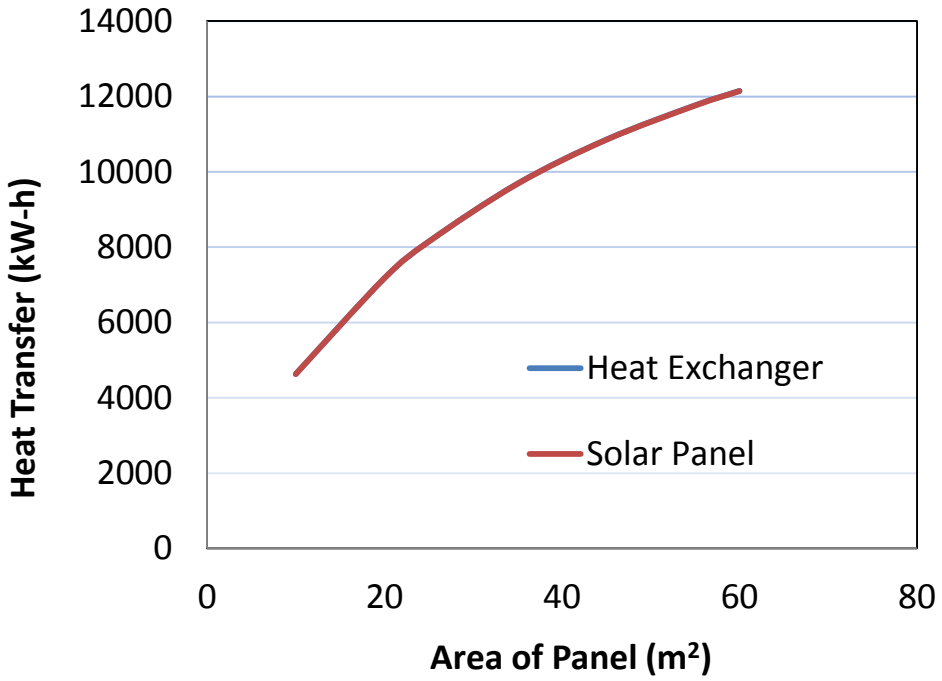

Figure 45: Yearly useful heat gain in solar array and yearly heat transfer in heat exchanger as a function of the solar array area for Minneapolis, MN.

The next parameter is important since it gives the fraction of the home's heating load that can be delivered as a function of the area of the panel. This is seen in Figure 46, which shows that a rather large solar array is required to meet about 50% of the home's total heating demand.

Furthermore, 60 m^2 (646 ft^2) is a large solar array for a 2000 ft^2 home. It would take a rather large south facing roof, 646 ft^2, to accommodate such a solar array.

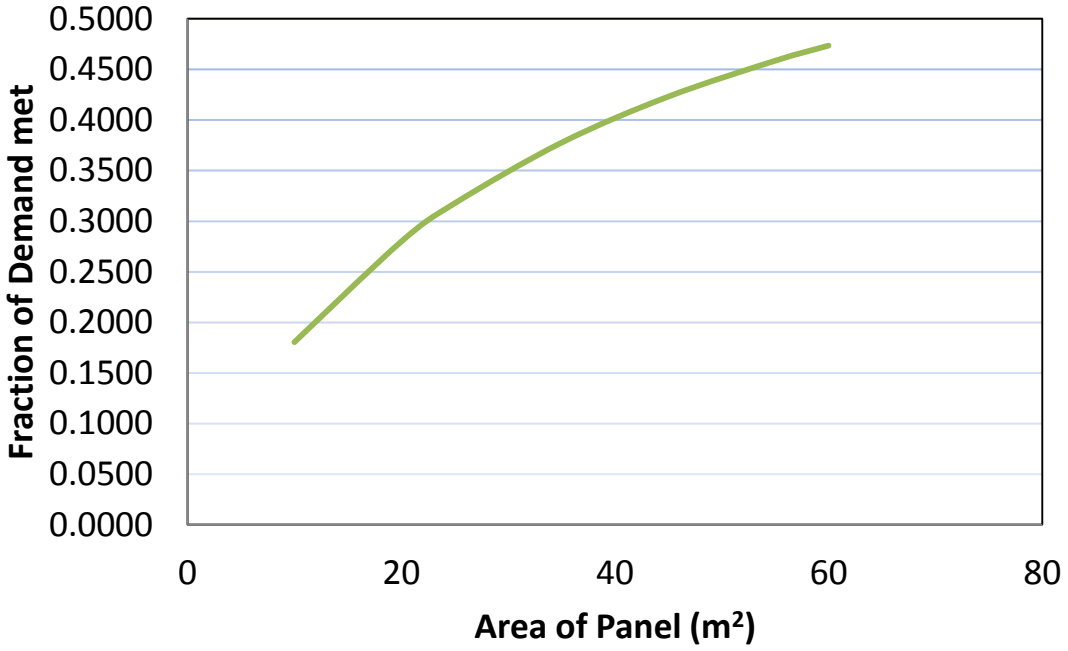

Figure 46: Fraction of heat load delivered as a function of the solar array area for Minneapolis, MN.

5.2.3 Tilt of Solar Panel

The tilt of a solar panel determines the amount of energy intercepted by the panel. As it is desired to get the most from a solar thermal system, there is a need to orientate and tilt the solar panels in way that they will capture the most energy from the sun. There is no question about which direction the panels should be orientated. In the northern hemisphere, fixed solar panels should point due south, and in the southern hemisphere, solar panels should point due north. The optimum tilt angle of the solar panels is a little bit more involved. If the goal is to capture the most solar energy over the course of a year, one tilt angle should be used. However, if the desire is to collect the most energy during the winter, when heating demand is high, another tilt angle should be used. In this survey work, an optimum tilt is found that maximizes the amount of solar energy captured during the winter. If the latitude at which the solar panels are located is between

25°and 50°, the recommended tilt angle for winter is $latitude \times 0.875 + 19.2^{o}$ [50]. Since the latitude of Minneapolis is 44.83°, the recommended tilt angle is 58.4°. Instead of just accepting this recommendation outright, a survey was done to see what is the optimum tilt angle for the particular situation being studied here. Figure 47 shows that the recommended optimum tilt angle of 58.43° is correct for the system being studied here. At this tilt angle, a 25 m^2 solar array collects slightly over 8000 kW-h of energy to the ethylene glycol flowing through it. For this system the yearly useful heat gain in the solar collector is the same as the yearly heat transfer in the heat exchanger, these two curves fall over the top of one another in Figure 47.

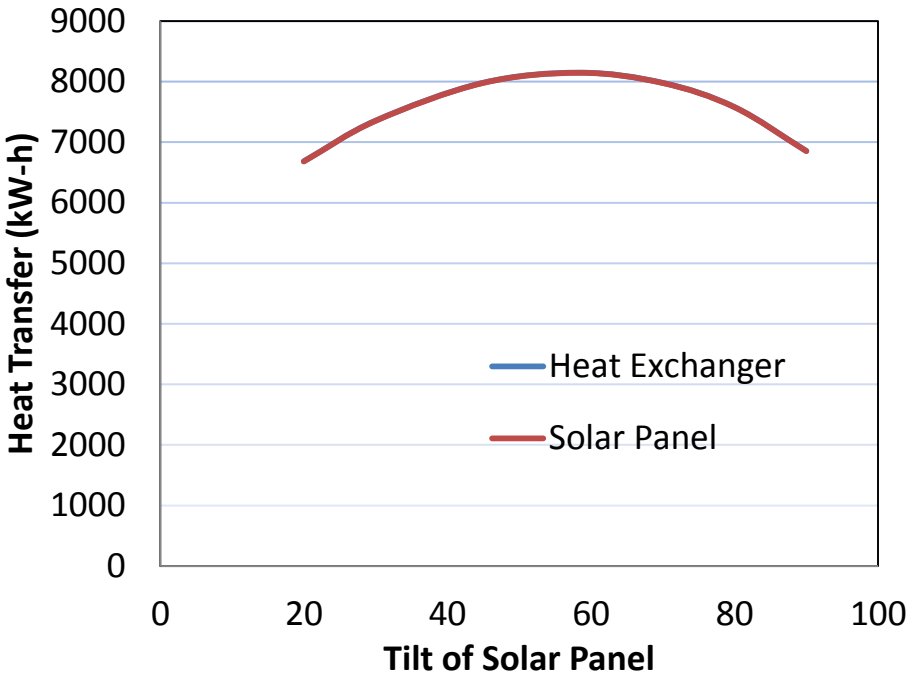

Figure 47: Yearly useful heat gain in solar array and yearly heat transfer in heat exchanger as a function of the panel tilt for Minneapolis, MN.

Figure 48 depicts the fraction of heat load met with the solar system as a function of the tilt of the panels. Like the energy gain plot in Figure 47, the fraction of demand plot also shows the optimum tilt angle is about 58.4°. At the optimum tilt, about 32% of the heat load of the home is met with the solar system. This fraction of demand plot goes to 25% for a tilt angle of 90°.

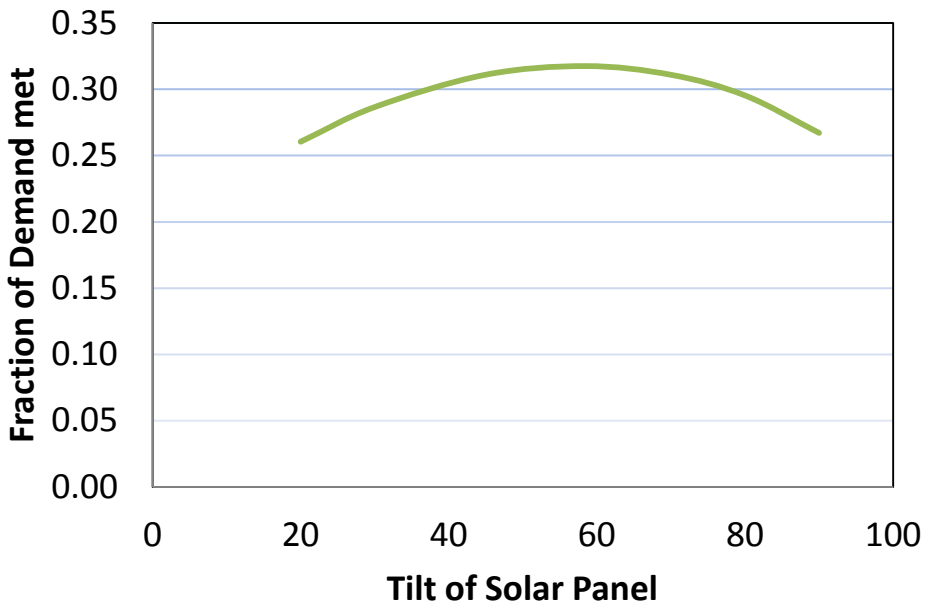

Figure 48: Fraction of heat load delivered as a function of the panel tilt for Minneapolis, MN.

5.2.4 Arrangement of Solar Panels

The arrangement of panels refers to placing solar panels in series or parallel with respect to the ethylene glycol flow. In this survey, the overall area is kept constant. A series arrangement of solar panels is obtained by connecting the outlet port of one solar panel to the input port of the next solar panel. A parallel arrangement of solar panels is accomplished by splitting the ethylene glycol flow between the solar panels. In this survey, only one panel in series, two panels in series, and three panels in series are simulated. The total area of the solar array is kept constant at 25 m^2 for all of the arrangements. The results of using a parallel or series arrangement of solar panels is shown in Figures 49, 50, and 51. Figure 49 depicts the energy efficiencies for the solar array and for the entire system as a function of the length of the solar array. Figure 50 shows the useful energy collected by the solar array and the amount of heat transferred in the heat exchanger. Figure 51 shows the fraction of the energy demand that is met by the solar system. All three of these figures show no effect of having the solar array in a more series arrangement as compared to a more parallel arrangement. This same result was obtained in the one-hour results. Once again, it should be noted that this may not be the case if the ethylene glycol flow is greatly reduced. Both Figures 49 and 50 show only one curve, even though two quantities are plotted in

both of these figures. As in other graphs displayed in this thesis, the plots of the two respective quantities lie on top of one another.

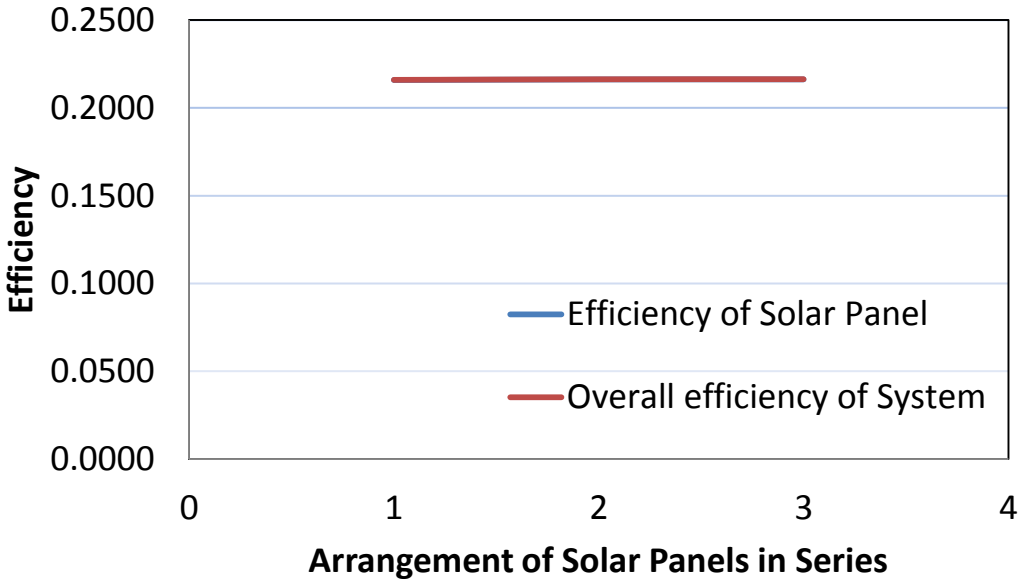

Figure 49: Efficiency of solar array and overall system efficiency as a function of the arrangement of the panels in series for Minneapolis, MN.

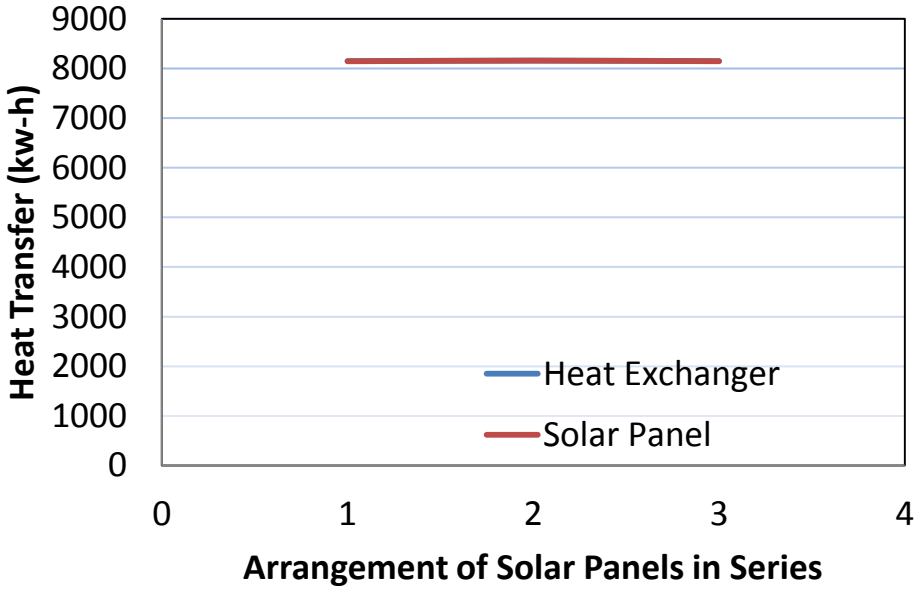

Figure 50: Yearly useful heat gain in solar array and yearly heat transfer in heat exchanger as a function of the arrangement of the panels in series for Minneapolis, MN.

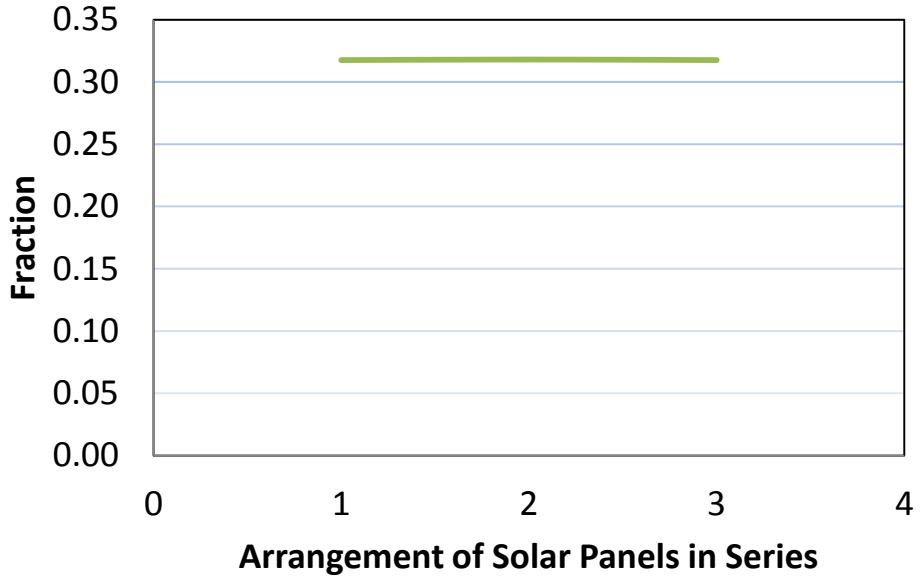

Figure 51: Fraction of heating load delivered as a function of the arrangement of the panels in series for Minneapolis, MN.

5.2.5 Ethylene Glycol Flow Rate

It was observed in the one-hour results presented in the first section of this chapter that increasing the ethylene glycol flow rate increases the energy gain and decreases the temperature rise of the ethylene glycol across the solar array. This correspondingly affects the efficiencies present in the system. Figure 52 depicts the solar array efficiency and the overall system efficiency as a function of the ethylene glycol flow rate. The rise in efficiencies can be seen in Figure 52, but after an ethylene glycol mass flow rate of 0.5 kg/sec, the efficiencies level off at a value near to 22%. Therefore, 0.5 kg/sec is a sufficient glycol mass flow rate to achieve effective system performance. Once again, the two efficiencies are equal and only one can be seen in the graph.

Figure 53 shows the energy captured by the solar array and the energy transferred in the heat exchanger. Figure 54 shows the fraction of the heating load that is met by the solar system. For all of these parameters, there are steep increases at low ethylene glycol mass flow rates, but the increases tend to level off at high flow rates. For this reason, it is felt that an ethylene glycol mass flow rate of 0.5 kg/sec is a reasonable mass flow rate at which to operate this system located in Minneapolis, MN.

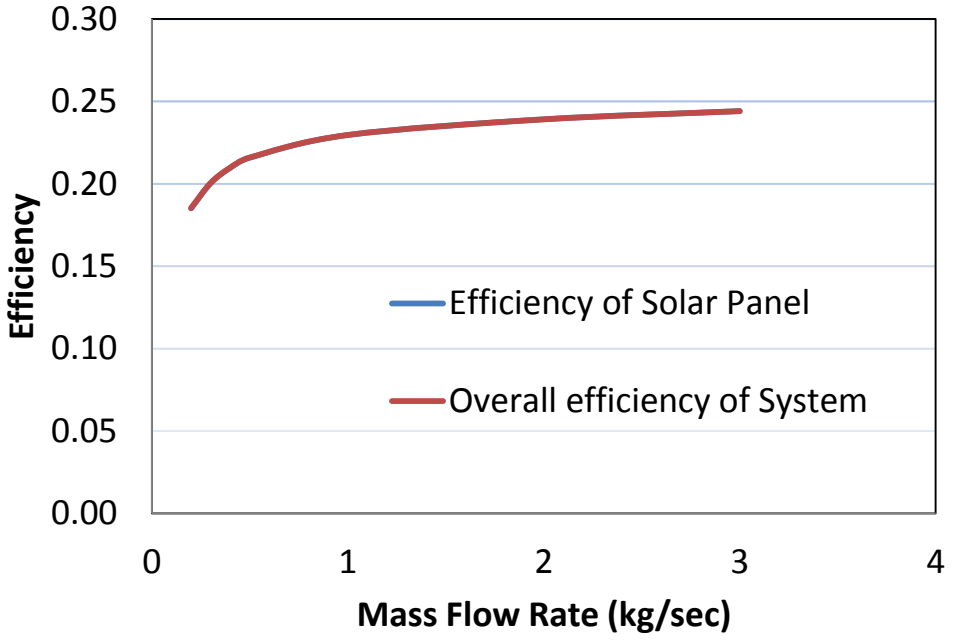

Figure 52: Efficiency of solar array and overall system efficiency as a function of the ethylene glycol mass flow rate for Minneapolis, MN.

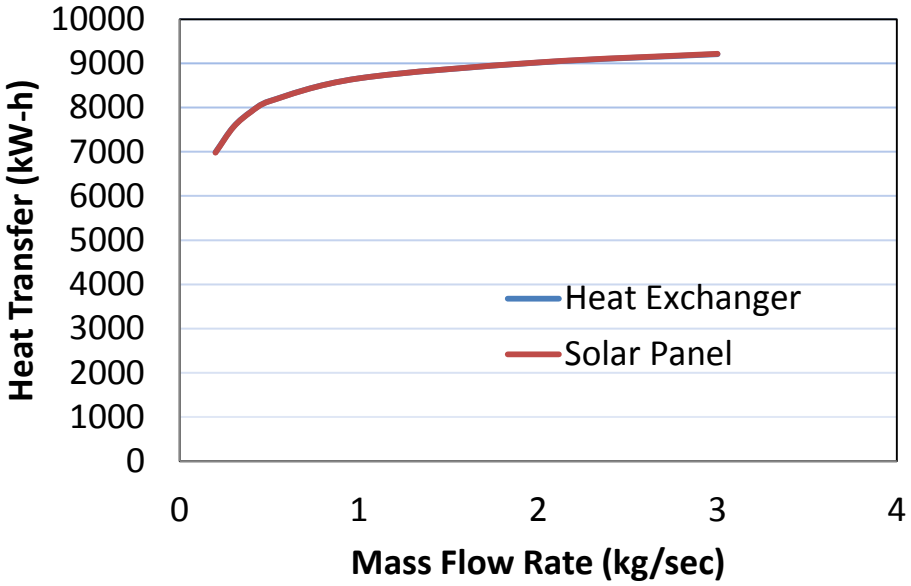

Figure 53: Yearly useful heat gain in solar array and yearly heat transfer in heat exchanger as a function of the ethylene glycol mass flow rate for Minneapolis, MN.

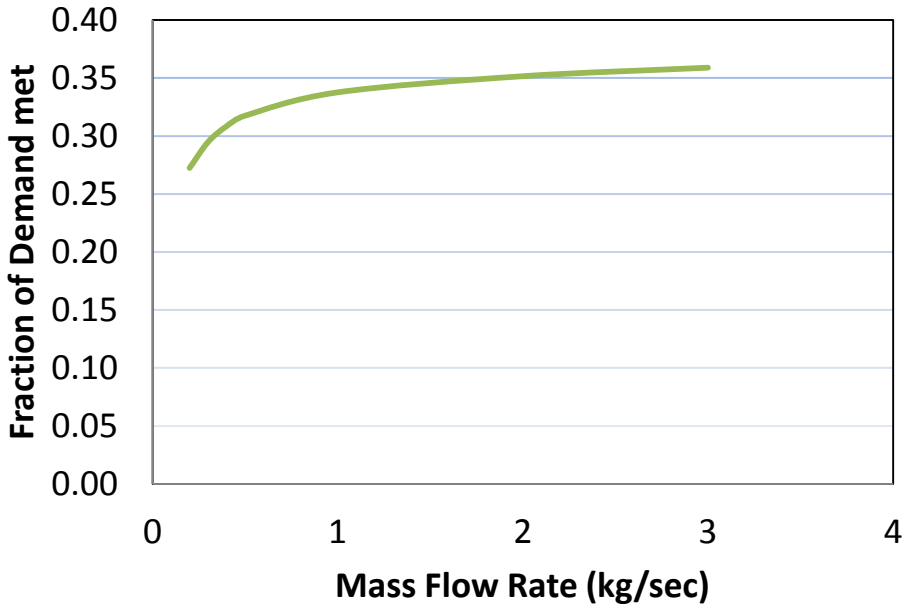

Figure 54: Fraction of heat load delivered as a function of the ethylene glycol mass flow rate for Minneapolis, MN.

5.2.6 Air Side Flow Rate

Figures 55, 56 and 57 show the efficiencies, energy flows, and fraction of heat load met, respectively, as a function of the air flow rate through the heat exchanger. The trends shown in these figures are similar to those shown in Figures 52, 53, and 54, respectively, as a function of the ethylene glycol flow rate. The difference is the rise at lower flow rates is not as pronounced. All three of these figures show that an air volumetric flow rate of 0.5 m^3/kg is sufficient to provide good performance of the solar system.

5.2.7 Size of Heat Exchanger

The size of the heat exchanger can be changed by varying three input parameters: the number of layers used in the heat exchanger, the flow length of the ethylene glycol, and the flow length of the air. In all the results presented in this thesis 93, layers of ethylene glycol-air flow paths are always used, and thus the height of the heat exchanger remains constant. The size of the

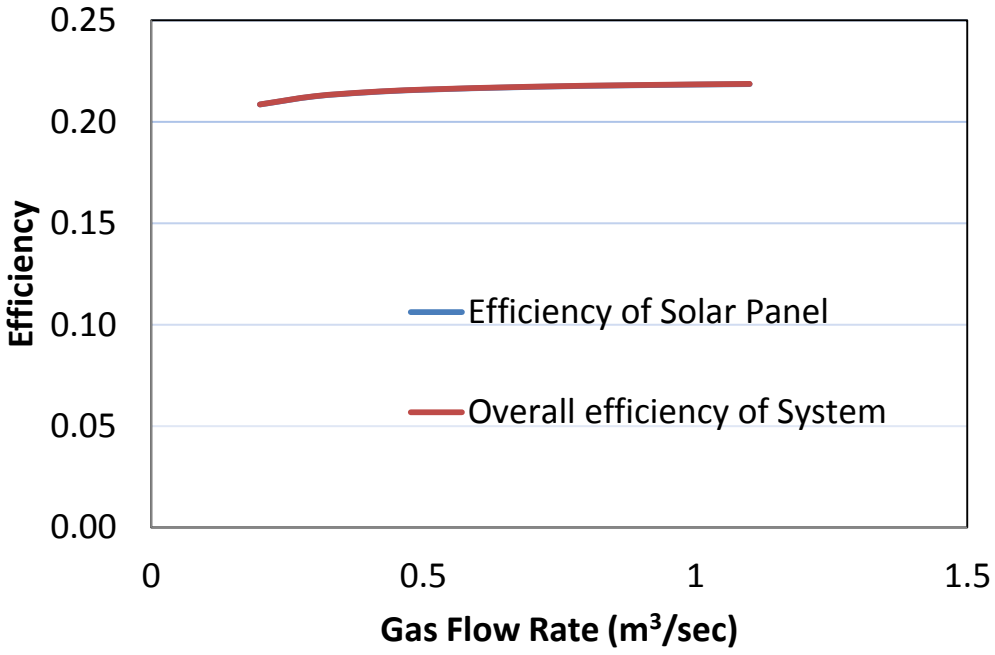

Figure 55: Efficiency of solar array and overall system efficiency as a function of the air volumetric flow rate for Minneapolis, MN.

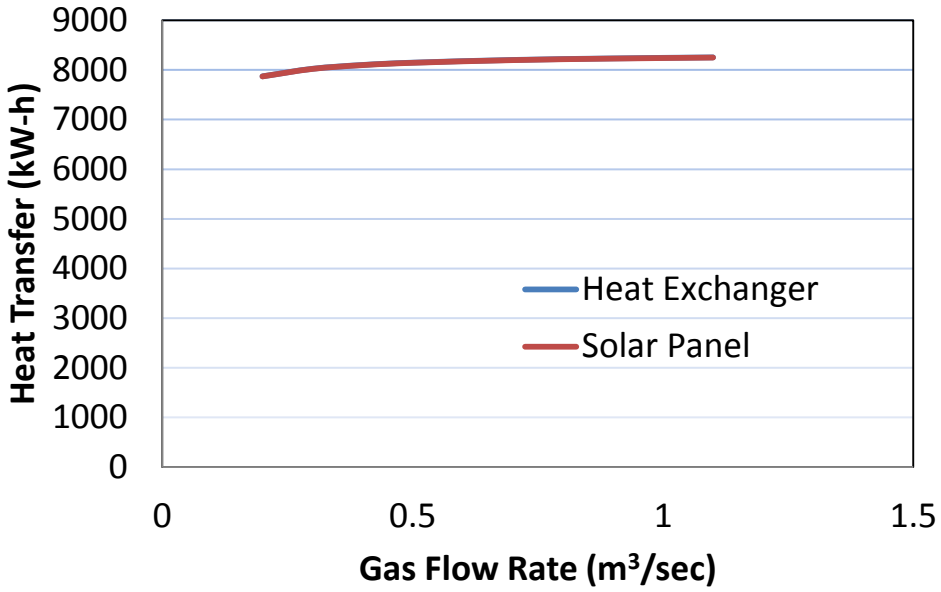

Figure 56: Yearly useful heat gain in solar array and yearly heat transfer in heat exchanger as a function of the air volumetric flow rate for Minneapolis, MN.

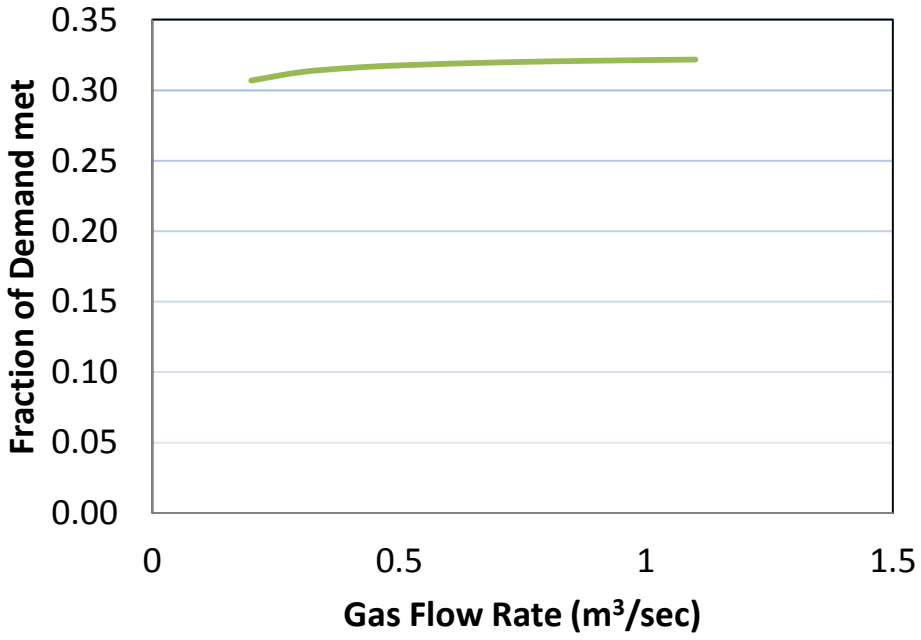

Figure 57: Fraction of heating load delivered as a function of air volumetric flow rate for Minneapolis, MN.

heat exchanger is varied by changing the flow length of the ethylene glycol or the flow length of the air.

Figures 58 and 59 shows the effect of changing the flow length of the ethylene glycol or the flow length of the air, respectively. Both of these figures show the overall efficiency of the solar system and the efficiency of the solar panels. As was the case for many of the results already shown, these efficiencies are the same, so only one line is visible on these plots. Whether the flow length of the heat exchanger is increased on the ethylene glycol side or the air side the results are similar, there is a small increase in the efficiencies at low flow rates and then changes become insignificant. For the heat exchanger length on the ethylene glycol side, the plot goes relatively flat at a flow length of 0.5 m. Because of other plots shown in this thesis, the base flow length chosen for the ethylene glycol side of the heat exchanger is 0.9 m. Figure 61 shows that a base flow length on the air side of the heat exchanger of 0.05 means the system is operating close to its peak efficiencies.

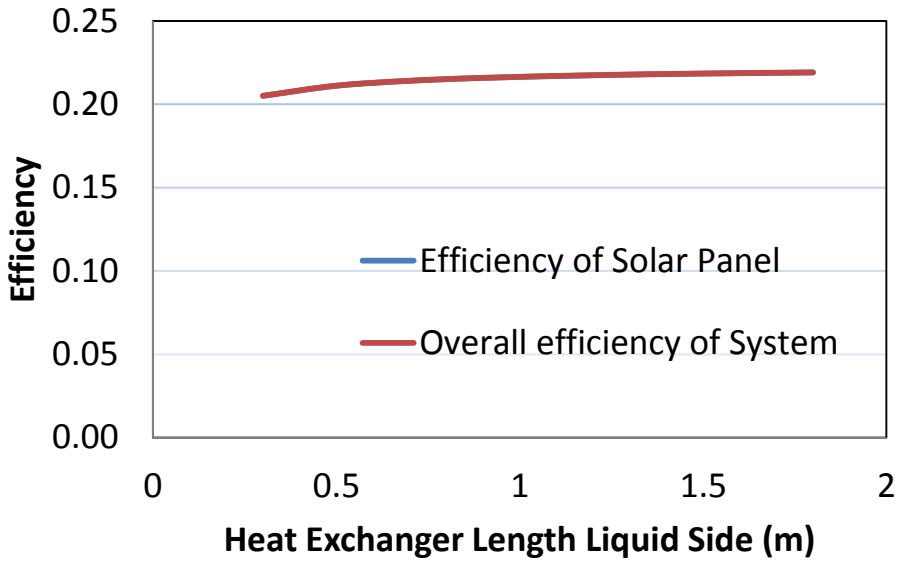

Figure 58: Efficiency of solar array and overall system efficiency as a function of heat exchanger length on ethylene glycol side for Minneapolis, MN.

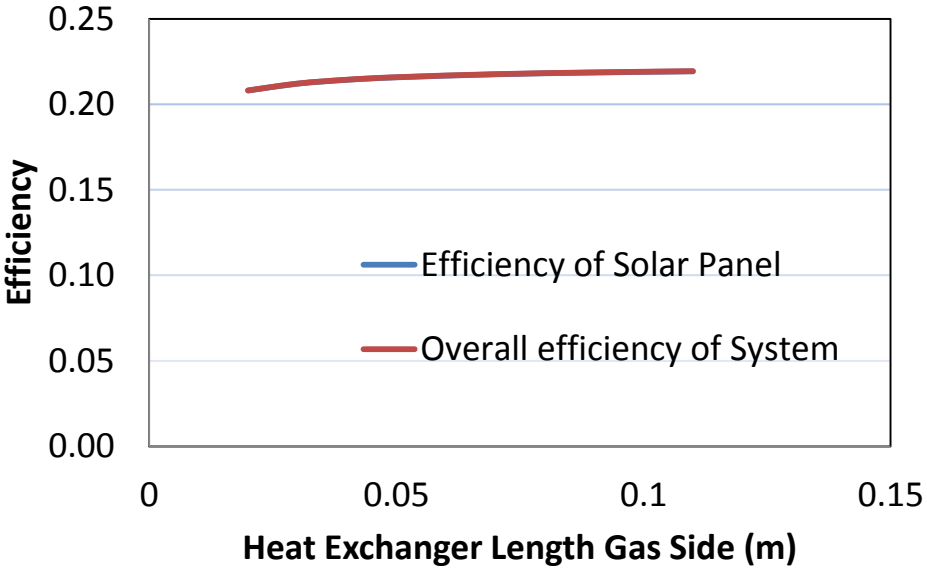

Figure 59: Efficiency of solar array and overall system efficiency as a function of heat exchanger length on air side for Minneapolis, MN.

Figures 60 and 61 show the energy flows in the solar system as a function of the ethylene glycol flow length and the air flow length, respectively. These figures are similar to the efficiency plots shown in Figures 58 and 59. There are some small increases at the smaller

lengths, but the curves flatten at larger flow lengths. A flow length of 0.9 m on the ethylene glycol side and 0.05 m on the air side are sufficient to have the solar system operating at near maximum heat transfer values. Figures 62 and 63, which are the fraction of heat load met by the solar system graphs, have the same behavior as the heat transfer and efficiency plots.

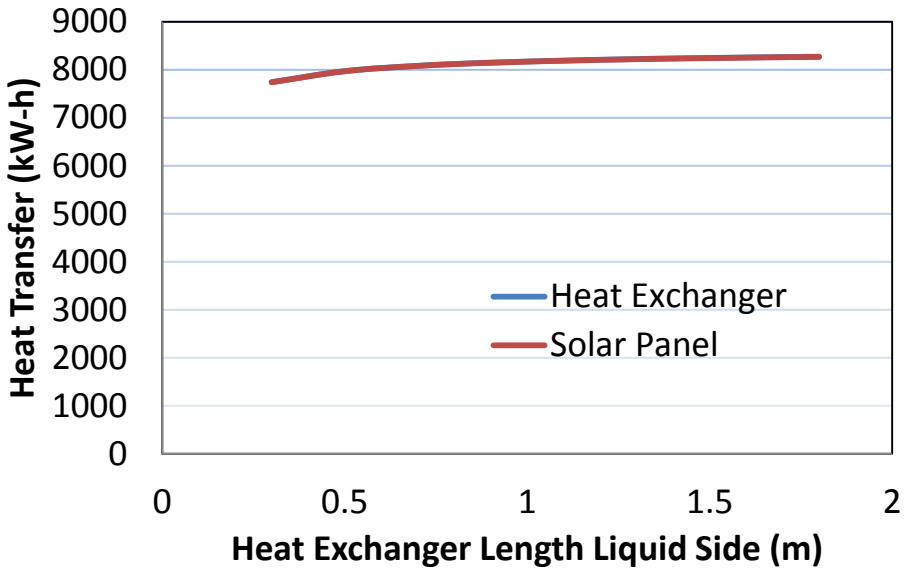

Figure 60: Yearly useful heat gain in solar array and yearly heat transfer in heat exchanger as a function of the heat exchanger length on the ethylene glycol side for Minneapolis, MN.

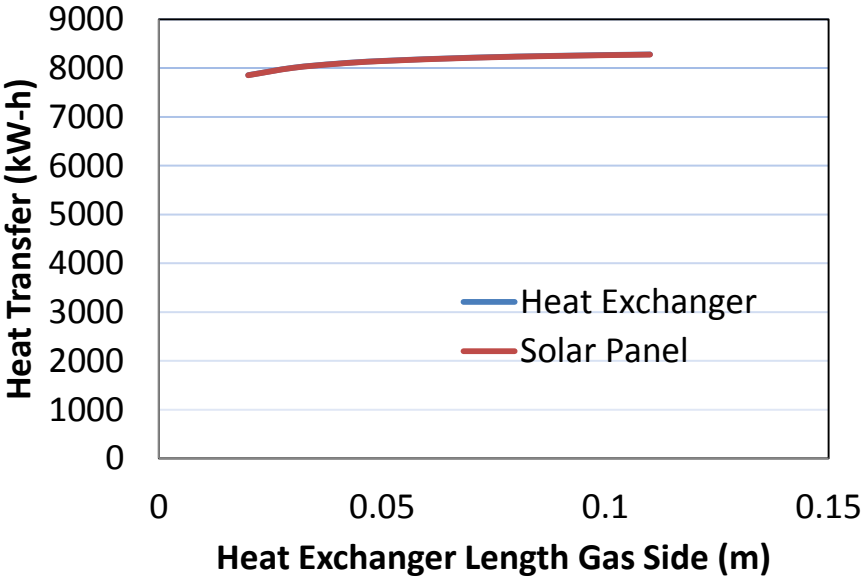

Figure 61: Yearly useful heat gain in solar array and yearly heat transfer in heat exchanger as a function of the heat exchanger length on the air side for Minneapolis, MN.

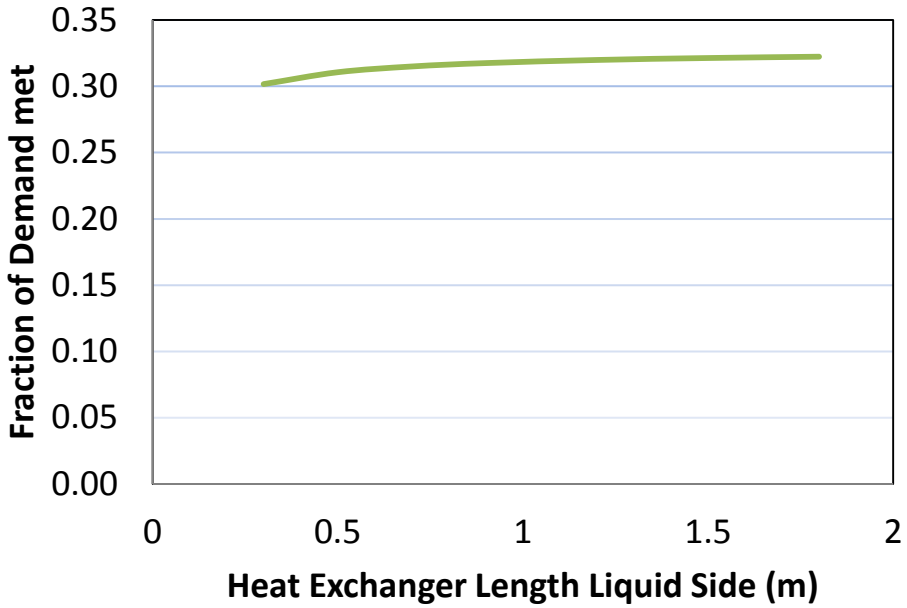

Figure 62: Fraction of heating load delivered as a function of heat exchanger length on the ethylene glycol side for Minneapolis, MN.

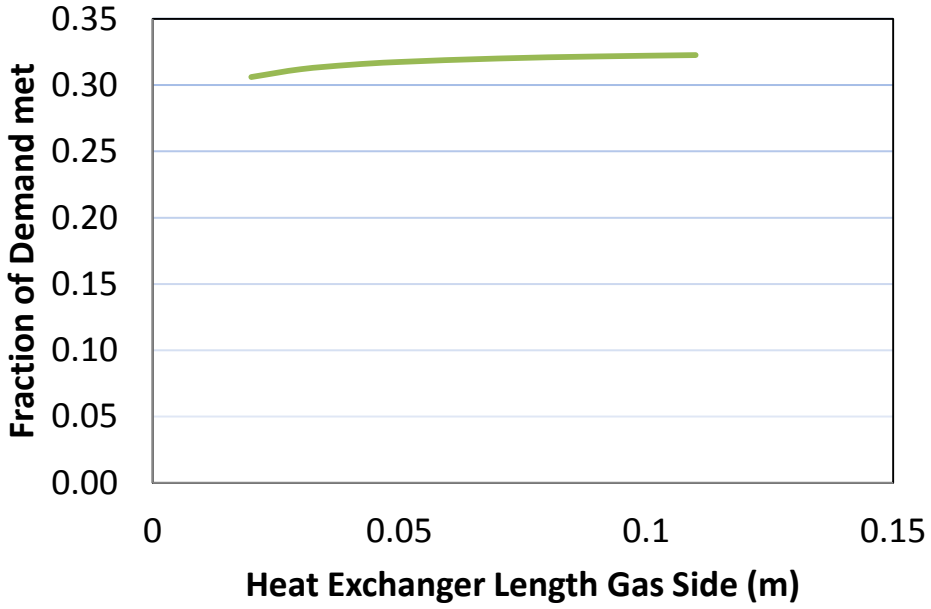

Figure 63: Fraction of heating load delivered as a function of heat exchanger length on the air side for Minneapolis, MN.

5.3 Results for Dayton, Ohio

The results in this section are for a 2000 ft^2 home with an average amount of insulation located in Dayton, OH. This location was chosen because it is the location of Wright State University, where this work is being carried out. This location has what could be considered a moderate winter and a moderate heating season length. This location receives optimal amounts of sunshine in the summer months, but does tend toward being cloudy during a number of the colder months. Just like Minneapolis, MN in Section 5.2, a number of design and operating parameters are surveyed. In fact, the same parameters are surveyed in the same order as for Minneapolis, MN. The reason for doing this is so the Dayton, OH results can be compared to the Minneapolis, MN results. The discussion of the results in this section will be less than that for the Minneapolis, MN results because many of the trends are the same, just the magnitudes have changed.

5.3.1 Detailed Hourly Results

The size of the solar system used for the detailed hourly results for the Minneapolis, MN analysis in Section 5.2 is also used for the Dayton, OH results. The solar array is 25 m^2, the flow length through the solar array is 2 meters, the width of the solar array is 12.5 m, the tilt of the panels is 44.9^o, and the tube spacing in the panels is 0.118 meters. The heat exchanger has 93 layers, an ethylene glycol flow length of 0.9 m, and an air flow length of 0.05 m. The mass flow rate of the ethylene glycol through the system is 0.5 kg/s, and the volumetric air flow rate through the heat exchanger is 0.5 m^3/s. Figure 64 shows four different plots that are given as a function of time in hours. This figure shows the same type of results for Dayton, OH that Figure 41 shows for Minneapolis, MN. The results for all four graphs in this figure look similar between Dayton and Minneapolis. Upon close inspection, it can be seen that the plots for Dayton, OH look a little smaller in magnitude and the lines are a little less dense. It is both the height and density of the lines that dictate the amount of energy being collected and delivered by the solar system. Later on, when the yearly integrated results are presented, more concrete comparisons between the energy values can be made. It should also be noticed the energy required to heat a home in Dayton, OH is less than that in Minneapolis, MN. Since these homes are almost identical, comparing the heating demand curves in the last graph in Figures 64 and 41 is valid. The amount of energy supplied by the solar system in Minneapolis appears to be more than the

amount supplied in Dayton. These conclusions will be made more concrete when yearly integrated results are presented. Since the solar systems used in both locations are exactly the same, these comparisons are valid.

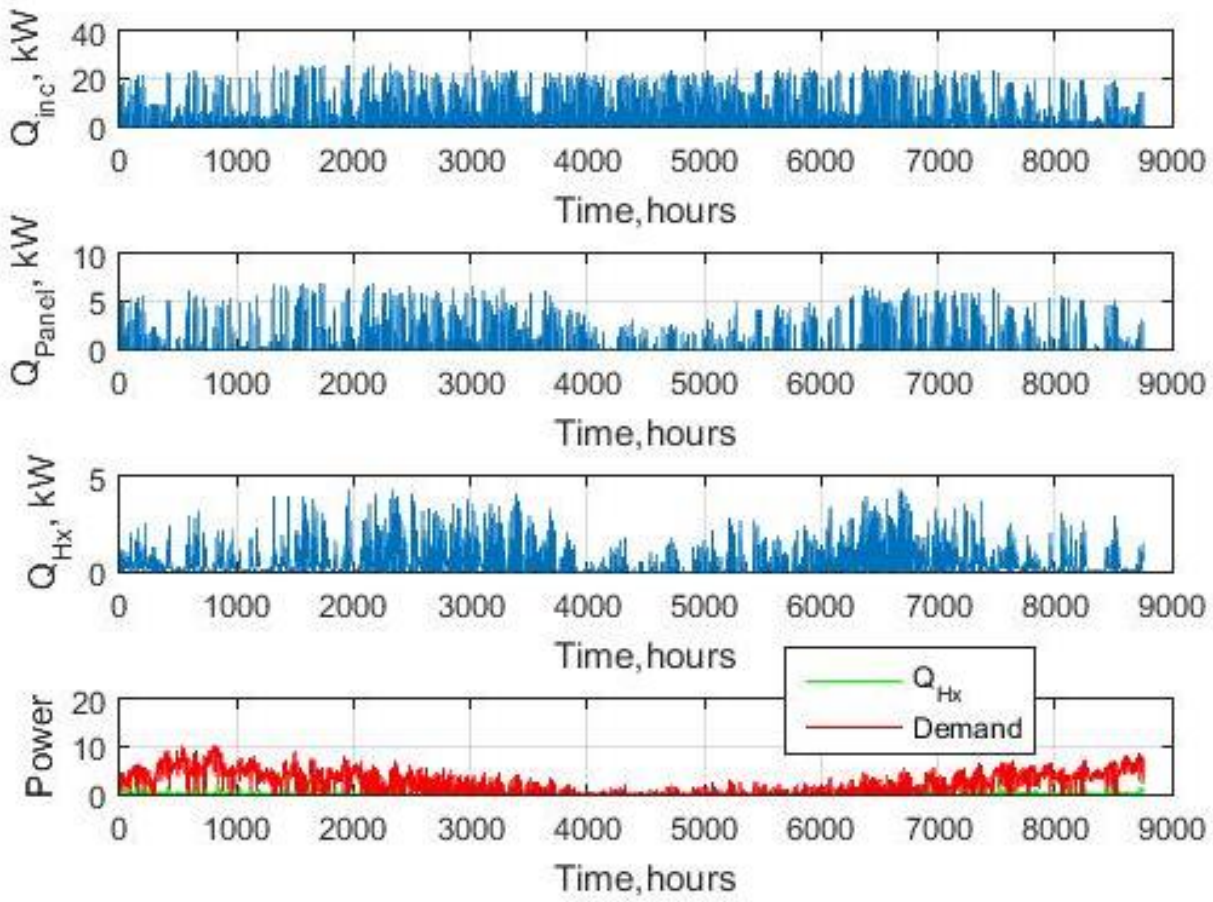

Figure 64: Hourly heat rates for Dayton, Ohio.

The temperatures shown in Figures 65 and 66 show all the system temperatures, the ethylene glycol inlet and exit temperatures from the solar array, the air inlet and exit temperatures from the heat exchanger, and the ambient temperatures throughout the year for Dayton, OH. Figure 65 for Dayton should be compared to Figure 42 for Minneapolis, and Figure 66 should be compared to Figure 43. The first thing that is noticed is the ambient temperatures for Dayton, OH do not get as low as those for Minneapolis, MN during the winter season. It is also noticed that the peak temperatures in the summer are similar for both locations. Minneapolis may not get as many of these high temperatures as Dayton, but they do reach about the same

peaks. The ethylene glycol temperatures at the inlet and exit from the solar array are similar; however, it does appear that the temperatures of the ethylene glycol for the system in Dayton reach higher peaks in the summer time. In the winter, Dayton appears to have fewer peaks in the temperatures. This is believed to be due to fewer sunny winter days in Dayton than in Minneapolis. The plots of the inlet air temperature to the heat exchanger are exactly the same in both locations because this is a set value. In these analyses, the indoor air temperature was maintained at 23^{o}C in both Minneapolis and Dayton. The outlet air temperatures are somewhat different, but there are no striking differences.

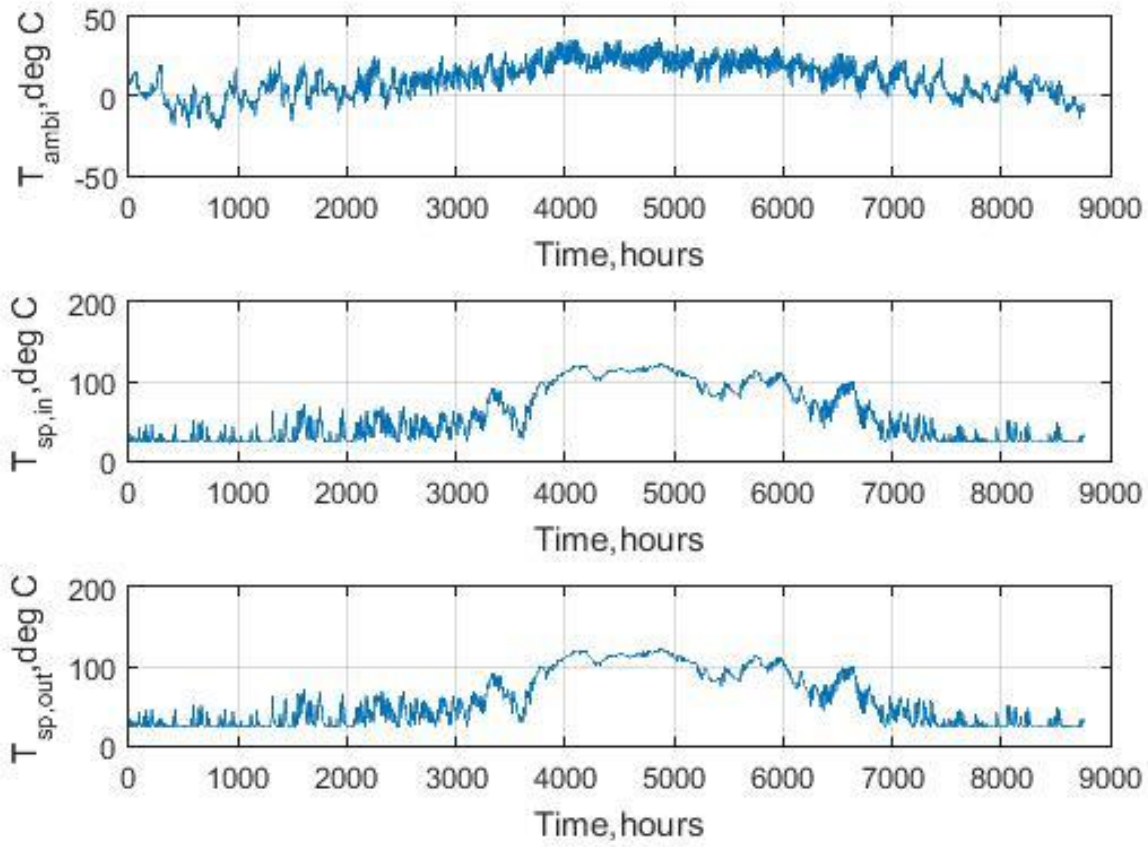

Figure 65: Hourly ambient and ethylene glycol temperatures for Dayton, Ohio.

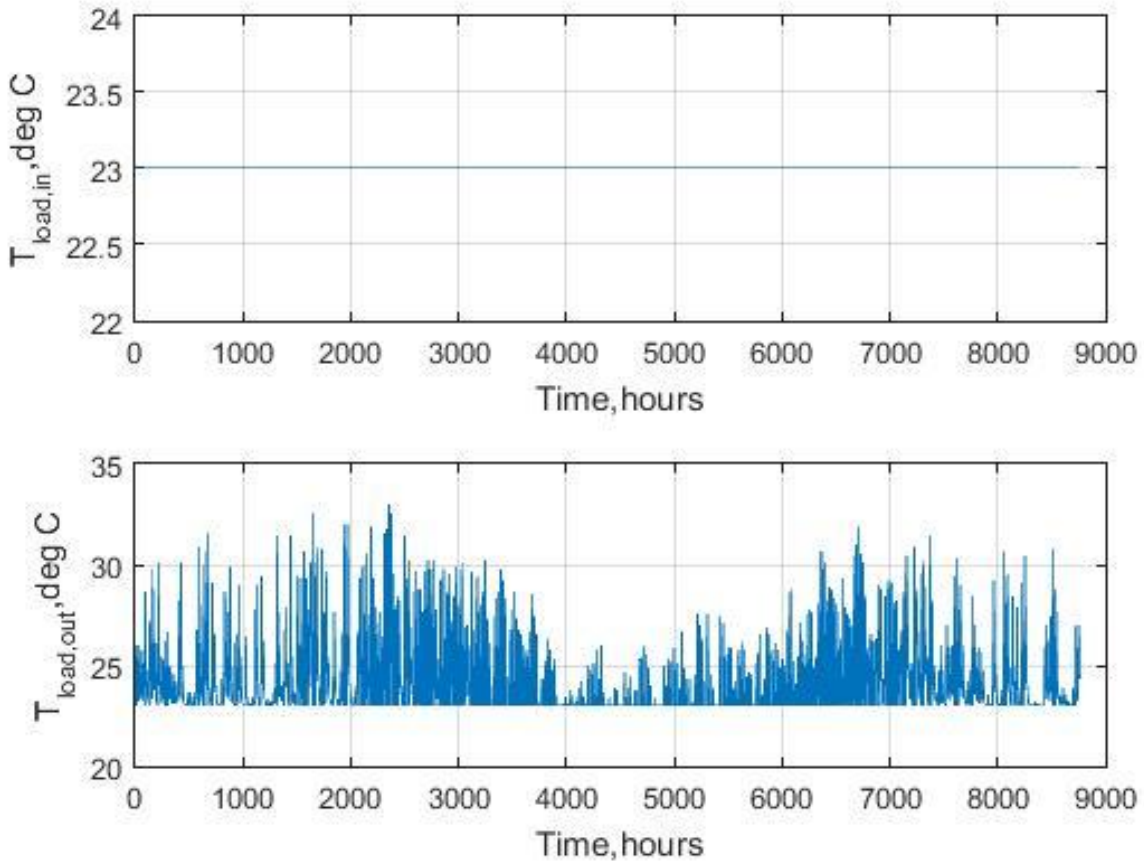

Figure 66: Hourly air temperatures for Dayton, Ohio.

In the remaining subsections of this section, yearly integrated results are presented for the 2000 ft^2 home in Dayton, OH. They are presented in the same order as the results for Minneapolis, MN. As previously mentioned, yearly integrated results provide a better means for comparing the performance of the same system located in Dayton, OH or Minneapolis, MN.

5.3.2 Area of Solar Array

Figure 67, as compared to Figure 44, shows that the solar array efficiencies and the overall system efficiencies at the Minneapolis and Dayton locations are about the same. Upon closer inspection, it is seen that these efficiencies are slightly higher in Minneapolis than Dayton. They are less than 1% point higher, but they are higher for all solar array areas.

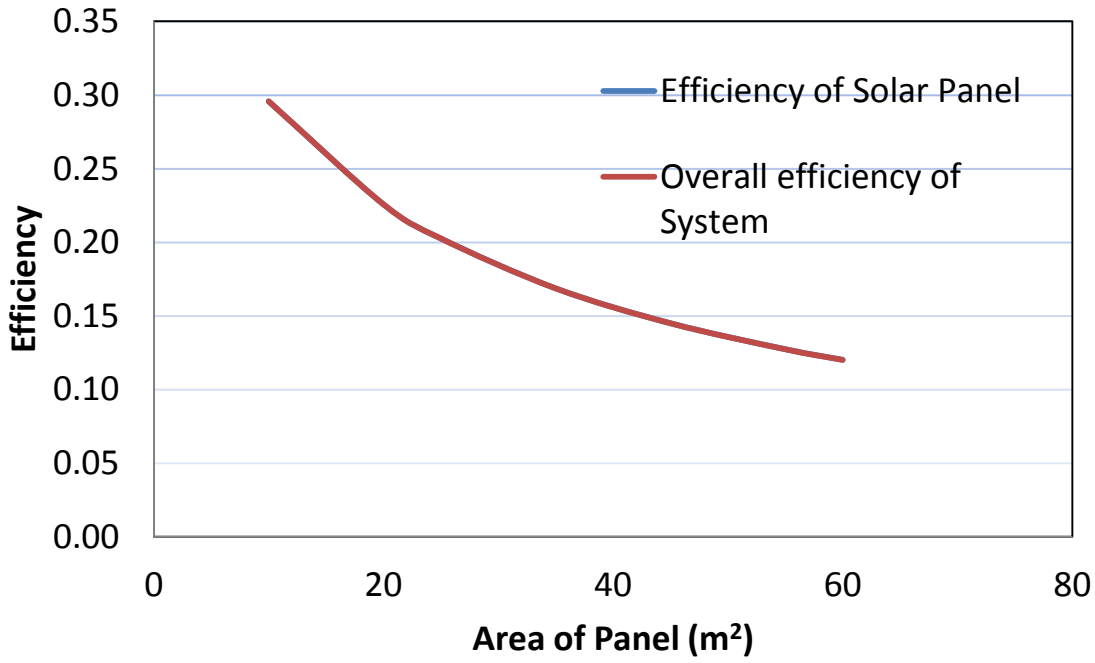

Figure 67: Efficiency of solar array and solar system as a function of the area of solar array for Dayton, Ohio.

The yearly heat collected by the solar array and the yearly heat exchanged in the heat exchanger are shown in Figure 68. The fraction of the heat load supplied by the solar system is given in Figure 69. These figures should be compared to Figures 45 and 46 for Minneapolis. The comparison of the heat transfer plots is more dramatic than the efficiency plots. The Minneapolis system delivers noticeably more energy to the home than the Dayton system. For the 60 m^2 solar array, the Minneapolis system delivers more than 20% more energy. For the 10 m^2 array, the Minneapolis system delivers slightly more than 10% more energy than the Dayton system. When comparing these systems from a fraction of heat load perspective, the differences are not as dramatic as from a heat transfer perspective. From this perspective, the Dayton system satisfies a slightly greater fraction of its heat load than the Minneapolis system using a solar array area of 10 m^2, but the Minneapolis system delivers a slightly higher fraction over the Dayton system for a 60 m^2 solar array.

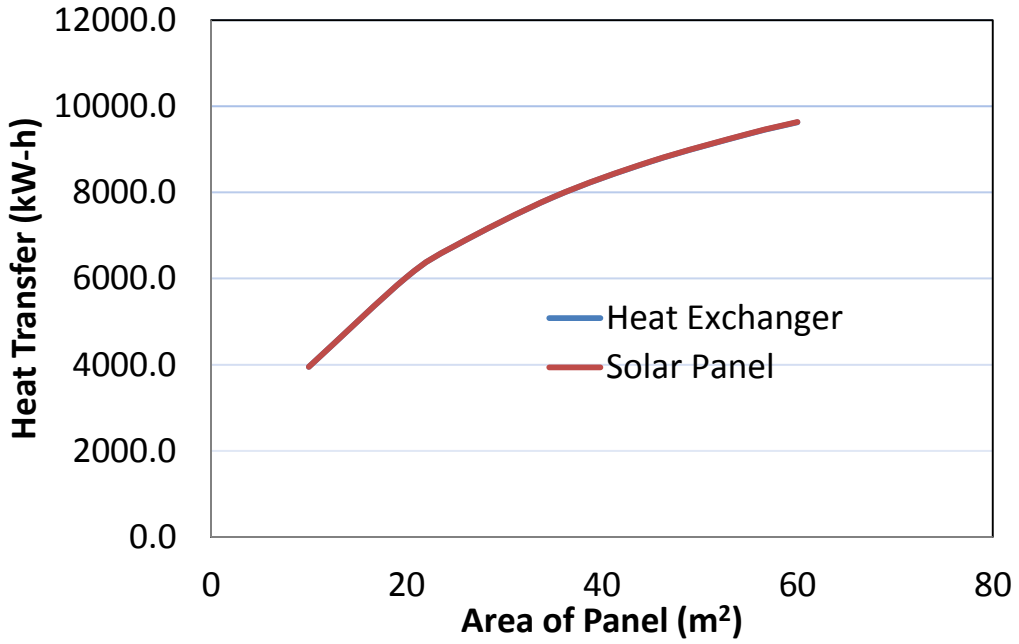

Figure 68 : Efficiency of solar array and solar system as function of the area of solar array for Dayton, Ohio.

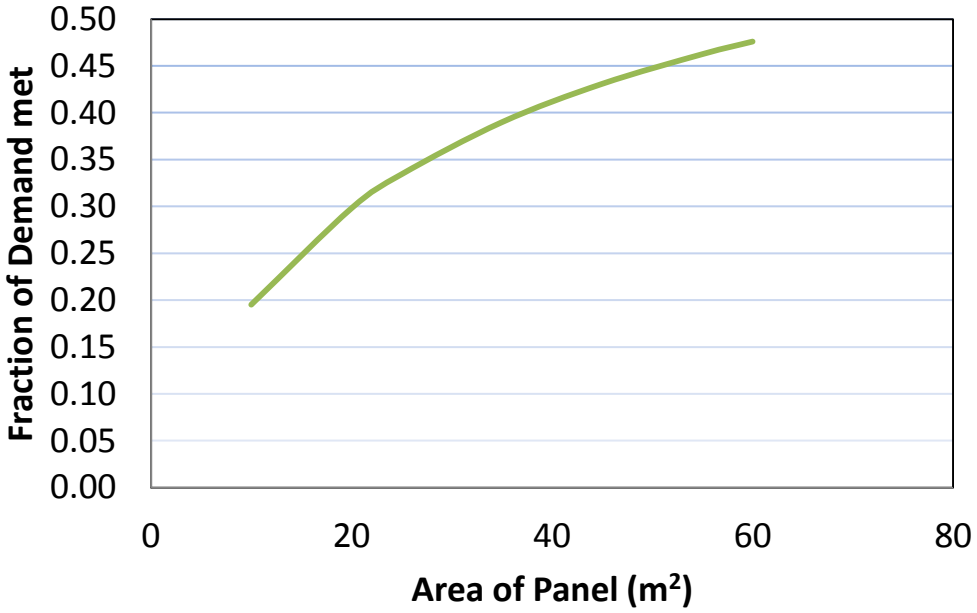

Figure 69: Fraction of heat load delivered as a function of the solar array area for Dayton, Ohio.

5.3.3 Tilt of Solar Panel

The latitude of Dayton, OH is 39.8°, therefore according to the equation $ude \times 0.875 + 19.2^{o}$ [45], the tilt angle of the solar thermal panels should be 44.9°. The tilt angle survey results for Dayton, OH are shown in Figures 70 and 71. Figure 70 shows the yearly-integrated energy gains in the solar array and the yearly heat transfer in the heat exchanger. Figure 71 shows the fraction of the home's heat load supplied by the solar system. All of these results show the optimum tilt angle to be very close to 44.9°. For tilt angles between 40 to 55 degrees, there is very little difference in the heat rates or heat load fraction. Thus, having the exact optimum tilt angle is not critical. In this work, we have used the optimum tilt angle calculated with the equation $latitude \times 0.875 + 19.2^{o}$ [50].

The optimum tilt angle for Minneapolis, MN was determined to be 58.4°. This is 14° more tilt than for Dayton, OH. This difference is more than the difference in the latitudes of the two locations, which is about 5°. The yearly heat transfers for Dayton peak out at slightly below 7000 kW-h, whereas those for Minneapolis peak out at slightly above 8000 kW-h. The Minneapolis system captures 7 to 23% more energy than the Dayton system. The fractions of the heat loads supplied by the systems in the two locations are about the same, but slightly more of the Dayton heat loads are supplied by its solar system than the Minneapolis solar system.

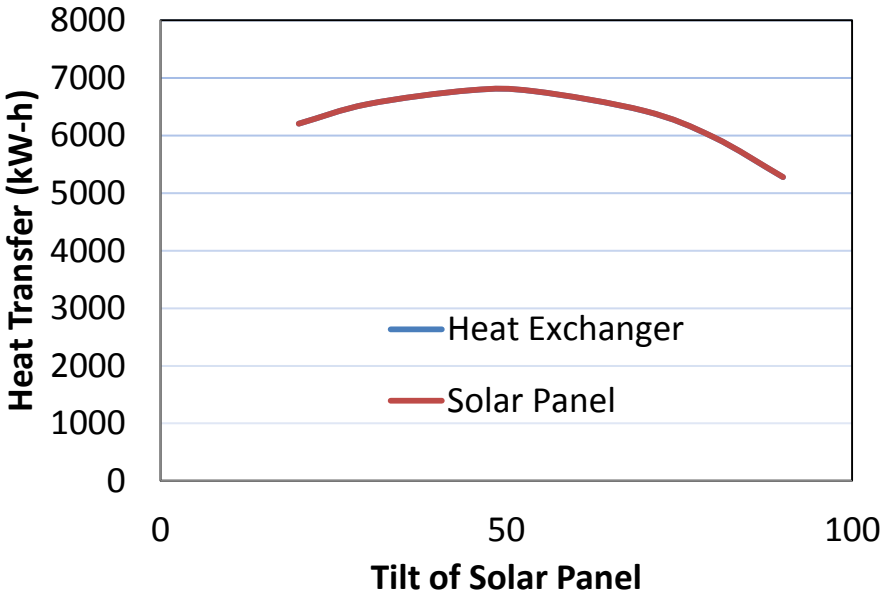

Figure 70: Yearly useful heat gain in solar array and yearly heat transfer in heat exchanger as a function of the panel tilt for Dayton, Ohio.

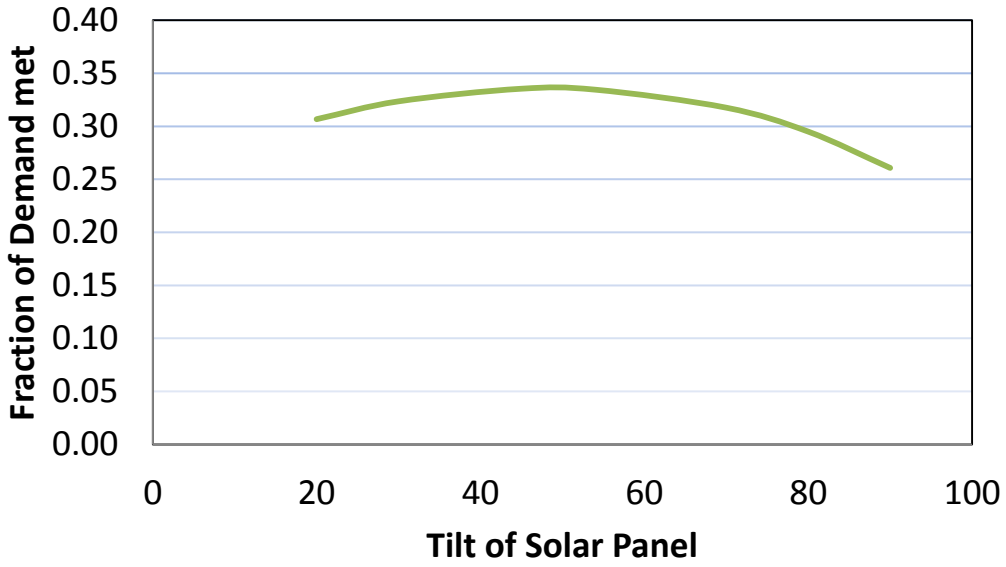

Figure 71: Fraction of heat load delivered as a function of the area of solar array for Dayton, Ohio.

5.3.4 Arrangement of Solar Panels

The survey results for the arrangement of the solar panels for the Dayton, OH location are shown in Figures 72, 73, and 74. Just like the results for Minneapolis (see Figures 49, 50, and 51), there is no dependence on the arrangement of the solar panels as long as the surface area of the solar array and the ethylene glycol flow rate through the array remain constant. Figure 72 and Figure 49 show that the solar array efficiency and the overall system efficiency are 1% point higher in the Minneapolis location as compared to the Dayton location. Figure 73 and Figure 50 show that the heat transfers are 17% more at the Minneapolis location as compared to the Dayton location. Figure 74 and Figure 51 show that the Dayton system supplies 1.4% points more of its heat than the Minneapolis system. Thus, even though the Minneapolis system supplies more energy to the home, it supplies a small fraction of its heat load as compared to the Dayton system. This simply means the Dayton heat loads are less than the Minneapolis heat loads.

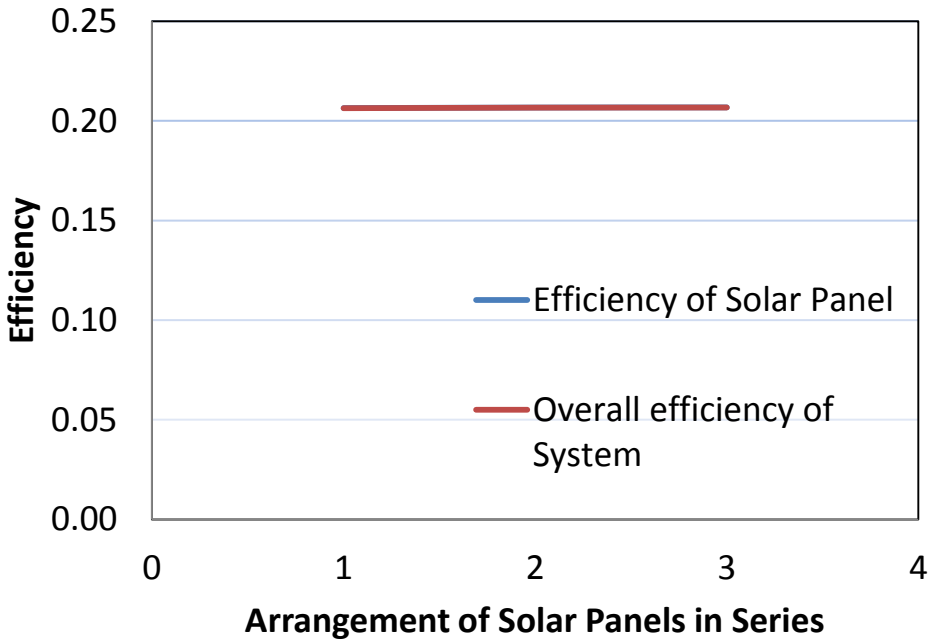

Figure 72: Efficiency of solar array and overall system efficiency as a function of the arrangement of the panels in series/parallel for Dayton, Ohio.

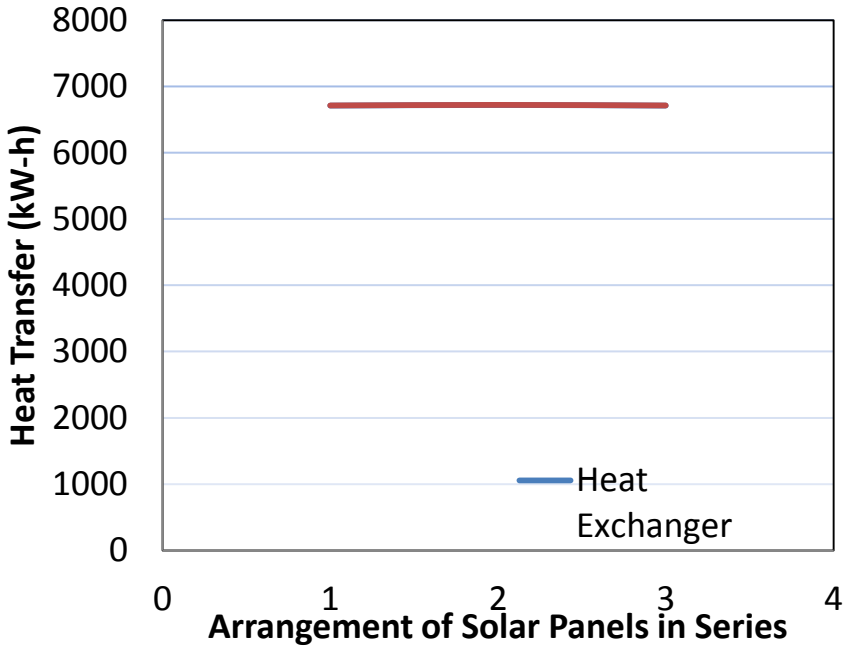

Figure 73: Yearly useful heat gain in solar array and yearly heat transfer in heat exchanger as a function of the arrangement of panels in series/parallel for Dayton, Ohio.

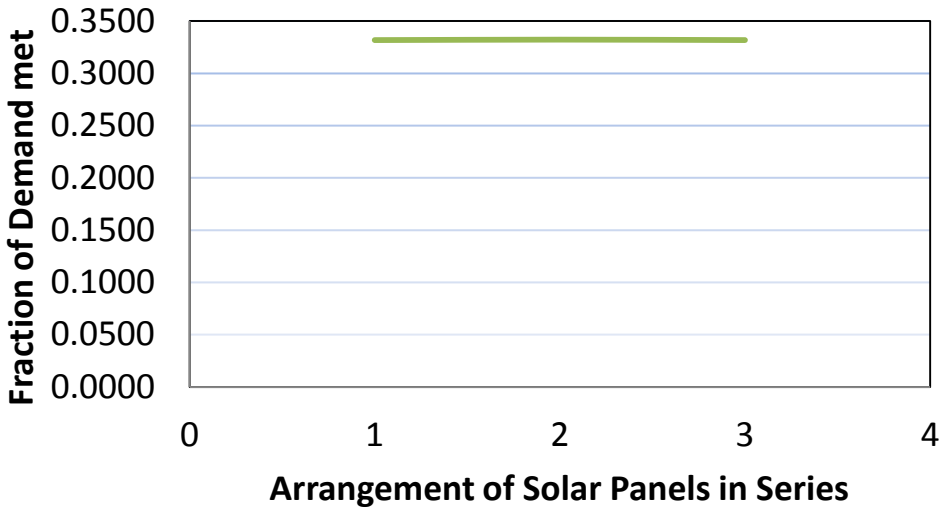

Figure 74: Fraction of heat load delivered as a function of the arrangement of panels in series/parallel for Dayton, Ohio.

5.3.5 Ethylene Glycol Flow Rate

Figures 75, 76, and 77 show the performance of the Dayton solar system as a function of the ethylene glycol flow rate. These plots should be compared to the corresponding figures for the Minneapolis solar system shown in Figures 52, 53, and 54. When this is done, it is seen that the trends are the same in the efficiencies, yearly heat transfer, and heat load fractions, but the magnitudes are a little different. Just like the Minneapolis ethylene flow rate results, the Dayton results show that an ethylene glycol flow rate of 0.5 kg/s is a reasonable ethylene glycol mass flow rate at which to operate this solar system when it is located in Dayton, OH. This same flow rate was deemed effective for the Minneapolis system as well.

5.3.6 Air Side Flow Rate

The air side flow rate results for Dayton, OH are shown in Figures 78, 79, and 80. The corresponding Minneapolis, MN results are shown in Figures 55, 56, and 57, respectively. All of the results between Dayton and Minneapolis are similar, but the magnitudes are slightly different. For Dayton, OH, the peak efficiency value is 20.9%, the peak heat flow is 6800 kW-h, and the peak heat load fraction is 33.6. The corresponding quantities for Minneapolis are 21.9%,

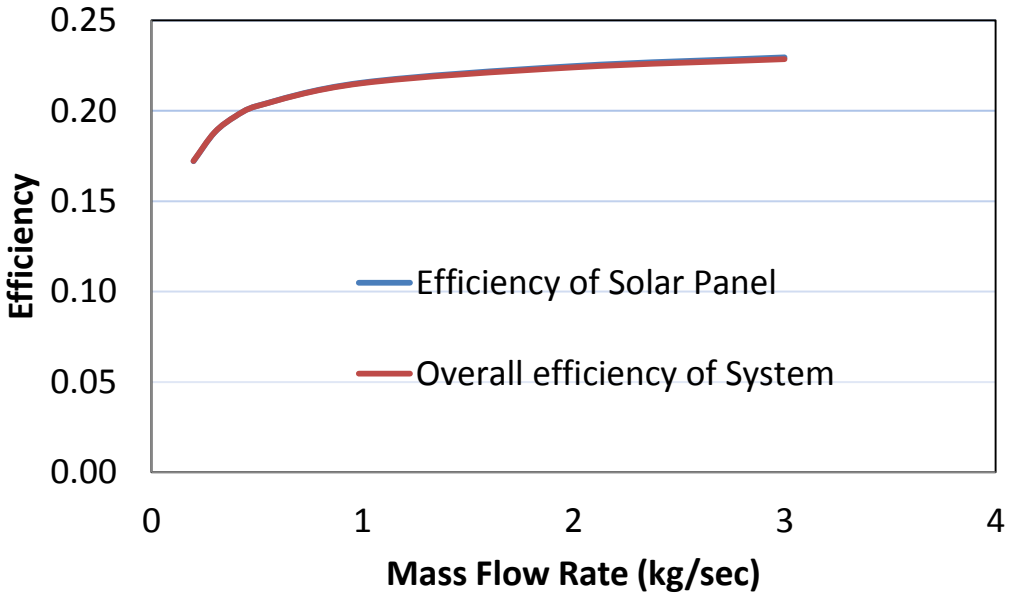

Figure 75: Efficiency of solar array and overall system as a function of the ethylene glycol mass flow rate for Dayton, Ohio.

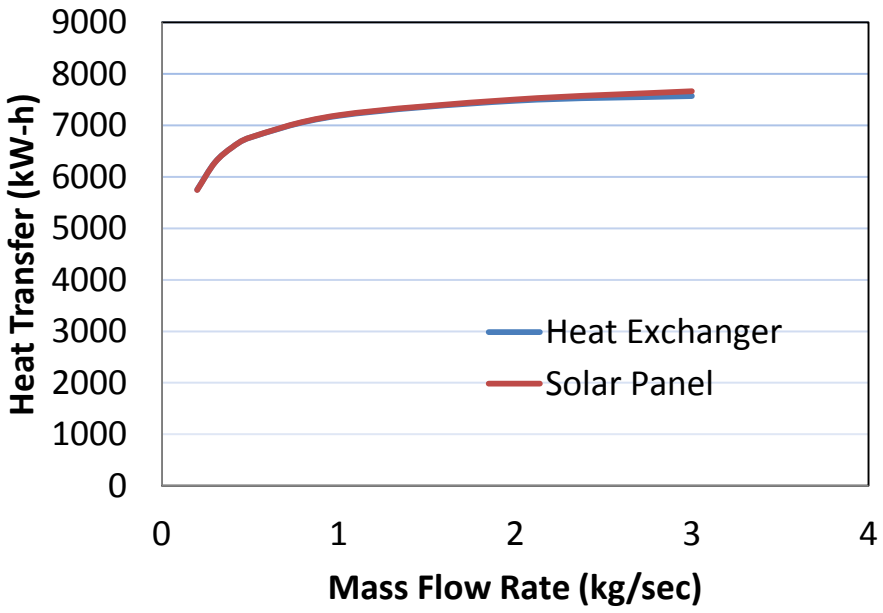

Figure 76: Yearly useful heat gain in solar array and yearly heat transfer in heat exchanger as a function of the ethylene glycol mass flow rate for Dayton, Ohio.

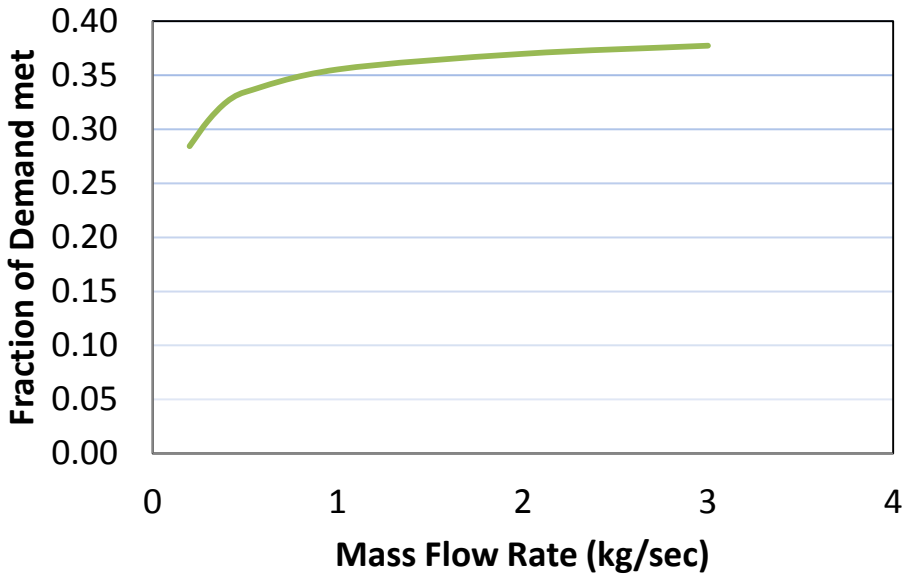

Figure 77: Fraction of heating load delivered as a function of the ethylene glycol mass flow rate for Dayton, Ohio.

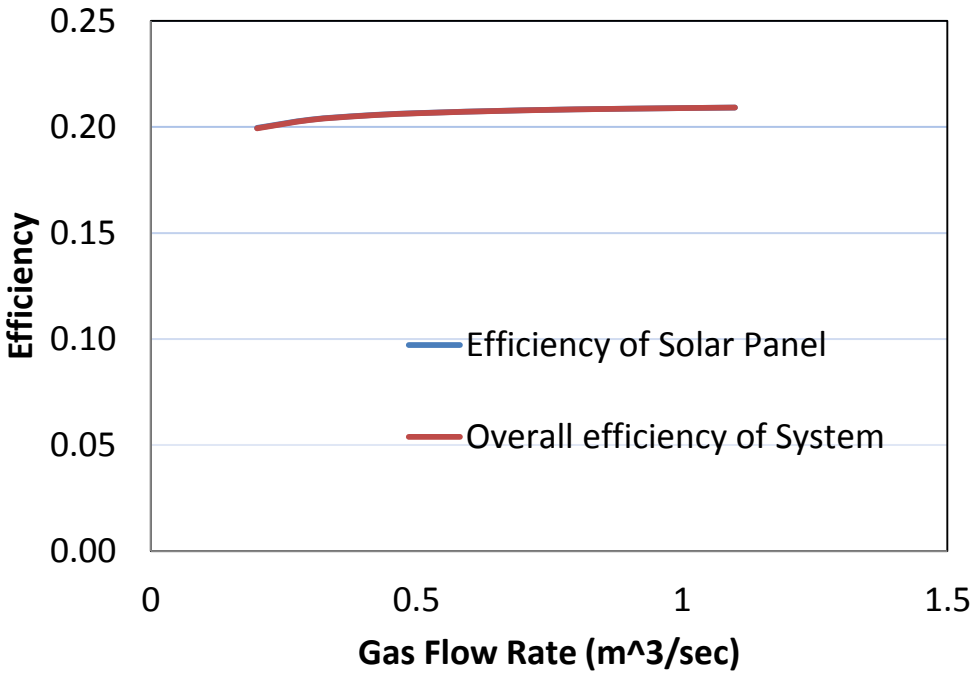

Figure 78: Efficiency of solar array and overall system efficiency as a function of the air volumetric flow rate for Dayton, Ohio.

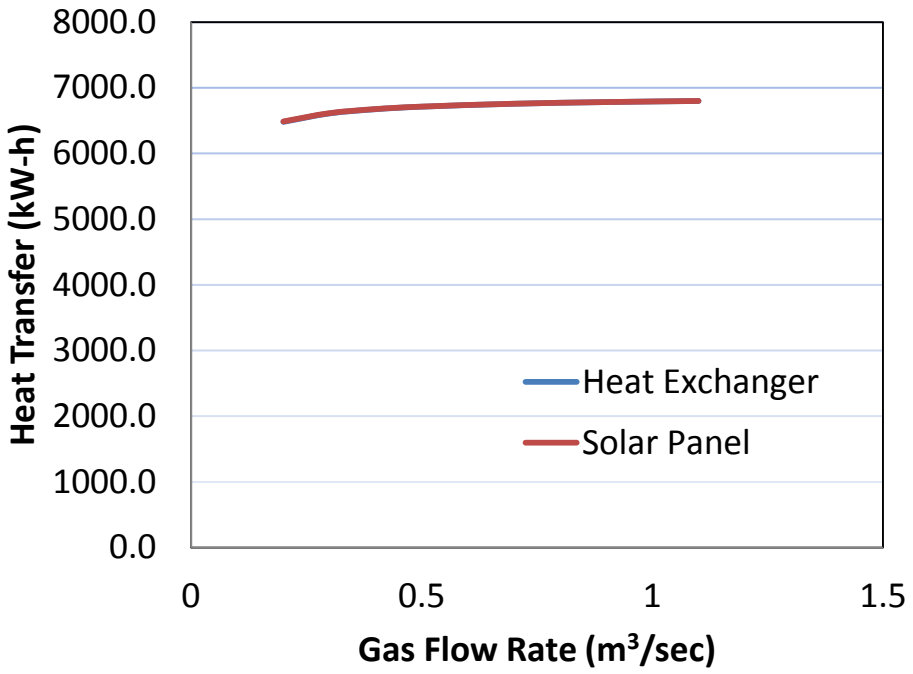

Figure 79: Yearly useful heat gain in solar array and yearly heat transfer in heat exchanger as a function of the air volumetric flow rate for Dayton, Ohio.

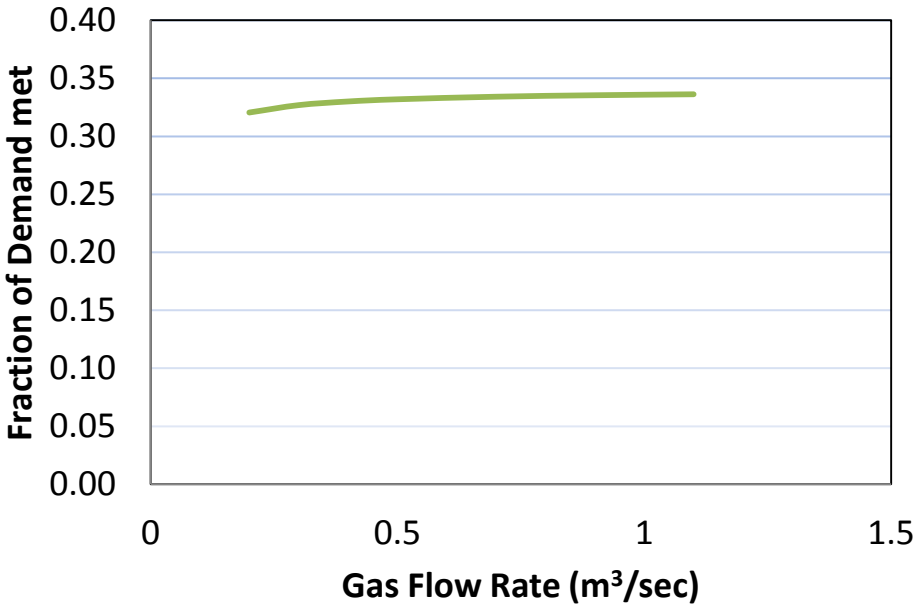

Figure 80: Fraction of heating load delivered as a function of air volumetric flow rate for Dayton, Ohio.

8250 kW-h, and 32.2%, respectively. The major difference is that the Minneapolis system supplies more heat than the Dayton system, but has a slightly lower fraction of energy supplied percentage. More energy is supplied by the Minneapolis system because there is more sun in Minneapolis. Another reason for more energy being supplied in Minneapolis is that the heat loads are larger and longer lasting. Longer lasting heat loads mean more energy can be collected by the solar panels. If a system does not use the energy it collects, the temperature of the ethylene glycol increases, preventing more energy from being collected in the solar panels, thus limiting solar energy collection. The heat load fractions being larger in Dayton than Minneapolis, even though more heat is collected in Minneapolis, is due to the heating loads being smaller in Dayton. Just like the Minneapolis air flow rate results, the Dayton results show that air volumetric air flow rate of 0.5 m^3/s is a reasonable air flow rate at which to operate this solar system when it is located in Dayton, OH.

5.3.7 Size of Heat Exchanger

This subsection shows the effects of increasing the ethylene glycol flow length and the air flow length in the heat exchanger for a solar system located in Dayton, OH. Figures 81 and 82 show efficiency numbers as a function of the ethylene glycol flow length and the air flow length, respectively. The corresponding Minneapolis results are shown in Figures 58 and 59, respectively. Figures 83 and 84 show the yearly heat rates as a function of the ethylene glycol flow length and the air flow length, respectively. The corresponding Minneapolis results are shown in Figures 60 and 61, respectively. Figures 85 and 86 show the heat load fractions as a function of the ethylene glycol flow length and the air flow length, respectively. The corresponding Minneapolis results are shown in Figures 62 and 63, respectively. All six of the Dayton figures look very similar to the corresponding six Minneapolis figures in shape and curvature, with small differences in magnitude. The Minneapolis results show higher efficiencies and yearly heat transfers, whereas the Dayton results show slightly higher heat load fraction results. Both the Dayton and Minneapolis results indicate that an ethylene glycol flow length of 0.9 m and an air flow length of 0.05 m are reasonable design lengths for heat exchanger in these solar systems.

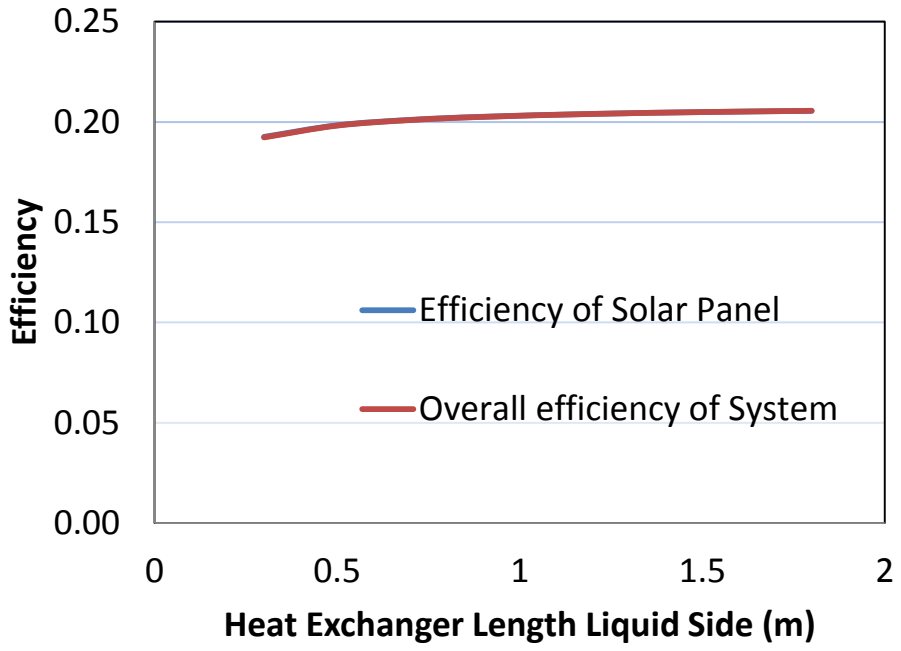

Figure 81: Efficiency of solar array and overall system efficiency as a function of heat exchanger length on ethylene glycol side for Dayton, Ohio.

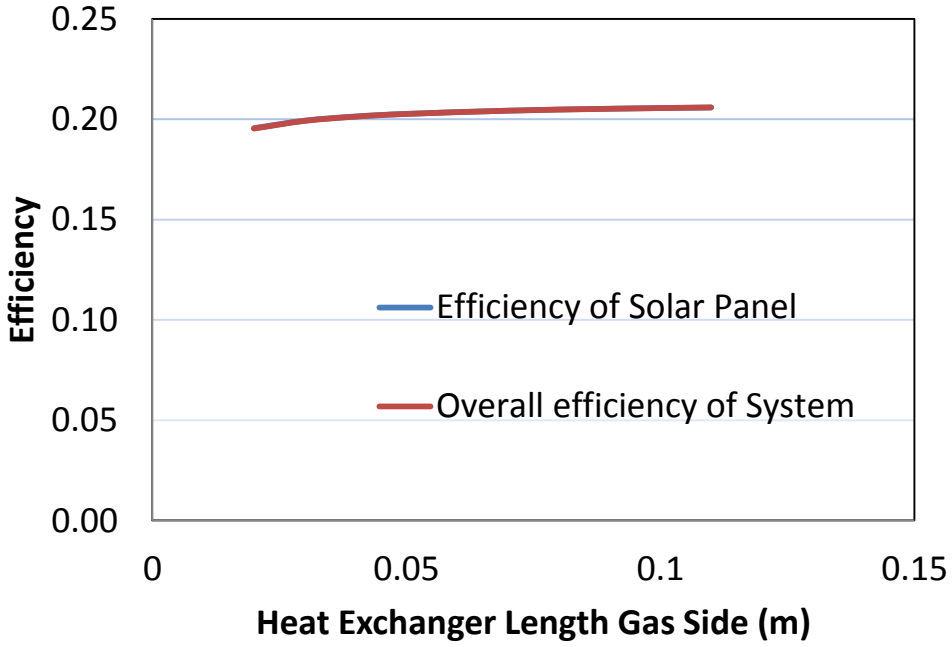

Figure 82: Efficiency of solar array and overall system efficiency as a function of heat exchanger length on air side for Dayton, Ohio.

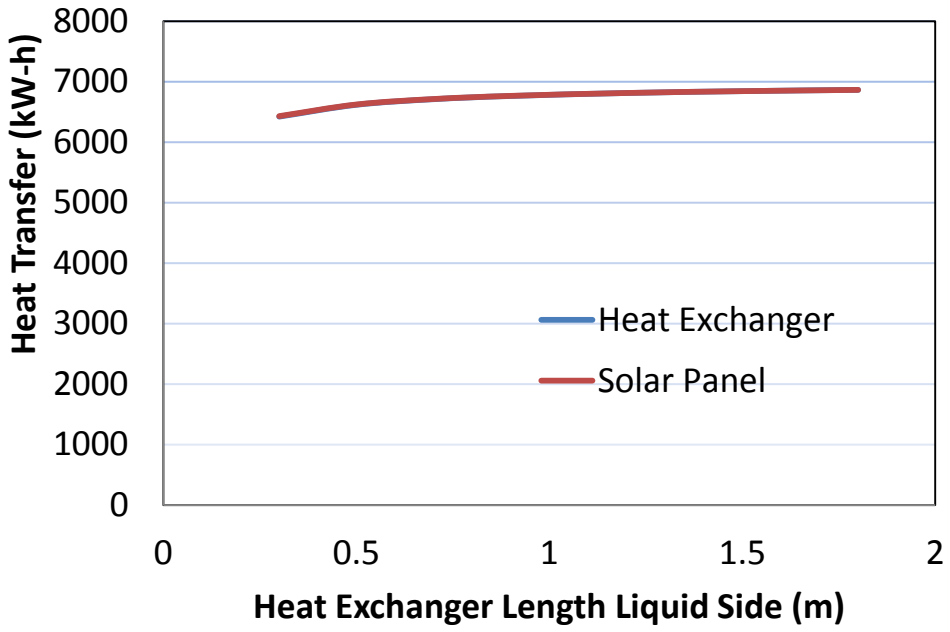

Figure 83: Yearly useful heat gain in solar array and yearly heat transfer in heat exchanger as a function of the heat exchanger length on the ethylene glycol side for Dayton, Ohio.

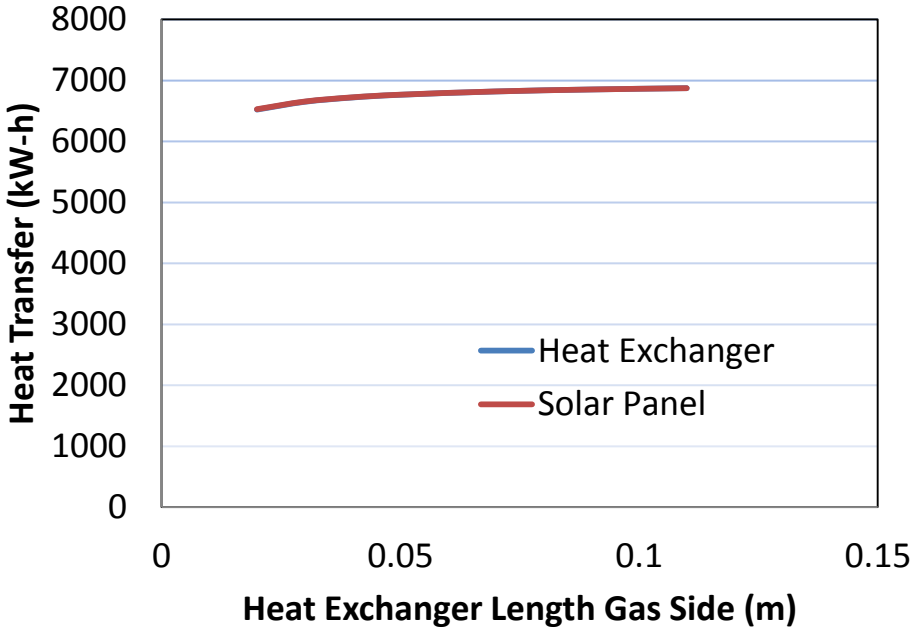

Figure 84: Yearly useful heat gain in solar array and yearly heat transfer in heat exchanger as a function of the heat exchanger length on the air side for Dayton, Ohio.

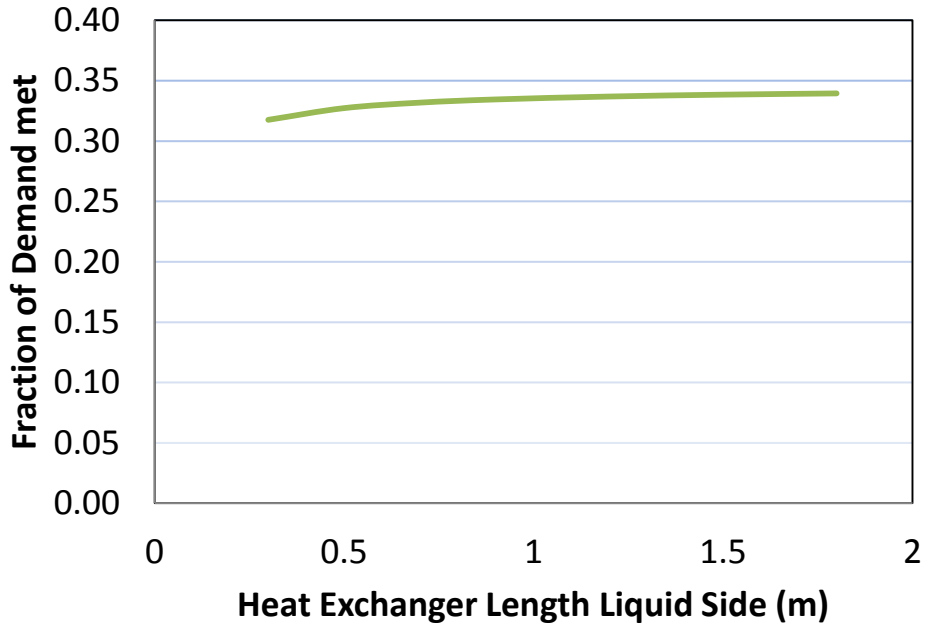

Figure 85: Fraction of heating load delivered as a function of heat exchanger length on the ethylene glycol side for Dayton, Ohio.

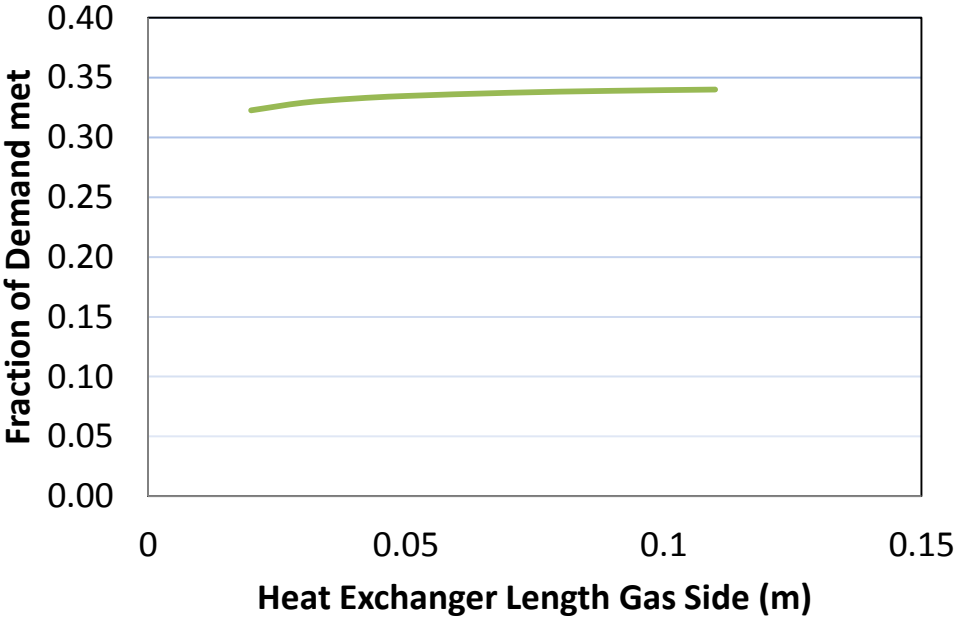

Figure 86: Fraction of heating load delivered as a function of heat exchanger length on the air side for Dayton, Ohio.

Chapter 6. CONCLUSIONS

The objective of this work was to study and gain understanding of simple solar thermal systems used for space heating. These systems are not as popular as solar thermal hot water heating systems, but there is still a desire to understand the abilities of such systems. This objective has been met by producing a large number of computational results for such systems composed of solar panels, a heat exchanger, and a small amount of thermal storage.

In order to produce these results, computer modules were written and integrated into a Wright State developed computer code called Solar_PVHFC. One of the computer modules simulates liquid solar thermal panel performance, and the other module simulates heat exchanger performance. In addition, system control routines were integrated into the solar thermal panel performance module. The thermal energy storage was handled by assuming the system had sufficient fluid storage for one hour, the time increment used for the calculations done in this thesis, and there was no mixing of fluid in this container. These two computer modules were integrated into Solar_PVHFC so that the detailed solar resource calculations performed by Solar_PVHFC could be utilized in this solar thermal system analysis.

Once this computer code was written and checked for accuracy, a large number of results were produced, including one-hour results for standard solar panel testing conditions and yearly results for solar thermal space heating systems in Minneapolis, MN and Dayton, OH. Sixty-one figures of results are presented in this thesis. These results study both design parameters and

operating parameters. The design parameters studied are the area of the solar array, the tilt of the solar panels, the arrangement of the solar panels, and the size of the heat exchanger used. The operating parameters studied are the mass flow rate of the working fluid passing through the solar panels, which also passes through the hot side of the heat exchanger, and the volumetric flow rate of the home air passing through the cold side of the heat exchanger. Because two different locations were studied, the effect of location can also be determined. Of the two locations studied, Minneapolis, MN is considered a cold region with high heating loads, and Dayton, OH is considered a moderate region with moderate heating loads.

The results shown in this thesis indicate the area of the solar array has the largest effect on the space heating produced by the solar system. Increasing the area of the solar array increases the heat delivered to the home and increases the fraction of the demand met. The two parameters that decrease with increasing array area are the efficiency of the solar array and overall efficiency of the solar thermal system. Furthermore, increases in the energy delivered to the home are not linear with respect to array area. The benefits of increasing solar array area become less as the area increases.

In regards to the optimum tilt angle of the solar panels, Landau ‘s equation [45] appears to provide optimum heat delivery to the home. The optimum tilt angle for Minneapolis, MN is 58.4^{o}, and the optimum tilt angle for Dayton, OH is 44.9^{o}. Both of these tilt angles are greater than the latitude of the given locations. These larger tilt angles are obtained because the heating demands occur in the winter time when the sun is low in the sky. Another useful conclusion found from the tilt angle studies is that there is a weak sensitivity to the accuracy with which this optimum tilt angle needs to be maintained. Being off by 2 or 3 degrees will not affect the performance of the solar system noticeably.

This study found that placing solar panels in series or parallel to produce the solar array will not change the performance of the system as long as the overall array area remains constant and the liquid flow rate through the array remains the same. This result may not hold up for liquid flow rates below those studied in this work, but no noticeable changes were seen in any of the results produced for the panel arrangement studies done here. Arrangements of one, two, and three solar panels in series were investigated as part of this work.

The size of the heat exchanger does affect the results, but oversized heat exchangers do not deliver any significant improvements in performance. The results in this thesis indicate that a

minimum heat exchanger size should be maintained, but further increases are not worth the additional capital equipment costs.

The survey of the fluid flow rates through the system, either liquid or gas, produced similar results to the heat exchanger size surveys. Certain minimum flow rates should be maintained, but increasing them significantly above these minimum rates does not yield noticeable benefits. Although higher flow rates may slightly increase heat delivery to the home, higher flow rates also require more pumping power. Thus, using the minimum flow rates that deliver close to the maximums is advantageous.

It was interesting to note that the same solar thermal system delivered more energy to the home in Minneapolis, MN compared to Dayton, OH. There are two possible reasons for this behavior. The first explanation is that better sun conditions exist in the winter for Minneapolis, MN. The second explanation is Minneapolis has greater heat loads and thus uses more of the energy captured by the solar array quickly. The more heating a home needs, the more solar energy the solar array will collect. This occurs because the fluid running through the solar array and the hot side of the heat exchanger increases in temperature when energy is not extracted from it. Higher working fluid temperatures mean higher heat losses to the surroundings from the solar array. It is also interesting to note that the Minneapolis system delivered more heat to the home and had higher panel efficiencies and higher system efficiencies, but supplied a slightly smaller fraction of the total yearly heating load. Overall, it can be said that solar thermal systems used for space heating are better utilized in Minneapolis, MN conditions as compared to Dayton, OH conditions.

From the results of this thesis work, it can also be noted that it takes a fairly large solar thermal system to supply, 20 to 50% of a home's heating needs. Without doing an economic analysis, it is not possible to answer the question as to whether this is worth it, but the size of the solar array and the fraction of heat load met seem to indicate that solar thermal space heating systems with minimum energy storage are not worth installing. One of the problems with such a system is matching the demand to the supply. For Dayton, OH, most solar energy is available in the summer, but the major heating requirements occur in the winter. This is a mismatch between supply and demand. The means to overcome this mismatch is to install large amounts of thermal storage, which is costly.

In the future, it would be beneficial to add an economic analysis to the solar thermal system computer model developed for this thesis work. Such an analysis would help to answer the question, of whether solar thermal systems with minimum storage are worth it?

Chapter 7. Bibliography

[1] M. Gustafson, "A Computational Approach to Simulating the Performance of a 24-Hour Solar Hydrogen Fuel Cell Electric Power Plant," Wright State University , Dayton, OH, 2013.

[2] "Lawrence Livemore National Laboratory," 2015. [Online]. Available: https://www.llnl.gov/news/americans-using-more-energy-according-lawrence-livermore-analysis. [Accessed 8 May 2015].

[3] [Online].Available:http://climatechange.lta.org/wp-content/uploads/cct/2015/04/energy_consumption_by_source_2014.jpg. [Accessed 8 May 2015].

[4] "Solar Energy Program," Buereau of Land Management, [Online]. Available: http://blmsolar.anl.gov/program/. [Accessed 9 May 2015].

[5] "Enviromental and Energy Study Institute," [Online]. Available: http://www.eesi.org/papers/view/fact-sheet-solar-water-heating?/solar_water_0506. [Accessed 9 May 2015].

[6] "CaliforniaSolarCenter,"[Online].Available: http://californiasolarhttp://www.greenenergyohio.org/page.cfm?pageID=1345. [Accessed 9 May 2015].

[7] E.Martinot, "Renewable Energy Policy Network," 2015. [Online]. Available: http://www.ren21.net/wp-content/uploads/2015/07/REN12-GSR2015_Onlinebook_low1.pdf. [Accessed 10 June 2015].

[8] "Clean Technica," [Online]. Available: http://cleantechnica.com/2014/04/24/us-solar-energy-capacity-grew-an-astounding-418-from-2010-2014/ . [Accessed 10 June 2015].

[9] "Department of Energy,USA," [Online]. Available: http://energy.gov/lpo/mojave. [Accessed 12 June 2015].

[10] "Department of Energy,USA," [Online]. Available: http://energy.gov/lpo/solana. [Accessed 12 June 2015].

[11] "Home Power," [Online]. Available: http://www.homepower.com/articles/solar-electricity/project-profiles/solar-success-northeast . [Accessed 13 June 2015].

[12] "Bechtel," [Online]. Available: http://www.bechtel.com/expertise/power/renewable/solar-photovoltaic/. [Accessed 12 August 2015].

[13] "Solar Energy USA," [Online]. Available: : http://solarenergy-usa.com/install/84-panel-solar-pv-install-in-greenville-sc/. [Accessed 12 August 2015].

[14] "Solar Energy USA," [Online]. Available: : http://solarenergy-usa.com/install/19-panel-off-grid-solar-home-in-cumming-ga/. [Accessed 10 September 2015].

[15] "Full Spectrum Solar," [Online]. Available: http://www.fullspectrumsolar.com/ourservices_spaceheating.html.

[16] "Department of Energy,USA," [Online]. Available: https://www1.eere.energy.gov/solar/pdfs/solar_timeline.pdf. [Accessed 12 September 2015].

[17] M. Kainth and V. K. Sharma, "Latest Evolutions in Flat Plate Solar Collectors Technology," *IJME*, vol. 1, no. 1, pp. 7-11, 2015.

[18] E. Tasdemiroglu, "Seasonal Performance of an Active Space Heating System," *Renewable Energy*, vol. 1, no. 1, pp. 9-12, 1991.

[19] M. Chekerovska and R. V. Filkoski, "Efficiency of Liquid Flat-Plate Solar Energy Collector with Solar Tracking System," *Thermal Science*, vol. 19, no. 5, pp. 1673-1684, 2015.

[20] T. V. Esbensen and V. Korsgaard, "Dimensioning of the solar heating system in the zero energy house in Denmark," *Solar Energy*, vol. 19, no. 2, pp. 195-199, 1977.

[21] A. Manickavasagan, "An Experimental Study on Solar Flat Plate Collector Using an Alternative Working Fluid," *Pertanika J. Sci. & Technology*, vol. 2, no. 13, pp. 147-167, 2005.

[22] W. Lin, W. Gao and T. Liu, "A parametric study on the thermal performance of cross-corrugated solar air collectors," *Applied Thermal Engineering*, vol. 26, no. 10, pp. 1043-

1053, 2006.

[23] H. Ayoub, "Improving the Energy Capture of Solar Collectors (For Cloudy Regions by Using Controlled Tracking System)," University of Strathclyde Engineering, Glasgow,United Kingdom, 2012.

[24] H. Zhong, G. Li, R. Tang and W. Dong, "Optical performance of inclined south–north axis three-positions tracked solar panels," *Energy,* vol. 36, no. 2, pp. 1171-1179, 2011.

[25] P. Dupeyrat, C. Ménézo, M. Rommel and H.-M. Henning, "Efficient single glazed flat plate photovoltaic thermal hybrid," *Solar Energy,* vol. 85, no. 7, pp. 1457-1468, 2011.

[26] M. M. Hassan and Y. Beliveau, "Modeling of an integrated solar system," *Building and Environment,* vol. 43, no. 5, pp. 804-810, 2008.

[27] F. Mehdaoui, M. Hazami, N. Naili and A. Farhat, "Energetic performances of an optimized passive Solar Heating Prototype used for Tunisian buildings air-heating application," *Energy Conversion and Management,* vol. 87, pp. 285-296, 2014.

[28] R. Oonk, W. Beckman and J. Duffie, " Modeling of the CSU heating/cooling system.," *Solar Energy,* vol. 17, no. 1, pp. 21-28, 1975.

[29] J. Cadafalch, "A Detailed Numerical Model for Flat-Plate Solar Thermal Devices," *Solar Energy,* vol. 83, no. 12, pp. 2157-2164, 2009.

[30] J. A. B. W. A. Duffie, Solar Engineering of Thermal Processes, New York,USA: Wiley Interscience, 1991.

[31] Z. Jiandong, T. Hanzhong and C. Susu, "Numerical simulation for structural parameters of flat-plate solar collector," *Solar Energy,* vol. 117, pp. 192-202, 2015.

[32] G. A. Zueva and J. Magiera, "Mathematical Model of Heat Transfer in a Solar Collector and Its Experimental Validation," *Theoretical Foundations of Chemical Engineering,* vol. 35, no. 6, pp. 604-608, 2001.

[33] M. Hamed, A. Fellah and A. B. Brahim, "Parametric sensitivity studies on the performance of a flat plate solar collector in transient behavior," *Energy Conversion and Management,* vol. 78, pp. 938-947, 2014.

[34] X. Lan, S. Wu, Q. Zhang and Y. Li, "Theoretical investigation on thermal performance of heat pipe flat plate solar collector with cross flow heat exchanger," *Heat Mass Transfer,*

no. 48, pp. 1167-1176, 2012.

[35] H. Gunerhan and A. Hepbasli, "Exergetic modeling and performance evaluation of solar water heating systems for building applications," *Energy and Buildings,* vol. 39, no. 5, pp. 509-516, 2007.

[36] A. Oliva, M. Costa and C. Segarra, "Numerical simulation of solar collectors: The effect of nonuniform and nonsteady state of the boundary conditions," *Solar Energy,* vol. 47, no. 5, pp. 359-373, 1991.

[37] A. Hasan, "Sizing solar space heating system : A case study," *Renewable Energy,* vol. 16, no. 1, pp. 720-724, 1999.

[38] A. M. Saleh, "Modeling of Flat-Plate Solar Collector Operation in Transient States," Purdue University, Fort Wayne,Indiana, 2012.

[39] B. Liu and R.C.Jordan, "The Long- Term Average Performance of Flat Plate Solar Energy Collectors," *Solar Energy,* no. 7, p. 53, 1963.

[40] S. A. Kalogirou, "Solar thermal collectors and applications," *Progress in Energy and Combustion Science* , vol. 30, pp. 231-295, 2004.

[41] J. A.Duffie and W. Beckman, Solar Engineering of Thermal Processes, Fourth Edition, Hoboken, New Jersey: John Wiley & Sons, 2013.

[42] H. Hottel and B.B.Woertz, "The Performance of Flat Plate Solar Heat Collectors," *ASME,* no. 91, p. 64, 1942.

[43] D. J. Menart, *Chapter6 Flat Plate Collectors,* Dayton,Ohio: Wright State University, 2008.

[44] "Thermal Systems," [Online]. Available: http://me1065.wikidot.com/automotive-heat-exchangers.

[45] F. P. Incropera and D. P. Dewitt, Fundamentals of Heat and Mass Transfer, New York,USA: Library of Congress Cataloging, 2002.

[46] "Heat Transfer," [Online]. Available: http://heattransfer.asmedigitalcollection.asme.org/data/Journals/JHTRAO/27906/005101jhr1.jpeg. [Accessed 10 April 2016].

[47] "Solar Rating & Certification Corpooration," [Online]. Available: www.solar-rating.org. [Accessed 5 September 2016]

[48] "SRCC Document RM-2016," 16 4 April. [Online]. Available: www.solar-rating.org. [Accessed 5 September 2016]

[49] "Certified solar collector," [Online]. Available: www.solar-rating.org/summarypage. [Accessed 12 September 2016]

[50] C. R. Landau, "Optimum tilt of solar panels," 2015. [Online]. Available: http://www.solarpaneltilt.com/. [Accessed 14 September 2016].